Ilias Papadopoulos

Contactless Photovoltaic Cell Power Transfer

Contactless Photovoltaic Cell Power Transfer

By

Ilias Papadopoulos

in partial fulfilment of the requirements for the degree of

Master of Science

in **Sustainable Energy Technology**

at the Delft University of Technology,

to be defended publicly on Monday November 29th, 2021.

Student Number: 5006090

Project Duration: December 1st, 2020 – November 29th, 2021

Supervisor: Dr. Patrizio Manganiello

Thesis Committee: Dr. Arno Smets, Professor, PVMD/ESE, TU Delft

Dr. Patrizio Manganiello, Assistant Professor, PVMD/ESE, TU Delft

Dr. Zian Qin, Assistant Professor, DC&S/ESE, TU Delft

Table of Contents

Abstract

One of the main reasons that the efficiency drops from cell to module is the conduction losses. To increase the efficiency of the PV module, the produced charge carriers in the semiconductor materials should be transferred to the PV module terminals with minimum conduction losses. As an alternative to the conventional cells and modules interconnections, in this thesis project, efficient ways to incorporate Wireless Power Transfer (WPT) techniques into PV cell and module architecture are being sought.

The main objectives of this research are to understand how WPT techniques can be efficiently incorporated into PV devices, such as PV cells and modules, find out whether these techniques in theory and in practice are efficient enough and suggest the best design approach as a guideline for near future prototyping.

Many different WPT methods were studied in theoretical level, such as the Capacitive Power Transfer (CPT), the Inductive Power Transfer (IPT) and the Magnetic Resonant Coupling (MRC). Based on the main advantages and disadvantages of these methods, the most efficient seems to be the MRC, which eventually was used as the main method of transferring power wirelessly in the systems of this thesis project.

The systems that were developed and studied consist of a PV generator made of a single IBC solar cell or a PV generator that consists of 16 connected in series IBC solar cells, an inverter that converts the direct current (DC) of the generators into alternating current (AC) and two resonant circuits, the primary and the secondary one. Between these circuits, the power is transferred wirelessly from the primary to the secondary one, through the magnetic field that is created.

During this project, the main mathematical models were developed and were used for simulations in both Matlab and Simulink. The main goals of these simulations were to find out which type of coils, as far as the shape, the cross section and the values of turn width, turn spacing, distance between the coils and

number of turns are concerned, and which compensation topology would help the systems to develop higher efficiencies.

According to the results, when ideal DC to AC conversion at the primary side of the system is assumed, the most ideal option seems to be the Series-Series compensation topology with planar coils of circular shape and rectangular cross-section, for which the systems developed efficiencies higher than 85% when the circuits were connected with one solar cell and above 98% when the circuits were connected with one module of 16 solar cells.

1 Introduction

1.1 General Information

Nowadays, the energy consumption increases year by year. The main reasons of it are the rapid development of the society, as well as the increment of the world population. People consume energy for many different reasons and purposes, such as to power up and charge their electronic devices, to transport, to heat their homes and to produce goods and food. Usually, the highest consumption of energy per resident is made in countries and nations that are wealthy and technologically developed [1].

Since the world population is continuously growing, in 21st century, one of the most significant challenges is the reduction of the energy consumption. Some studies predict that until 2040 the energy demand will have risen due to the fact that in many countries, such as in India and China, the life expectancy is rapidly increasing and this will lead to higher demand of energy [1].

The growing energy demand is strongly related to another challenge that humankind is facing and this is the use of fossil fuels, such as coal, oil and gas to cover this demand. Fossils fuels are solar energy of million years stored in the form of chemical energy. The consumption of these fossil fuels by people is faster than their generation through the photosynthetic process in nature and this is a huge problem. Major amounts of oil and gas are produced with many different ways. Some of them, such as the extraction of oil from tar sands (Canada) and the production of gas with hydraulic fracturing (USA), are unconventional [2].

Another challenge, related to the previous ones, is the production of greenhouse gases and organic chemicals, such as carbon dioxide (CO_2), by burning fossil fuels and methane (CH_4), ozone (O_3) and nitrous oxide (N_2O). The additional amounts of these, that are caused by human activity, are stored in the oceans and atmosphere and leads in climate change, global warming and long-term environmental pollution [2],[3].

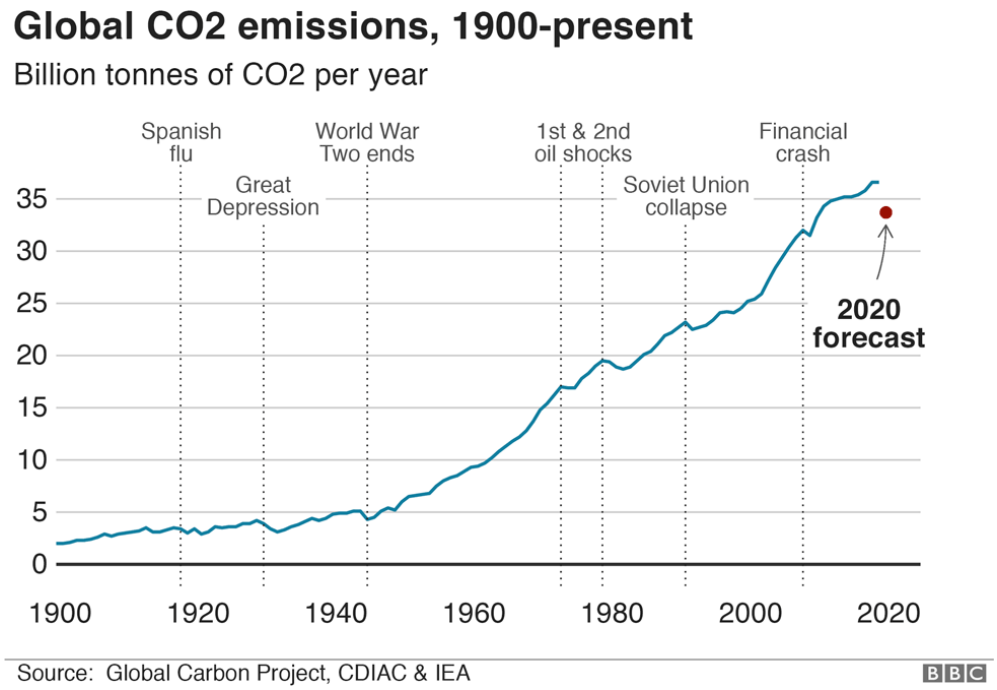

Figure 1.1: Global CO_2 Emissions between 1900 and 2020 [4]

Therefore, due to the gigantic use of fossil fuels and the huge production of greenhouse gases, phenomena such as the global warming and the environmental pollution are unavoidable. To avoid phenomena like these, renewable energy sources and technologies, such as solar panels, wind turbines, and hydro turbines, will play a crucial role [2].

For the majority of processes that happen on the surface of the Earth, sun is the main energy source. In particular, the evaporation of water due to sunlight has as a result the creation of clouds and rain and atmosphere's temperature difference, caused by the solar irradiation, results in the creation of wind [2].

In general, many different types of energy, such as thermal, kinetic, electric and chemical energy, can be produced by solar energy through the solar systems. One way of using solar energy is through direct conversion of solar radiation into electricity by using photovoltaic (PV) technology. The photovoltaic systems contain cells that convert the sunlight into electricity. The light enters the solar cell and is effectively trapped by the antireflection layer (optical coating) of the cell. In this way, the reflection losses are minimized. The amount of electrical

power that will be generated from each cell is determined by the intensity of the sunlight [2],[5].

1.2 History of PV Technology

Late in 1950s, the first photovoltaic cells were produced. In 1960s were used to provide electrical power for earth-orbiting satellites. Since 1960 and until 1970s, the research on the semiconductor based solar cells, the establishment of new technologies for polycrystalline Si (poly-Si) and thin-film solar cells and the improvements in performance, manufacturing and quality of the PV modules had as a result the increase of the production capacity and the decrease of the costs. Later, in the 1980s, PV technology became even more popular, especially for electronic devices, such as watches, calculators, lanterns, radios and other small battery charging applications [2],[6].

After the 1970s energy crises, major efforts to develop PV power systems for commercial and residential use were begun. At the same period, there was a significant increase of the international applications for PV systems to power health clinics, refrigerators, water pumps, telecommunications, as well as off-grid households and they still remain a major portion of today's worldwide market [6].

The last decades, one of the main renewable energy technologies is the PV systems. PV systems are a commercially and technically grown technology, able to generate and supply electricity by using solar energy. In 2018, PV systems were the second most popular energy source, since around 480 GW of capacity were installed in global scale. In 2019, 94 GW of power capacity were added from PV systems, surpassing the additional capacities of wind, fossil fuels and nuclear energy together [1],[7].

Finally, there is a significant reduction of PV technologies' costs and a continuous research for improved performance. Before 2000, the performance ratio of the PV systems was around 70%. However, today, this ratio has increased and it is in a range between 80 and 90%. So, PV systems will have the opportunity to become

one of the major global energy suppliers and it is predicted that they will deliver 2840 GW by 2030 and this will rise to 8519 GW by 2050, eventually [1],[7],[8].

1.3 Components of PV Systems

The basic components of PV systems are the solar cells. Due to its limited size, from each solar cell a small amount of power is generated. However, for most of the applications and devices this is not practical, since to operate there is a requirement for specific amounts of voltage and current. So, a number of solar cells are connected together to create a solar module (PV module), many solar modules are connected together to form a solar panel (PV panel) and many solar panels are connected together to form a solar array (PV array) and produce a substantial amount of power (Figure 1.2) [2].

Photovoltaic systems, except for the solar panels, include many other components too. These components are the so-called balance of system (BOS) and have a major role, since they manage to store and distribute electricity in safe and efficient ways. Depending on whether the system is connected to the grid or whether is designed as a stand-alone system, different components are required. The components of the greatest importance are the cables, the DC-DC converters, the inverters, the mounting structure, the charge controllers and the energy storage [2].

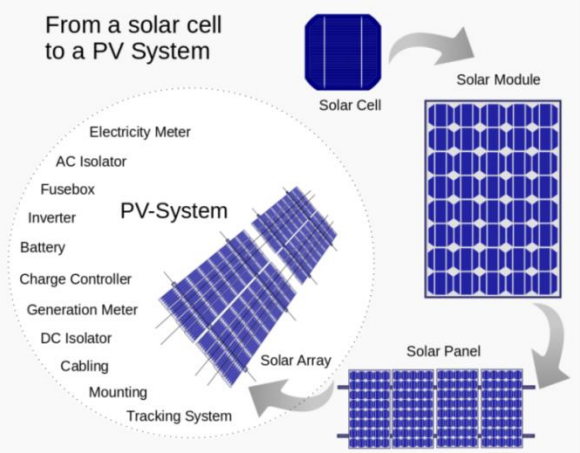

Figure 1.2: From Solar Cell to PV System [9]

1.4 Types of Solar Cells

Usually, the solar cells are named after the semiconducting material that they are made of. In order to absorb sunlight, these materials should have certain characteristics. There are solar cells that are designed to handle the sunlight that reaches the Earth's surface and there are cells that are deployed for use in space too. In PV systems, solar cells can be categorized into three different generations of solar cell technologies and each generation includes different types of solar cells [10].

1.4.1 First-Generation Solar Cell Technology

Solar cells that are made of crystalline silicon (c-Si) are included in the first-generation solar cell technology. The c-Si solar cells can also be characterized as wafer-based, conventional or traditional cells. In comparison to other materials, silicon makes the c-Si solar cells more economical and at the same time more efficient. The two main types of c-Si solar cells are the mono-crystalline silicon (mono-Si) and the poly-crystalline silicon (poly-Si) or multi-crystalline silicon solar cells [7],[10].

1.4.1.1 Mono-Crystalline Silicon Solar Cells

Mono-crystalline silicon solar cells (Figure 1.3) consist of silicon, in which the crystal lattice of the entire solid is continuous, unbroken to its edges and free of any grain boundaries. Mono-crystalline silicon can be prepared intrinsic, consisting only of pure or doped silicon and very small amounts of other elements added to change its semiconducting properties [10].

In 2006, the average module efficiency for the mono-crystalline PV panels was 14.7%. Since then and until 2019, this percentage had a steady rise, reaching 18%. Now, in lab conditions, the highest efficiency is 24.4% and this positive trend is expected to continue through 2030 [7],[8].

1.4.1.2 Poly-Crystalline Silicon Solar Cells

Poly-crystalline silicon or polysilicon (Figure 1.3) is a high purity form of silicon that is used as a raw material by the photovoltaic industry. As a material, polysilicon has a typical metal flake effect, which is given by the small crystals, also known as crystallites that it consists of. Most of the times, polysilicon and multisilicon are used as synonyms. However, multi-crystalline, as a term, usually refers to crystals larger than 1 mm [10].

Poly-crystalline solar cells are less efficient in comparison to mono-crystalline solar cells. In 2006, the average module efficiency was equal to 13.2% and by 2019 had reached 17%. Now, in lab conditions, the highest efficiency for the poly-crystalline PV modules is 20.4% [7],[8].

Due to the reduced power conversion efficiency, higher number of poly-crystalline solar cells is required to generate a specific amount of power. However, poly-crystalline solar cells are more affordable to purchase than the mono-crystalline ones, due to the lack of homogeneity [10].

1.4.2 Second-Generation Solar Cell Technology

The second-generation solar cell technology includes the thin-film solar cells (Figure 1.3). Thin-film solar cells can be created by a variety of different materials. These materials are divided into two main families. These are the silicon-based thin-film materials, such as amorphous silicon (a-Si) and micromorph silicon (a-Si/c-Si) and the non-silicon based thin-film materials, such as cadmium telluride (CdTe), gallium arsenide (GaAs) and copper indium gallium selenide (CIGS) [7],[10].

The production of thin-film solar cells is less expensive in comparison to the production of silicon solar cells, since lower amount of materials is required. However, they are less efficient than the silicon ones, they require more surface area to generate the same amount of power and have shorter lifetime [10].

1.4.3 Third-Generation Solar Cell Technology

In the third-generation of solar cells, a number of thin-film technologies, also known as emerging photovoltaics, are included. Many of these use organic materials or inorganic substances. However, most of them have not yet been commercially applied and are still in development. Some examples of third generation solar cells are the dye-sensitized solar cells (DSSC), the biohybrid solar cells, the polymer solar cells and the perovskite solar cells [10].

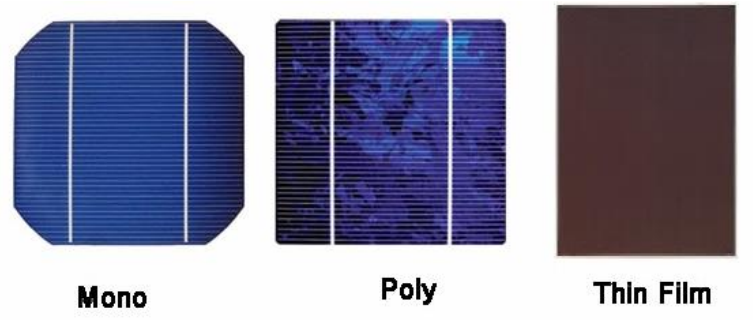

Figure 1.3: Mono-crystalline, Poly-crystalline & Thin-film Solar Cells [11]

1.5 High Efficiency Concepts for Silicon Solar Cells

In this chapter, three different examples of high efficiency solar cell concepts, based on crystalline silicon technology, will be presented. These are the Passivated Emitter Rear Locally (PERL) solar cell concept, the Interdigitated Back Contact (IBC) solar cell concept and the Silicon Heterojunction (SHJ) solar cell concept [2].

1.5.1 Passivated Emitter Rear Locally Diffused (PERL) Concept

The PERL solar cell concept (Figure 1.4) is the first high efficiency concept that was developed at the University of New South Wales between the late 1980s and the early 1990s, reaching conversion efficiencies of around 25%. In the PERL concept, silicon cells of advanced architecture are being used, known as PERL or PERC (Passivated Emitter Rear Cell) solar cells. As far as the construction is concerned, the difference between a PERC solar cell and a mono-crystalline solar cell is not

significant. The main improvement is the integration of a back-surface passivation layer that improves the efficiency of the cells, since it reduces the electron recombination, increases the light absorption and allows higher internal reflectivity [2],[7].

Nowadays, PERC and IBC solar cells that are mentioned in Section 1.5.2 are on course to become the dominant commercial solar cells. In 2017, according to the International Technology Roadmap for PV systems, the PERC solar cells constituted 20% of the PV industry [12].

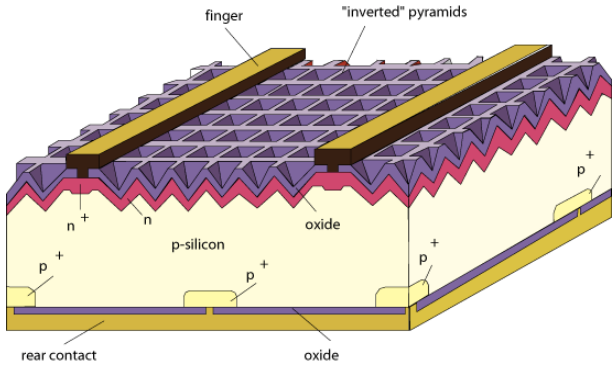

Figure 1.4: Structure of a PERL/PERC Solar Cell [13]

1.5.2 Interdigitated Back Contact (IBC) Solar Cells

IBC solar cells (Figure 1.5) are a second successful solar cell concept. The main idea of this concept is the eradication of shading losses at the front metal contact grid. For the collection of charge carriers at the n- and p-sides, all the contacts that are responsible are positioned at the back of the crystalline wafer-based solar cell [2].

One of the main advantages of IBC solar cell concept is the use of mono-crystalline float-zone n-type wafers. In comparison to p-type wafers, n-type wafers have some important advantages, like for instance they do not suffer from light induced degradation and they are not so sensitive to impurities, such as iron. Another advantage of IBC solar cells is that since the metal fingers are at the back

side of the cell, their cross-section can be made much larger, and therefore the shading losses can be avoided [2].

Despite the fact that this technology of solar cells is more complicated than other solar cell technologies, it can reach some of the highest efficiencies and eradicate the main reasons that cells lose power, fail or break [2].

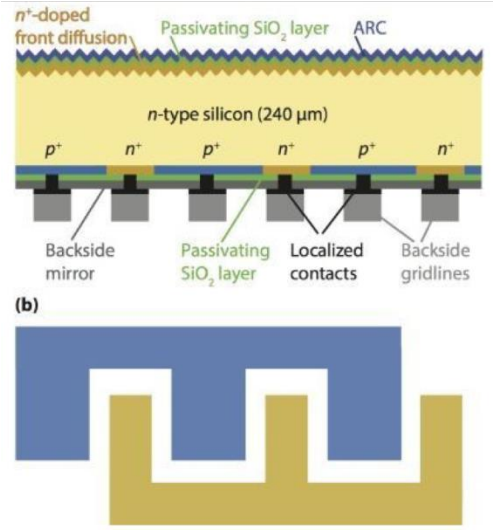

Figure 1.5: Structure of an IBC Solar Cell [2]

1.5.3 Silicon Heterojunction (SHJ) Solar Cells

The last high efficiency concept is the SHJ solar cell concept (Figure 1.6). Heterojunction is a junction that consists of a p-doped semiconductor material and an n-doped semiconductor, made from another material. On the other hand, a homojunction is a junction fabricated by different doping types within the same semiconductor material [2].

SHJ solar cells consist of two junctions. The junction at the front side, which is formed by using a thin layer of intrinsic amorphous silicon (a-Si) and a thin layer of p-doped amorphous silicon and the junction at the back side, which is similar to the one at the front side. This junction is formed by using a thin layer of intrinsic amorphous silicon deposited on the wafer surface and a thin layer of n-doped amorphous silicon on the top of the intrinsic layer [2].

One of the main advantages of SHJ concept is the presence of the amorphous silicon layer, which acts as an excellent passivation layer. This approach results in the highest possible charge carrier lifetimes and thus c-Si wafer-based heterojunction solar cells are able to realize the highest open circuit voltages among the different crystalline silicon technologies [2].

Another advantage of this concept is that the amorphous silicon layers are deposited with the use of the cheap plasma-enhanced chemical vapor deposition (PE-CVD) technology at low temperatures, lower than 200^{o}C. So, the cost of making the front and the back surface fields in SHJ solar cells is very low [2].

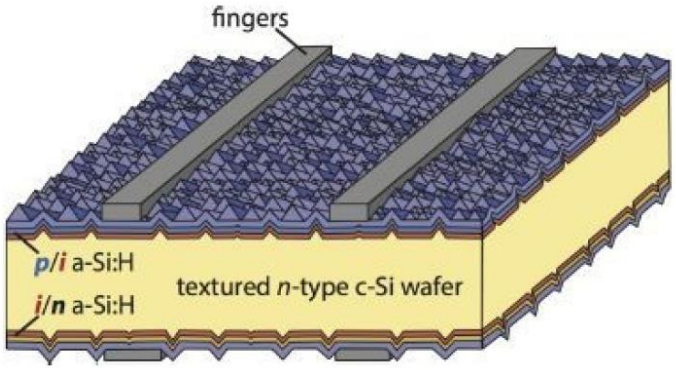

Figure 1.6: Structure of a Silicon Heterojunction Solar Cell [2]

1.6 Interconnection Technologies

To make a proper design of a solar module and choose the most ideal materials, a variety of solar cell properties should be taken into consideration. Usually, the most common PV modules are the wafer-based modules, comprised of 60 solar cells, with 156 mm edge length and arranged in 6 strings of 10 cells each. These modules are mainly used at residential rooftops. For commercial use, wafer-based PV modules, comprised of 72 solar cells are used [14],[15].

The last decades, PV modules were comprised of solar cells with 156 mm edge length. However, to decrease the manufacturing costs and increase the efficiency, wafer-based solar cells with edge lengths of 166, 182 and 210 mm (Figure 1.7) are used and many others are still in development. This results in larger PV modules

and thus larger PV panels. Therefore, higher amounts of power can be produced [14].

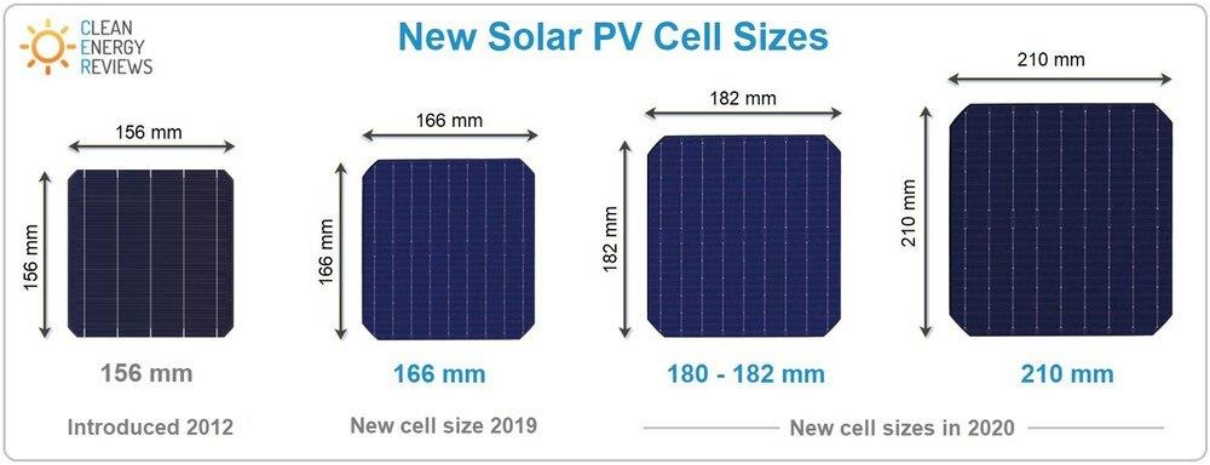

Figure 1.7: New Solar Cell Sizes [14]

The connections between the solar cells and the modules, to form a solar module and a solar panel, respectively, are called interconnections. Different types of contact, such as electrical, mechanical and thermal contact, between the solar cells and the modules can be provided by these interconnections. There are many different types of interconnection technologies and they are divided into two main categories, the conventional, such as ribbons and wires technologies, and the unconventional ones, such as the back contact cells technologies [16].

1.6.1 Conventional Interconnection Technologies

1.6.1.1 Ribbons & Wires

The most common way to interconnect the cells of c-Si modules is by using flat wires made of copper that are called ribbons (Figure 1.8). They consist of soft temper copper, bearing a solder coating of thickness between 10 and 25 μm. Usually, cell soldering processes depend on the solder from the ribbon coating and do not need any additional solder material. Also, for quality assurance, the establishment of a uniform solder coating thickness on both sides of the ribbon is very important [15].

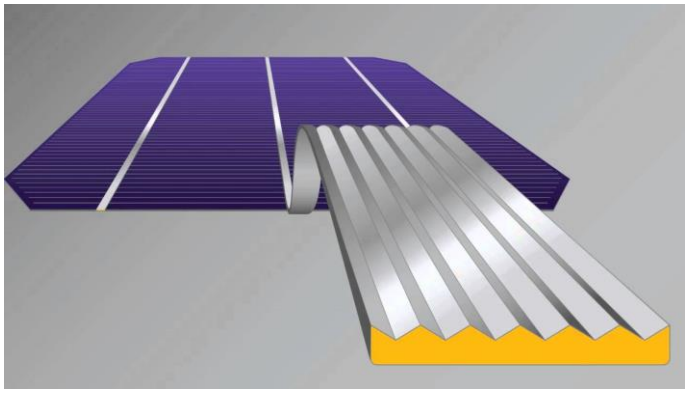

Figure 1.8: Photovoltaic Ribbon [16]

Elongation at fracture, also known as fracture strain, is another important mechanical parameter. Copper displays ductile fracture with necking after plastic deformation. During the module operation, ribbons experience extreme strain, especially in the gaps between the solar cells. So, for the cell interconnections, fracture strains higher than 25% are preferable [15].

Lastly, in cell interconnection, instead of copper, aluminum could be used too. It might have lower conductivity than copper, but its cost is much less. However, using aluminum results in problems that are related to joint formation, such as increased mismatch, in relation to thermal expansion, and reduced ductility [15].

1.6.1.2 Soldering Process

In PV applications and especially when wafer-based silicon solar cells are involved, the interconnection process that is used is the so-called infra-red (IR) reflow soldering. An electrically conductive and mechanically stable joint in between metal parts is established through soldering, by means of an additional metal with a lower melting point, the solder. During the process, all parts are heated above solder's melting temperature, without reaching the melting point of the parts to join. The molten solder spreads over the solid surfaces and after cooling it, a solid joint is created [13],[14].

The temperature at which the solid becomes a liquid is called melting point and the materials that can be used for given real world applications are defined by it.

In most applications, materials in solid and not in melted state are chosen to be used. However, in the case of solders things are different. Melting is the main role of solders during which two or more electrical components join together. Solders comprise many alloy compositions, with melting points between 90°C and 400°C [17].

To stabilize the solder joints, sufficient wetting is necessary and to prevent surface oxidation, wetting measurements are applied in an inert atmosphere. In most of the soldering applications, including common solar cell interconnection, the use of fluxes is necessary to remove oxidized layers from the interfaces and to improve and accelerate the wetting of the parts to be joined. The persistence of these layers, and consequently the amount of the required flux, are affected by the storage time and the conditions of the cells and ribbons [15].

Finally, there are two phases in the soldering process, the stringing or tabbing and the bussing. The first involves the interconnection of solar cells with each other to form strings, whereas the last deals with the assembly of the strings of solar cells to form PV modules [16].

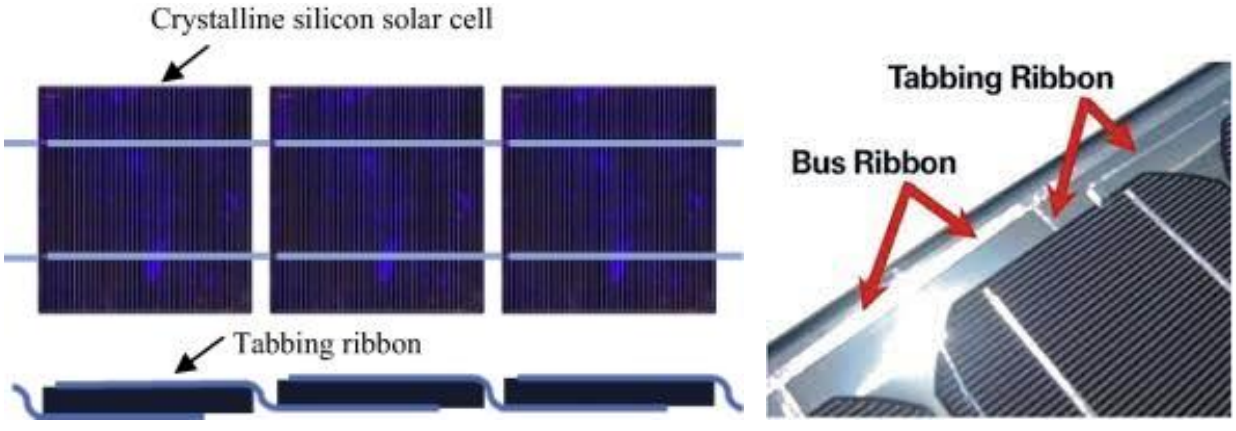

Figure 1.9: Interconnection of Solar Cells – (a) Crystalline Silicon Solar Cells Interconnected in Series with Tabbing Ribbon, (b) Interconnected Solar Cells with Tabbing and Bussing Ribbons [16]

1.6.2 Unconventional Interconnection Technologies

As mentioned before, the unconventional interconnection technologies are mainly concepts of back-contact solar cells technology, which means that both the materials that are being used for the interconnections and the circuitry are behind the cells. Examples of these concepts are the emitter wrap-through (EWT), the metallization wrap-through (MWT), the back-junction back-contact (BJBC), the honeycomb design (HD), the pin up modules (PUM) and many others [16].

The main advantages of these concepts are the decreased stress in the soldered joints, the reduced shadowing losses as a result of metal grids, the increased surface area for higher current generation and the advanced module aesthetics [16].

1.6.3 Challenges of the Conventional Interconnection Technologies

In the conventional interconnection technologies, one of the main challenges is the series resistance losses. The metallization for contact formation and the tabbing for current collection are the causes of these losses. To reduce them, thinner wafers should be used, to ensure low-stress interconnection between the cells and at the same time to reduce the cost of the material and enable the modules manufacture [16].

Another challenge is the shadowing losses. For wider solar cells, thicker ribbons are required for higher current conduction, since when the width of the cross section of the interconnection ribbon increases, the shadowing losses increase too. This increase is proportional. To reduce the shadowing losses, the thickness of the ribbon strip should be reduced by applying built-up stresses in the soldered joints or in other words, by releasing the stresses due to the difference in thermal expansion coefficient between the interconnection material and the silicon or due to the bending of the interconnection material [16],[18].

Finally, as far as the IR soldering process is concerned, there is another challenge too and has to do with the induced thermo-mechanical stress in the solder joints

of the solar cells. This stress leads to accelerated fatigue and results in module failure during field operations. To avoid this, laser soldering is preferred, because it can be controlled better, it is more precise, fast and efficient, especially for smaller spots and areas of soldering and there is no physical contact during the process, which could result in cell breakage [16].

1.7 Main Goals of the Thesis Project

One of the main reasons that the efficiency drops from cell to module is the conduction losses. To increase the efficiency of the PV module, the produced charge carriers in the semiconductor materials should be transferred to the PV module terminals with minimum conduction losses. As an alternative to the conventional cells and modules interconnections, in this thesis project, efficient ways to incorporate Wireless Power Transfer (WPT) techniques into PV cell and module architecture are being sought. WPT could be also a possible way of reducing, or even eliminating some of the main drawbacks of the conventional interconnections and the soldering process.

The main goals of this research are to understand how WPT techniques can be efficiently incorporated into PV devices, such as PV cells and modules, find out whether these techniques in theory and in practice are efficient enough and suggest the best design approach as a guideline for near future prototyping.

To model the main systems of this thesis project, research on different WPT techniques was made first. From these techniques, the most promising seemed to be the Magnetic Resonant Coupling (MRC). After selecting it as the main method, the models were developed. For these models, two different PV generators were considered, one made of a single IBC solar cell and one that consists of 16 IBC solar cells, connected in series. IBC solar cells were chosen to be used as PV generators, because they can reach some of the highest efficiencies (24.2%) and eliminate the main reasons that cells lose power, fail or break.

The PV generators send direct current (DC) into the inverter and the inverter converts the DC into alternating current (AC) to send it to the resonant circuits.

Between the transmitter coil and the receiver coil of the circuits a magnetic field is being created. Through this field the energy transfers from the primary compensation network to the secondary one. To study the performance of these models, different types of coils were researched and tested, mathematical models were developed and simulations were ran in Matlab and Simulink.

To sum up, in Chapter 1, some general information about the PV systems, the types of solar cells and the interconnections between the solar cells and the modules were given. In Chapter 2, information about the WPT and the different types of WPT techniques is given. In Chapter 3, the main mathematical models that were used for the simulations in Matlab and Simulink are developed. In Chapter 4 the results of the simulations are presented and discussed. And finally, in Chapter 5, the main conclusions and subjects for future research are given.

2 Wireless Power Transfer

2.1 General Information

After the second industrial revolution, electrical energy became one of the most significant forms of energy. Nowadays, devices such as mobile phones, laptops and many others need electricity to work and the most common ways to deliver power to them are through wires or with the use of batteries, which can store a certain amount of energy [19].

However, providing energy through wires is not always convenient or safe. Multiple problems can be arisen, such as breakdowns, friction and aging. Also, during the conventional wired power transfer, the produced sparks can cause damages to the electric equipment and become a threat to human safety [19],[20],[21].

Furthermore, battery-powered devices are affected by some main problems, such as the short battery life, due to the limited capacity of the batteries and the high initial cost, due to installation of a large number of batteries. An alternative and promising solution is the so-called Wireless Power Transfer or Wireless Power Transmission (WPT) which is the transmission of power from a source to an electrical load over an air gap without using any physical contact, such as wired connection. Through WPT, the batteries of the devices can be charged without the use of wires, even when they move around [19],[22].

Therefore, the main advantages of WPT, compared to the conventional power transfer methods, are safety (no breakdowns), reduction of the size and the weight of the devices (no wires) and charging from long distances [19].

2.2 Wireless Power Transfer History

The foundation of electricity and electromagnetism was established in the early 19th century by scientists, such as the French scientist André Marie Ampère (1775-1836) and the English scientist Michael Faraday (1791-1867). The laws of Ampere

and Faraday formed the pillars of modern electrical engineering. Based on their work, the Scottish scientist James Clerk Maxwell (1831-1879) managed to develop the so-called Maxwell's equations for electromagnetic fields and waves [23].

The concept of Wireless Power Transfer is not new, since around 1890 Nikola Tesla (1856-1943) had a vision of a wirelessly powered world. Based on Ampere's, Faraday's and Maxwell's scientific principles, Tesla attempted to develop WPT technologies with the use of coupled alternating magnetic field. For over a century, Tesla's inventions, such as the Tesla Coil to transfer power to light bulbs, the AC machines, the AC power generation and transmission, the radio transmitters and receivers, the X-ray machines and the world's first remote-controlled technology have been used [19],[23].

During the same period of time M. Hutin and M. LeBlanc made a device to power electrical vehicles wirelessly with inductive coupling. However, their invention did not receive much of attention, since the electrical vehicle technologies were not much developed at that time [19].

Tesla did not personally succeed to transfer power all around the world, but he was and still is an inspiration for other scientists to work and further develop the WPT technologies. In Japan, at the middle of 1920s, H. Yagi and S. Uda worked on WPT by using antennas to transmit power at the frequency of 68 MHz. They managed to transfer 200 mW to the receiving antenna (rectenna) when the transmitting antenna had 3 W. At the same time, in the United States of America, H.V Noble achieved WPT with transmitting and receiving antennas at the frequency of 100 MHz and he managed to transfer 15 kW at a distance of approximately 12 m [19].

After the Second World War, many other efforts had been made. For instance, W. C. Brown in USA tried WPT with microwaves. Also, in 1968, Peter Glaser proposed the Space Based Solar Power, which was a method to produce energy outside the Earth's atmosphere from the sun and then transmit it wirelessly [19].

Finally, at 1990s, the University of Auckland worked on the so-called Inductive Power Transfer (IPT) which is one of the WPT methods. This method was the only one that was used commercially for small devices, such as toothbrushes and shavers. Several years ago, MIT published a paper for WPT with the use of magnetic resonance coupling, which is what Tesla was trying to do. These days, WPT are gaining more attention and many companies and universities are working to develop and evolve the WPT methods and techniques [19],[23].

2.3 Categories of Wireless Power Transfer Methods

Based on the distance of transmission, the maximum power and the method used to achieve power transmission Wireless Power Transfer (WPT) methods can be classified in different categories. Focusing on the distance of transmission, the two main categories that the WPT methods can be divided into are the near field (non-radiative) WPT method and the far field (radiative) WPT method [19].

Near field WPT method is being used for short distances, shorter than one wavelength, and includes two subcategories of WPT methods, the Electrodynamic Induction and the Electrostatic Induction. From these two methods, the most common is the first one [19].

On the other hand, the far field WPT method is being used for longer distances, longer than one wavelength, and includes two subcategories too. These are the Microwave Power Transfer and the Laser or Light Power Transfer [19].

In Figure 2.1 the different categories of WPT methods are shown.

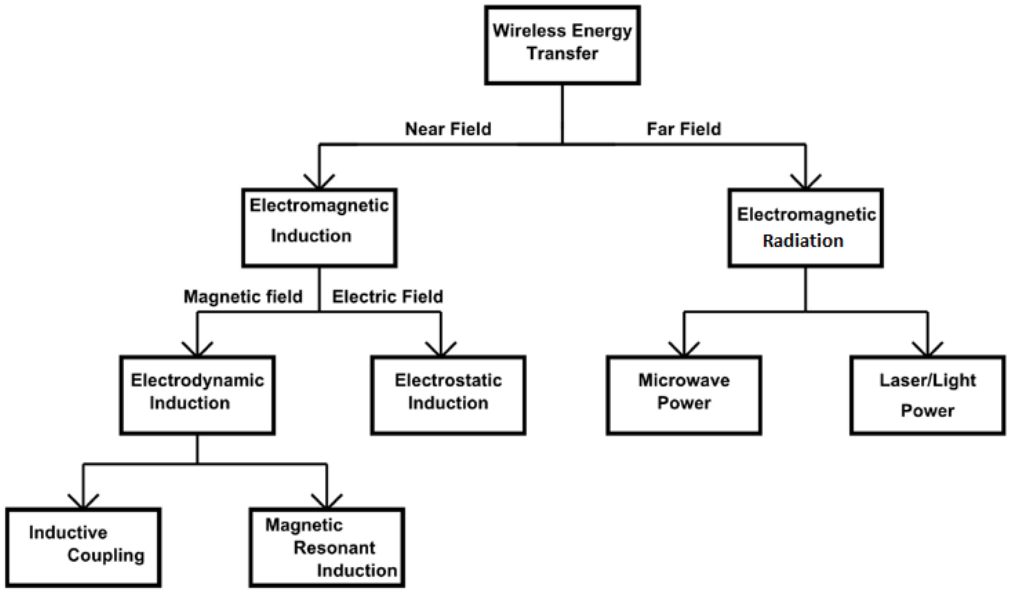

Figure 2.1: Various Ways Used for Achieving Wireless Power Transfer Technology [24]

2.4 Inductive & Capacitive Power Transfer

The most common WPT methods are the Electrodynamic Induction and the Electrostatic Induction or the so-called Capacitive Power Transfer (CPT). Electrodynamic Induction includes two sub-categories. These are the Inductive Coupling or Inductive Power Transfer (IPT) and the Magnetic Resonant Induction (MRI) or Magnetic Resonant Coupling (MRC) [25].

Between IPT and CPT, the most common of them is the first, since is applicable to many different power levels and gap distances. On the other hand, due to constraints on the developed voltage, CPT method is only applicable for power transfer applications with small gap distances (less than 1 mm) [25].

2.4.1 Inductive Power Transfer (IPT)

As mentioned in the introduction part of this chapter, one of the most used WPT methods is the Inductive Coupling or the so-called Inductive Power Transfer (IPT). The main part of an inductive WPT system is the magnetically coupled windings, which can be modeled with two coupled inductors, as shown in Figure 2.2 [23],[26].

R_1 and R_2 are the resistances of the primary and secondary windings, respectively, L_1 and L_2 are the self-inductances of the primary and secondary windings, respectively, M_{12} is the mutual inductance between the two windings and R_L is the load resistance [23].

In a coil, when the magnetic field around its turns changes, an induced electromotive force (emf) is generated in it. When emf is induced in the same circuit, the so-called self-induction (*L*) effect happens. On the other hand, when emf is induced into an adjacent coil in the same magnetic field, then it can be said that is magnetically induced or is induced by mutual induction (*M*). So, when two or more coils are magnetically connected together under a common magnetic flux, they have the property of mutual inductance, which is also the main property of other devices, such as transformers, motors, generators and many others [27].

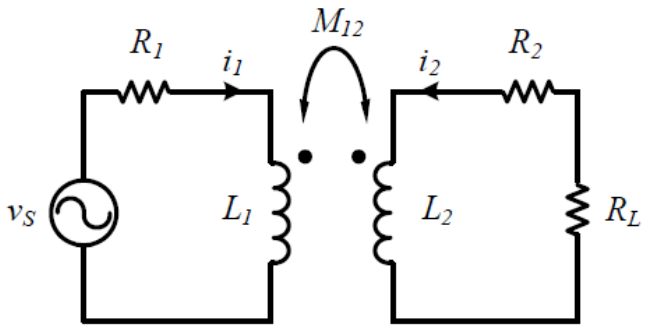

Figure 2.2: Representation of an Inductive WPT System [23]

IPT method has evolved rapidly and can cover a wide range of applications, such as charging or powering electrical vehicles, wireless sensors, medical implants, laptops, electric toothbrushes and cell phones. Sometimes, it is even used because there are no other possible solutions to transfer power to a location, like for instance in some chemical labs [26].

Most of the times, IPT method is used for small distances in a range of few mm to at most a few cm and realize high efficiencies, such as in cell phones chargers, with efficiencies above 70% and in chargers for electrical cars, with efficiencies higher than 90%. However, since the need for transferring power wirelessly in

bigger ranges rises, more research is being carried out on this subject. In 2007, researchers at Massachusetts Institute of Technology (MIT) managed to successfully power a light bulb over a distance of 2 m and reaching an efficiency of around 40%, by implementing Wireless Power Transfer. In 2016, in the Korea Advanced Institute of Science and Technology (KAIST), a group of researchers was able to transfer 10 W over a distance of 7 m [26],[28],[29].

The long distance IPT transfer method has some main drawbacks too. First of all, due to complex and bulky designs, it is still not economical enough for commercial purposes. Also, its installation cost is much higher than the installation cost of conventional systems and it is less efficient than a transformer [26].

Since in this thesis project there is no need for transferring power in long distances, IPT method represents a good candidate.

2.4.2 Capacitive Power Transfer (CPT)

CPT method is a WPT method that uses electric fields, instead of magnetic fields. In this method there are two circuits, the transmitter circuit and the receiver one (Figure 2.3). Each of these circuits is connected with two metallic plates. Each pair of plates forms a capacitance and the gap between them is the so-called dielectric [19].

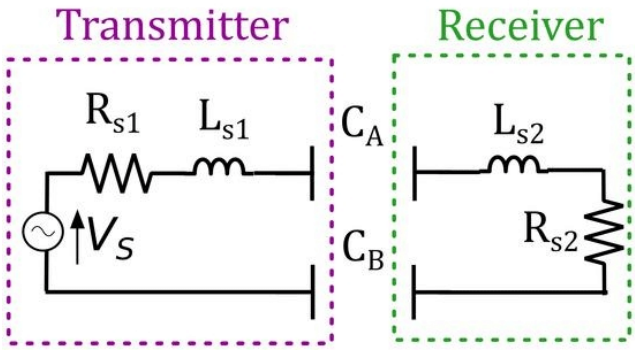

Figure 2.3: Representation of a Capacitive WPT System [30]

Transfer of power through CPT method has some advantages. The main being the low eddy-current losses, the low cost and weight and the high misalignment performance [19].

However, in general, CPT method still remains a non convenient method to be used, since there are a few drawbacks too. First of all, to transfer any significant amount of power (over 1 kW) high voltages are required and the intensity of the electric field could harm a human body, especially when this amount of power should be transferred in gap distances higher than 1 mm [25].

Under dry atmospheric conditions, the highest electric field possible is around $3\ {}^{\mathrm{kV}}/_{\mathrm{mm}}$. So, for applications with distances higher than 1 mm CPT should be avoided, since between the transmitter and the receiver plates higher voltages can be developed [25].

Finally, another drawback is the possibility of a strong interaction between the electric and magnetic fields and any other object placed between the capacitive plates or coils. This interaction could reduce the amount of transferred power, and thus the efficiency of the system, by increasing the losses of it [25].

2.4.3 Magnetic Resonant Coupling (MRC)

Magnetic Resonant Coupling (MRC) is one of the most common and advanced categories of Electrodynamic Induction method. In this method, instead of using transformers, coils are connected to capacitors in different topologies in order to create resonance, typically for frequencies between 20 kHz and a few MHz [26].

MRC is the solution for the main problems of IPT. It can be used to improve the efficiency of IPT, especially for longer separation distances between the coils (from a few cm to a few m). To increase the efficiency, this method uses the benefit of resonance state of the system's coils and the resonance coupling, by getting the maximum power at the receiver side [31],[32],[33].

In other words, MRC is a form of inductive coupling with the main difference that it uses two resonant circuits instead of just two coils. More specifically, the basic

resonant circuits consist of one coil and one capacitor that resonate at the same resonant frequency. So, this allows the transmission of larger amounts of power, at higher efficiencies and for larger distances, in comparison to the non-resonating systems [19],[31],[33].

Usually, in MRC the coils are single-layer solenoids or flat spirals with less parasitic capacitances, in comparison to the coils that are used in IPT, that are made of multi-layer windings as can be seen in Figure 2.4 [33].

Figure 2.4: a) Single-layer Coil & **b)** Multi-layer Coil [33]

In Figure 2.5, a representation of a possible implementation of a basic MRC system is shown. C_1 and C_2 are the capacitances of the primary and the secondary circuits, respectively.

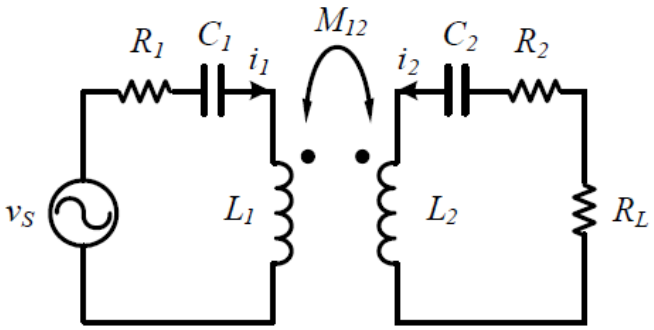

Figure 2.5: Representation of a possible Implementation of a MRC System [23]

Furthermore, MRC can be considered the most ideal method for residential devices and appliances, since the magnetic fields do not interact with materials, such as wood and metal and humans and other electronic devices do not affect

the power transfer, when they are placed between the coils, especially for distances of a few cm [33].

On the other hand, in MRC there are a few drawbacks and constraints. One of these is that when the distance between the resonant circuits is very small, the resonant frequency is split into two frequencies and the optimal power transfer is no longer done at the original resonant frequency. This means that if the system resonates at a frequency slightly different from the operating one and the effect is not detected, there will be a significant reduction of the amount of the transferred power and the efficiency [34],[19].

Other disadvantages of MRC are the increased resistive heating, in comparison to the direct-approach of power transfer through wires and the fact that it cannot be used in longer range applications than the ones that have already mentioned [33].

Finally, despite the drawbacks, MRC method can still be better than the IPT method, since it can achieve higher efficiencies for the same (few mm to few cm) or longer distances (few cm to few m), it allows the use of smaller planar coils that can be implemented in portable and implanted devices, it is safer for humans and animals, since there is not electromagnetic radiation during the energy transfer and it develops magnetic fields that are strong enough to not be affected by surrounding objects of any type of material [33].

So, based on the considerations above, MRC method seems to be the most ideal option in comparison to IPT and CPT. Thus, it has been the focus of this thesis project.

3 Magnetic Resonant Coupling

Magnetic Resonant Coupling (MRC) is based on compensating both the primary and the secondary circuits to be able to have resonance in both sides. There are many compensation topologies. However, since the circuits must be as simple as possible to allow future cell-level integration, the focus will be on the four main compensation topologies. These are the Series-Series (SS), the Series-Parallel (SP), the Parallel-Series (PS) and the Parallel-Parallel (PP) topologies and are shown in Figures 3.1 – 3.4, respectively [23].

I_1 and I_2 represent the current phasors in the primary and secondary circuits, V_s is the voltage source, V_{C1} and V_{C2} represent the voltages of the capacitors, V_{L1} and V_{L2} represent the voltages of the coils, R_1 and R_2 denote the equivalent resistances of the transmitting and receiving coils, C_1 and C_2 represent the capacitors of the circuits, L_1 and L_2 are the self-inductances of the coils, M_{12} is the mutual inductance of the coils and R_{Load} or R_L represents the load resistance.

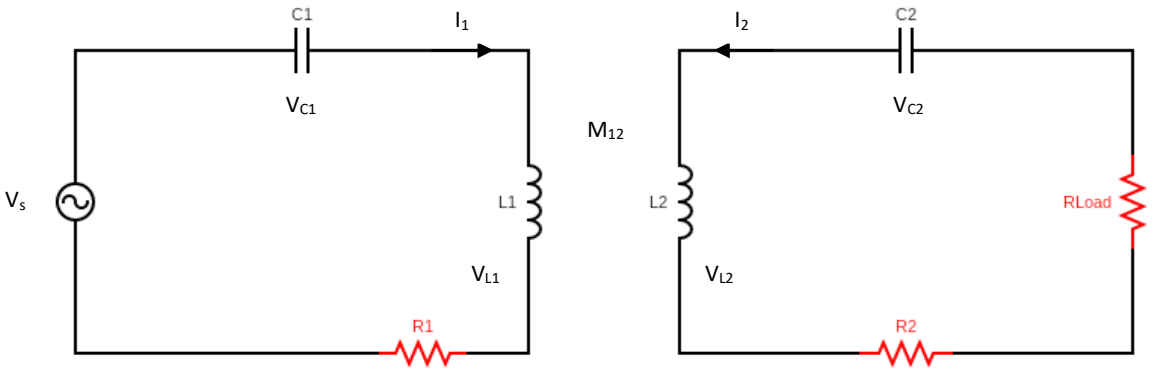

Figure 3.1: Series-Series Compensation Topology

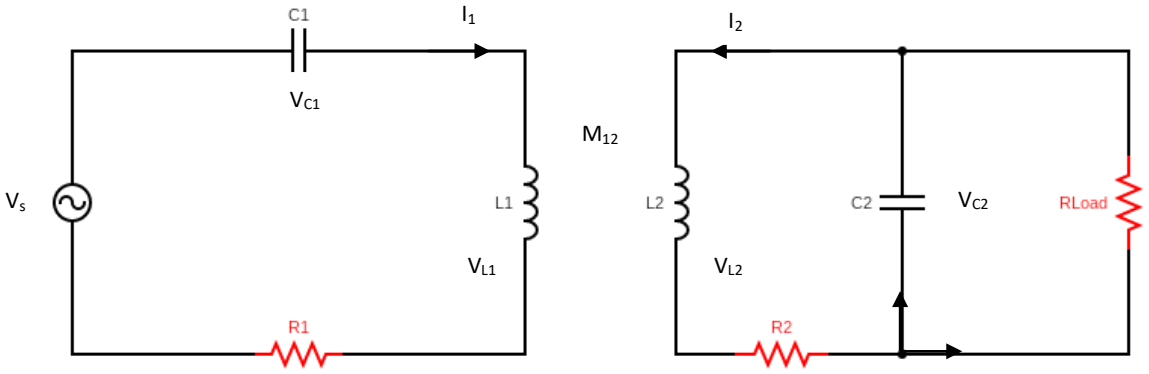

Figure 3.2: Series-Parallel Compensation Topology

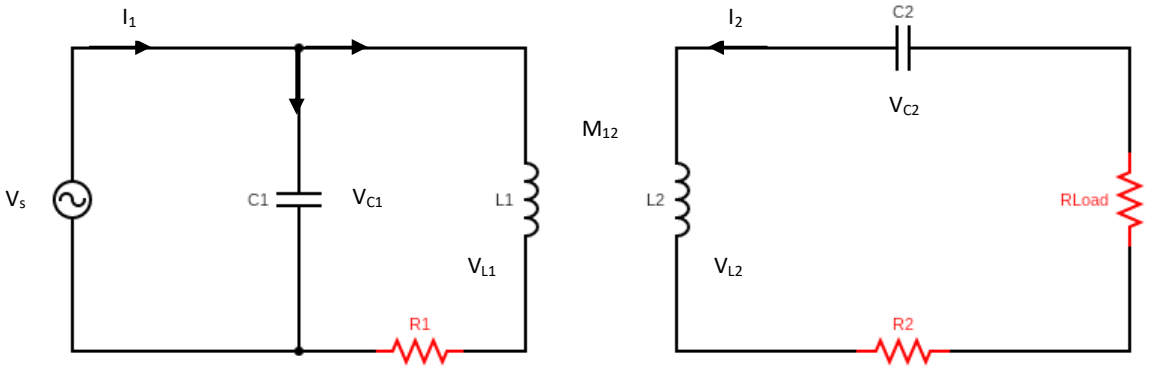

Figure 3.3: Parallel-Series Compensation Topology

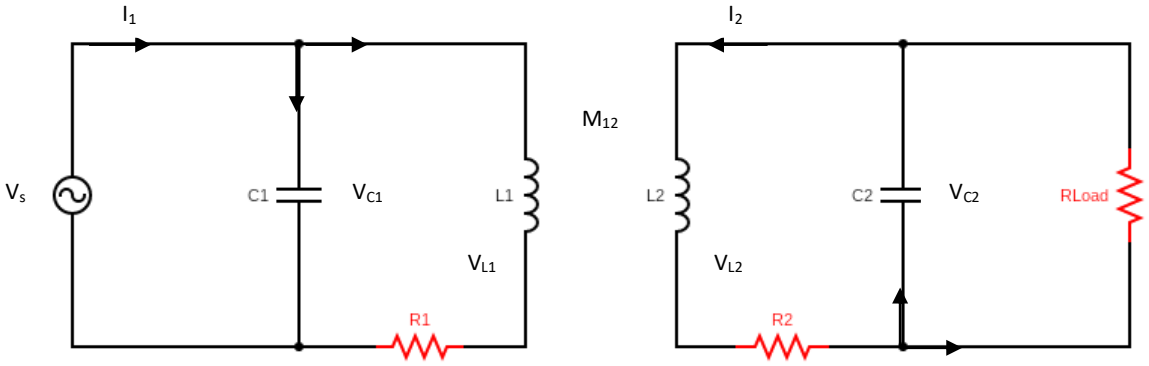

Figure 3.4: Parallel-Parallel Compensation Topology

3.1 Analysis of the Compensation Topologies

Kirchhoff's circuit laws are the easiest and the most common way to solve complex circuit problems. So, based on Kirchhoff's Voltage Law, the main equations of each compensation topology were developed. In Section 3.1.1, the analysis of the Series-Series compensation topology is presented. The rest of the compensation topologies are presented in Appendix A.

3.1.1 Series-Series Compensation Topology

In Series-Series compensation topology, shown in Figure 3.1, the corresponding equations of the circuit model are the following:

$$z_1 \cdot I_1 + j \cdot \omega_o \cdot M_{12} \cdot I_2 = V_s \tag{3.1}$$

$$(j \cdot \omega_o \cdot M_{12}) \cdot I_1 + z_2 \cdot I_2 = 0 \tag{3.2}$$

z_1 and z_2 are the impedances of the primary and the secondary sides, respectively, and are equal to:

$$z_1 = R_1 + j \cdot X_1 \tag{3.3}$$

$$z_2 = R_2 + R_L + j \cdot X_2 \tag{3.4}$$

Where X_1 and X_2 are the reactances of resonators and are equal to:

$$X_1 = (\omega_o \cdot L_1) - \frac{1}{\omega_o \cdot C_1} \tag{3.5}$$

$$X_2 = (\omega_o \cdot L_2) - \frac{1}{\omega_o \cdot C_2} \tag{3.6}$$

ω_o is the resonant angular frequency measured in $^{\mathrm{rad}}/_{\mathrm{s}}$.

The secondary current phasor can be derived from (3.2) and it is equal to:

$$I_2 = -\frac{I_1 \cdot M_{12} \cdot \omega_o \cdot j}{R_2 + R_L + j \cdot \omega_o \cdot L_2 \cdot -\frac{j}{C_2 \cdot \omega_o}} \tag{3.7}$$

By substituting (3.7) into (3.1), the voltage source can be calculated and it is equal to:

$$V_s = I_1 \cdot (R_1 + j \cdot \omega_o \cdot L_1 - \frac{j}{C_1 \cdot \omega_o}) + \frac{I_1 \cdot M_{12}^2 \cdot \omega_o^2}{R_2 + R_L + j \cdot \omega_o \cdot L_2 - \frac{j}{C_2 \cdot \omega_o}} \tag{3.8}$$

Then, the input impedance of the system can be calculated by using the following equation:

$$Z_{in} = \frac{V_s}{I_1} \tag{3.9}$$

By substituting (3.8) into (3.9), the impedance of the system can be calculated and it is equal to:

$$Z_{in} = \frac{V_s}{I_1} = R_1 + j \cdot \omega_o \cdot L_1 - \frac{j}{C_1 \cdot \omega_o} + \frac{M_{12}^2 \cdot \omega_o^2}{R_2 + R_L + j \cdot \omega_o \cdot L_2 - \frac{j}{C_2 \cdot \omega_o}} \tag{3.10}$$

The first term is the impedance of the primary circuit and the second term is the reflected impedance.

$$Z_{pr} = R_1 + j \cdot \omega_o \cdot L_1 - \frac{j}{C_1 \cdot \omega_o} \tag{3.11}$$

$$Z_r = \frac{M_{12}^2 \cdot \omega_o^2}{R_2 + R_L + j \cdot \omega_o \cdot L_2 - \frac{j}{C_2 \cdot \omega_o}} \tag{3.12}$$

In other words, in Series-Series compensation topology, the impedance of the system is equal to the sum of the primary impedance and the reflected impedance.

Also, the current gain can be derived as:

$$G = \left| \frac{I_2}{I_1} \right| \tag{3.13}$$

By substituting (3.7) into (3.13), the current gain can be calculated and it is equal to:

$$G = \left|\frac{I_2}{I_1}\right| = \frac{M_{12}\cdot\omega_o}{\left|R_2+R_L+j\cdot\omega_o\cdot L_2-\frac{j}{C_2\cdot\omega_o}\right|} \quad (3.14)$$

Finally, the efficiency of the system can be expressed as:

$$n_s = \frac{total\ output\ power}{total\ input\ power} = \frac{P_{sec}}{P_{pr}} \quad (3.15)$$

The total input power or total power of the primary circuit can be expressed as:

$$P_{pr} = V_s \cdot I_1^* \quad (3.16)$$

Where I_1^* is the conjugate of the current of the primary circuit.

The total output power or the total power of the secondary circuit can be expressed as:

$$P_{sec} = |I_2|^2 \cdot R_L \quad (3.17)$$

By substituting (3.8) into (3.16) and (3.7) into (3.17), the total input and output powers can be expressed as:

$$P_{pr} = V_s \cdot I_1^* = R_1 \cdot |I_1|^2 + j \cdot \omega_o \cdot L_1 \cdot |I_1|^2 - \frac{|I_1|^2\cdot j}{C_1\cdot\omega_o} + \frac{C_2\cdot M_{12}^2\cdot\omega_o^3\cdot|I_1|^2}{C_2\cdot R_2\cdot\omega_o+C_2\cdot R_L\cdot\omega_o+j\cdot\omega_o^2\cdot C_2\cdot L_2-j} \quad (3.18)$$

$$P_{sec} = |I_2|^2 \cdot R_L = \frac{R_L\cdot M_{12}^2\cdot\omega_o^2\cdot|I_1|^2}{\left|R_2+R_L+j\cdot\omega_o\cdot L_2-\frac{j}{C_2\cdot\omega_o}\right|^2} \quad (3.19)$$

By substituting (3.18) and (3.19) into (3.15), the efficiency of the system can be calculated.

3.2 Coils

There are two main categories of coils that can be used in a resonant system. These are the spiral planar or flat coils and the solenoid or helix coils (Figure 3.5).

The most ideal category is the spiral planar coils, since the turns of the coils are not concentrated at the outer circumferences, like in solenoid ones, but they are distributed across the radii. In this way, the coupling coefficient of the coils can be improved significantly [26],[35].

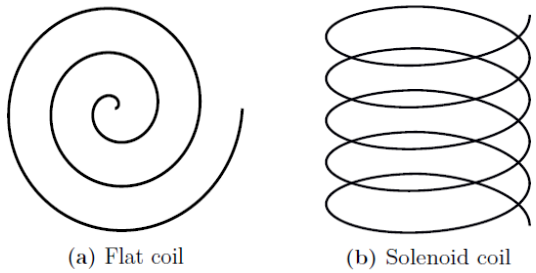

Figure 3.5: Different Coil Designs [26]

Furthermore, the spiral planar coils are more compact, robust and flexible to optimize the size. They can be fabricated on PCB, silicon or other flexible substrates and they can be processed in a variety of shapes, such as the circular, the square, the hexagonal and the octagonal spiral coils that are shown in Figure 3.6. The most commonly used are the circular and the square planar coils [35].

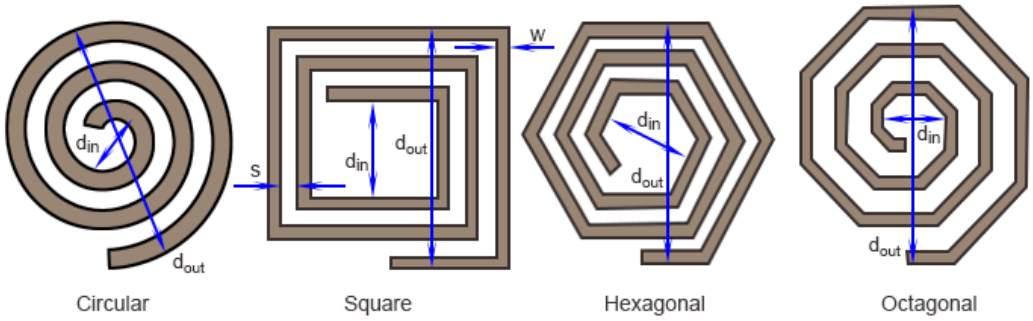

Figure 3.6: Different Types of Spiral Coils [36]

When a system made of two coils is created to implement Wireless Power Transfer, two of the most important parameters that define the efficiency of the system are the mutual inductance (M_{12}), measured in $^{\mathrm{H}}/_{\mathrm{m}}$ and described in Section 2.4.1 and the coupling coefficient (k_{12}). Coupling coefficient is a number that can express the degree of electrical coupling that exists between two circuits

and it can vary between 0 and 1. When the coupling coefficient is equal to 1, it is indicated that the coils are fully coupled and all the power from the transmitting coil is transferred to the receiving coil. On the other hand, when the coupling coefficient is equal to 0, it is indicated that no power is transferred [19].

The connection between the self-inductance of the coils (L_1 & L_2), the coupling coefficient and the mutual inductance can be expressed by equation (3.20) [19].

$$k_{12} = \frac{M_{12}}{\sqrt{L_1 \cdot L_2}} \tag{3.20}$$

3.2.1 Calculation of the Self-Inductances

In this chapter, simple and accurate expressions for the self-inductances of circular, square/rectangular, hexagonal and octagonal spiral planar coils will be presented. These expressions are improved mathematical models of Harold A. Wheeler's models [36],[37].

The self-inductance of a single-layer circular spiral coil can be expressed as:

$$L_{circ} = 31.33 \cdot \mu_o \cdot N^2 \cdot \frac{A^2}{8 \cdot A + 11 \cdot C} \tag{3.21}$$

Where μ_o is the vacuum permeability, equal to $4 \cdot \pi \cdot 10^{-7}\ {}^{\mathrm{H}}/_{\mathrm{m}}$, N is the number of turns of the spiral coil, A is the average radius of the coil, in meters, and C is the so-called width of the coil, in meters too.

The average radius and the width of the coil can be expressed as:

$$A = \frac{d_{in} + d_{out}}{4} \tag{3.22}$$

$$C = \frac{d_{out} - d_{in}}{2} \tag{3.23}$$

Where d_{in} is the internal diameter of the coil and d_{out} is the external diameter of the coil, both measured in meters (Figure 3.6).

On the other hand, the self-inductance of a single-layer square, hexagonal or octagonal spiral coil can be expressed as:

$$L_{sq,ex,oct} = K_1 \cdot \mu_o \cdot \frac{N^2 \cdot d_{avg}}{1+K_2 \cdot \rho} \tag{3.24}$$

K_1 and K_2 are empirical dimensionless coefficients that depend on the coil' shape (Table 3.1), d_{avg} is the average diameter of the coil in meters and ρ is the so-called filling ratio of the coil defined as:

$$d_{avg} = \frac{d_{in}+d_{out}}{2} \tag{3.25}$$

$$\rho = \frac{d_{out}-d_{in}}{d_{out}+d_{in}} \tag{3.26}$$

The hollowness of a spiral coil can be expressed by the filling ratio. For small fill ratio the spiral coil is hollow ($d_{out} \approx d_{in}$) and for large fill ratio the spiral coil is full ($d_{out} >> d_{in}$).

Table 3.1: Empirical Dimensionless Coefficients

Coil Layout	K_1	K_2
Square	2.34	2.75
Hexagonal	2.33	3.82
Octagonal	2.25	3.55

Finally, to describe and specify a coil, except for the number of turns, the inner diameter and the outer diameter, other parameters play a crucial role too, such as the turn width (w) and the turn spacing (s), measured in meters (Figure 3.6). Based on these, the external diameter of a spiral coil can be expressed as:

$$d_{out} = (2 \cdot N \cdot w) + \{[(2 \cdot N) - 2] \cdot s\} + d_{in} \tag{3.27}$$

So, the internal diameter of a spiral coil can be expressed as:

$$d_{in} = d_{out} - (2 \cdot N \cdot w) - \{[(2 \cdot N) - 2] \cdot s\} \tag{3.28}$$

3.2.2 Calculation of the Mutual Inductance

There are many different expressions that could be used to calculate the mutual inductance (M_{12}) of two coils. However, in this thesis project, for the numerical calculations of both circular and square/rectangular spiral coils, a conventional approximation method was used based on Neumann's formula and the accurate expressions of the mutual inductance of coaxial Archimedean spiral coils [38],[39],[40].

So, the mutual inductance between two perfectly aligned circular coils can be expressed as:

$$M_{12} = \sum_{i=1}^{N_1} \sum_{j=1}^{N_2} M_{ij} \tag{3.29}$$

Where *i* and *j* represent the i_{th} and j_{th} turn of the two coils, respectively and M_{ij} is the mutual inductance between the i_{th} approximate circular loop and the j_{th} approximate circular loop.

M_{ij} can be calculated as:

$$M_{ij} = \mu_o \cdot \sqrt{R_{1i} \cdot R_{2j}} \cdot \left[\left(\frac{2}{g} - g\right) \cdot K(g) - \frac{2}{g} \cdot E(g)\right] \tag{3.30}$$

Where *K(g)* and *E(g)* are the complete elliptic integrals of the first and second kind, respectively, R_{1i} and R_{2j} are the i_{th} and j_{th} external radii of the coils, respectively, measured in meters, and *d* is the distance between the coils, measured in meters too.

$$[E(g), K(g)] = ellipke(g)$$

The geometric factor *g* can be expressed as:

$$g = \sqrt{\frac{4 \cdot R_{1i} \cdot R_{2j}}{(R_{1i} + R_{2j})^2 + d^2}} \tag{3.31}$$

And the i_{th} and j_{th} external radii of the coils can be expressed as:

$$R_{1i} = r_{inner_1} + (i-1) \cdot (w_1 + s_1) \tag{3.32}$$

$$R_{2j} = r_{inner_2} + (j-1) \cdot (w_2 + s_2) \tag{3.33}$$

Where r_{inner1} and r_{inner2} are the internal radii of the coils measured in meters.

To calculate the mutual inductance between two rectangular planar coils, the simplest approach is to approximate the rectangular coils as circular ones, whose diameters are equal to the sides of the corresponding rectangular coils. Since the mutual inductance is proportional to the area covered by each filament, the mutual inductance between two rectangular coils of the same dimensions is $\left(4/\pi\right)^2$ times larger than between two circular coils. This number can be characterized as a *q* factor [35],[41].

So, the mutual inductance between two perfectly aligned rectangular coils can be expressed as:

$$M_{12} = q \cdot \sum_{i=1}^{N_1} \sum_{j=1}^{N_2} M_{ij} \tag{3.34}$$

However, for the calculation of the mutual inductance of the rectangular coils there are many other methods that could be used, such as the Finite Element Method (FEM), by using software packages, such as COMSOL. It should be mentioned that these methods can give more accurate results, but they are more complex and time-consuming.

3.2.3 Calculation of the Compensation Capacitances

Two systems that resonate at the same frequency exchange power efficiently. Therefore, it is beneficial if the transmitting and the receiving sides resonate at the same frequency (ω_o) [26].

The resonant frequency of a system can be expressed as:

$$\omega_o = \frac{1}{\sqrt{L \cdot C}} \tag{3.35}$$

Where *L* is the self-inductance of the coil, measured in Henry, and *C* is the capacitance of the circuit, measured in Farad.

Here, it is very important to mention that the resonant frequency and the compensation capacitances (C_1, C_2) can be expressed differently, depending on the compensation topology that is studied [42].

So, in Series-Series compensation topology and when the Wireless Power Transfer system operates at resonant frequency, the capacitances can be expressed as:

$$C_1 = \frac{1}{L_1 \cdot {\omega_o}^2} \tag{3.36}$$

$$C_2 = \frac{1}{L_2 \cdot {\omega_o}^2} \tag{3.37}$$

On the other hand, in Series-Parallel compensation topology, at resonant frequency, the capacitance of the secondary circuit has the same expression as (3.37), but the capacitance of the primary circuit can be expressed as:

$$C_1 = \frac{1}{\left(L_1 - \frac{M_{12}^2}{L_2}\right) \cdot {\omega_o}^2} \tag{3.38}$$

In equation (3.38), it is clear that both the self-inductances of the coils (L_1, L_2) and the mutual inductance (M_{12}) affect the capacitance of the primary circuit. In other words, the capacitance of the primary circuit and the difference between the self-inductance of the transmitting coil and the ratio of the square mutual inductance and the self-inductance of the receiving coil are inversely proportional.

In Table 3.2, the capacitances of each compensation topology, at resonance condition, are summarized [42].

Table 3.2: Compensation Capacitances of each Topology

Capacitances	SS	SP	PS	PP
C1	$C_1 = \frac{1}{L_1 \cdot {\omega_o}^2}$	$C_1 = \frac{1}{\left(L_1 - \frac{M_{12}^2}{L_2}\right) \cdot {\omega_o}^2}$	$C_1 = \frac{1}{L_1 \cdot {\omega_o}^2}$	$C_1 = \frac{1}{\left(L_1 - \frac{M_{12}^2}{L_2}\right) \cdot {\omega_o}^2}$
C2	$C_2 = \frac{1}{L_2 \cdot {\omega_o}^2}$	$C_2 = \frac{1}{L_2 \cdot {\omega_o}^2}$	$C_2 = \frac{1}{\left(L_2 - \frac{M_{12}^2}{L_1}\right) \cdot {\omega_o}^2}$	$C_2 = \frac{1}{\left(L_2 - \frac{M_{12}^2}{L_1}\right) \cdot {\omega_o}^2}$

3.2.4 Calculation of the Parasitic Resistances

In flat spiral coils the main power losses are the radiation and conduction losses. Usually, the size of WPT coils is relatively small, compared to the operating wavelength, and this is the main reason why conduction losses are the dominant losses and the radiation losses are negligible [43].

First of all, the DC resistance of a conductor is calculated as in (3.39) and depends on the coil length, the cross-sectional area and the electrical conductivity of the material [26].

$$R_{DC} = \frac{l}{\sigma \cdot A_{cs}} \tag{3.39}$$

A_{cs} is the cross-sectional area of the wire, measured in square meters, l is the length of the wire (coil) in meters and σ is the electrical conductivity of the material used in the wire, measured in $^{\mathrm{S}}/_{\mathrm{m}}$.

To get low coil resistance, the electrical conductivity of the material needs to be high. Table 3.3 is a list of electrical conductivities of a few common materials used in conductors [26].

Table 3.3: Conductivity of Materials

Material	Conductivity [S/m]
Copper	$5.8 \cdot 10^7$
Aluminum	$3.54 \cdot 10^7$

From Table 3.3 it is obvious that the material that would give the lowest coil resistance is copper. However, it has higher cost than aluminum, which means that depending on the characteristics of the system, the material should be selected in order to balance costs and losses.

When the cross-sectional area of the coil is circular, A_{cs} can be expressed as:

$$A_{CCS} = \pi \cdot r^2 \tag{3.40}$$

In equation (3.40), *r* is the radius of the circular cross-section (CCS), measured in meters, which is equal to half the cross-section width $\left({}^{w}/_{2}\right)$.

On the other hand, when the cross-sectional area of the coil is rectangular (RCS), A_{cs} can be expressed as:

$$A_{RCS} = w \cdot h \tag{3.41}$$

In equation (3.41), *w* is the width of the cross-section and *h* is the thickness of the conductor both measured in meters.

As far as the length of the wire is concerned, it depends on the shape of the planar coils [44],[45].

For circular coils (CC) it can be expressed as:

$$l_{CC} = \frac{\pi \cdot N \cdot (d_{out} + d_{in})}{2} \tag{3.42}$$

Whereas, for rectangular coils (RC) it can be calculated using the following expression:

$$l_{RC} = 4 \cdot N \cdot B_1 + (4 \cdot N^2 - 5 \cdot N) \cdot w \tag{3.43}$$

Where

$$B_1 = B_2 - 2 \cdot (N - 1) \cdot w$$

$$B_2 = d_{out} - w$$

Equation (3.39) allows calculating the so-called DC resistance. However, the effective resistance of the coil is affected by other effects that play a major role at high frequencies. These are the skin effect and the proximity effect.

At high frequencies, the current tends to concentrate at the edge of the conductor, causing the so-called skin effect. This reduces the effective cross-section of the conductor, and thus increasing its resistance value [43],[46].

Skin effect can be taken into account by defining a skin resistance, that is a product of the skin ratio and the DC resistance of the conductor [43],[46]. Based on this, the skin resistance can be expressed as:

$$R_{skin} = F_{skin} \cdot R_{DC} \tag{3.44}$$

Where F_{skin} is the skin ratio and for coils with circular cross-section can be expressed as:

$$F_{skin} = \frac{1}{4} + \frac{r}{2 \cdot \delta} + \frac{3}{32} \cdot \frac{\delta}{r} \tag{3.45}$$

Whereas, the skin ratio for coils with rectangular cross-section can be expressed as:

$$F_{skin} = \frac{1}{2} \cdot \frac{h}{\delta} \cdot \frac{\sinh\frac{h}{\delta} + \sin\frac{h}{\delta}}{\cosh\frac{h}{\delta} - \cos\frac{h}{\delta}} \tag{3.46}$$

In (3.45) and (3.46), δ is the skin depth, measured in meters [26]. The skin depth defines the area where the current flows and is equal to:

$$\delta = \sqrt{\frac{2 \cdot \rho}{\omega \cdot \mu}} = \sqrt{\frac{\rho}{\pi \cdot f \cdot \mu_o \cdot \mu_r}} = \frac{1}{\sqrt{\sigma \cdot \pi \cdot f \cdot \mu_o \cdot \mu_r}} \tag{3.47}$$

Where μ_o is the permeability of the free space (vacuum), measured in $^{\mathrm{H}}/_{\mathrm{m}}$, μ is the magnetic permeability of the conductor, measured in $^{\mathrm{H}}/_{\mathrm{m}}$, μ_r is the relative permeability of the conductor, σ is the conductivity of the conductor, measured in $^{\mathrm{S}}/_{\mathrm{m}}$ and ρ is the resistivity of the conductor in $\Omega \cdot \mathrm{m}$.

$$\mu_r = \frac{\mu}{\mu_o}$$

$$\omega = 2 \cdot \pi \cdot f$$

$$\sigma = \frac{1}{\rho}$$

Independently from the skin effect, proximity effect takes into account the influence of adjacent conductors, with the redistribution of the current under the influence of an external magnetic field [46].

Similarly to the skin resistance, the proximity resistance can be expressed as:

$$R_{prox} = F_{prox} \cdot R_{DC} \tag{3.48}$$

Where F_{prox} is the proximity ratio.

The total AC resistance of the conductor is influenced by both the skin and the proximity effects [46]. So, it can be expressed as:

$$R_{AC} = R_{skin} + R_{prox} = \left(F_{skin} + F_{prox}\right) \cdot R_{DC} \tag{3.49}$$

However, according to [43], in loosely-coupled coils, namely in coils with space between their turns, the proximity effect can be considered negligible and the AC resistance can be expressed as:

$$R_{AC} = R_{skin} = F_{skin} \cdot R_{DC} \tag{3.50}$$

This happens, since the current is able to be distributed around the cross-section of the coil, uniformly, in comparison to coils that are tightly-coupled, with no space between their turns and the current is distributed inconsistently [47].

4 Results

In this chapter, different combinations of coil parameters will be presented, to see (1) which type of planar coils, circular or rectangular, would be the best option for the Wireless Power Transfer, (2) which type of cross-section, circular or rectangular, is the most ideal and (3) which compensation topology is the most efficient. In all the systems and for all the cases, coils of the same dimensions and perfectly aligned were used.

Based on the mathematical models that were developed on Chapter 3, Matlab scripts were created to calculate the compensation capacitances (C_1, C_2), the self-inductances (L_1, L_2) and the parasitic resistances of the coils (R_1, R_2), as well as their mutual inductance (M_{12}) and coupling coefficient (k_{12}).

As mentioned in Section 3.2, the values of the mutual inductance and the coupling coefficient of the coils are of utmost importance, since the amount of energy that will be transferred wirelessly from the primary circuit to the secondary one, depends on these values. The higher these values are the tighter the coils are coupled and higher amounts of energy will be transferred.

In Section 3.2, it is mentioned that the range of the coupling coefficient is between 0 and 1. If the coupling coefficient is equal to 1, this means that the coils are perfectly coupled, if the k_{12} is higher than 0.5, it means that the coils are tightly-coupled and if k_{12} is lower than 0.5 the coils are loosely-coupled [19].

However, the parasitic resistances of the coils must be taken into consideration too, because if the systems have high values of mutual inductance and coupling coefficient and at the same time high values of parasitic resistances, then maybe the losses, such as eddy-current losses, will be high, thus reducing the efficiency of the systems.

4.1 Coils Design

As mentioned in Section 3.2, there are two main categories of coils. These are the solenoid and the spiral coils (Figure 3.5). For reasons that were explained in the same section, the most ideal category is the spiral ones. There are many different shapes of spiral coils, fabricated on the PCB, silicon, or other flexible substrates. The most common of them are the circular and the square or rectangular spiral coils (Figure 3.6). So, these are the main types of coils that were studied in this project.

4.1.1 Main Parameters of Coils

As mentioned in Section 3.2.1, to specify a coil, the main parameters are the external diameter of the coil (d_{out}), the turn width (w), the turn spacing (s) and the number of turns (N).

First of all, since IBC solar cells of 125x125 mm were used, the external diameter of the coils should be less than or equal to 125 mm. For this reason, d_{out} was chosen to be equal to 120 mm.

At this point, it should be mentioned that to adjust a coil at an IBC solar cell, either the metallization layer of the solar cell should be replaced by the coil, or the coil should be put on top of the metallization of the solar cell. The physical realization of such a device goes beyond the scope of this thesis; however, the results from this project can be used to design these novel solar cells.

From Figures 4.1 & 4.2, it can be observed that for both circular and rectangular coils, with turn width equal to 4 mm, turn spacing equal to 1 mm and number of turns equal to 7 and 8, when the distance between the coils (d) increases, the values of the mutual inductance and the coupling coefficient decrease.

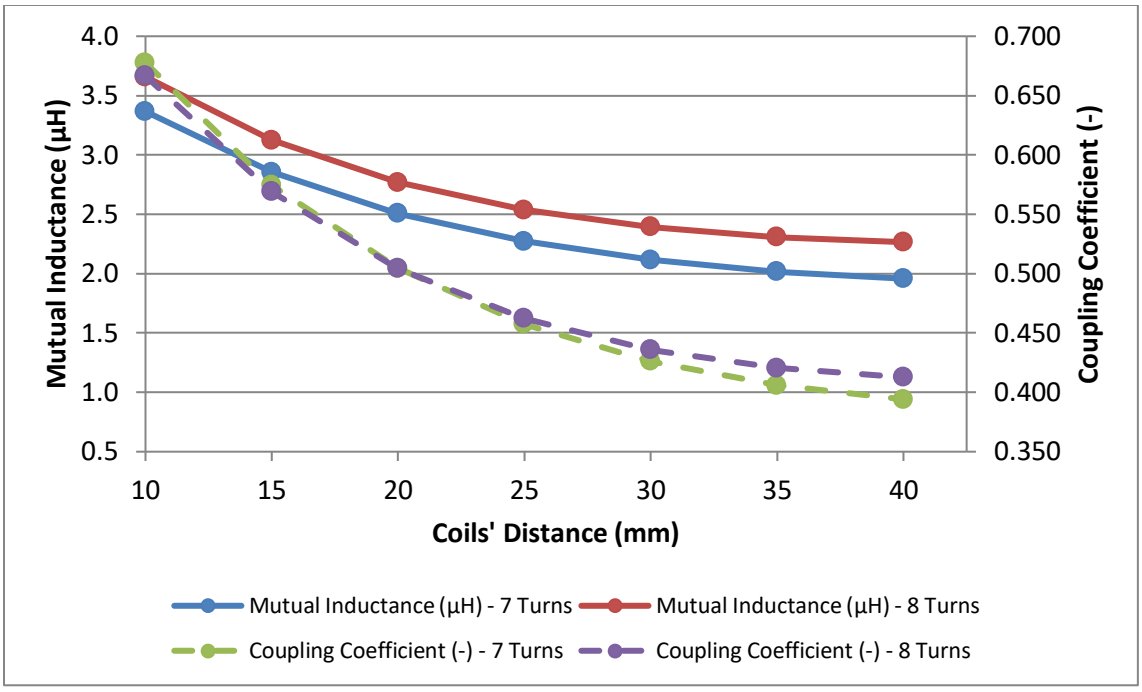

Figure 4.1: Circular Coils – Mutual Inductance & Coupling Coefficient vs. Coils' Distance (d_{out} = 120 mm, w = 4 mm & s = 1 mm)

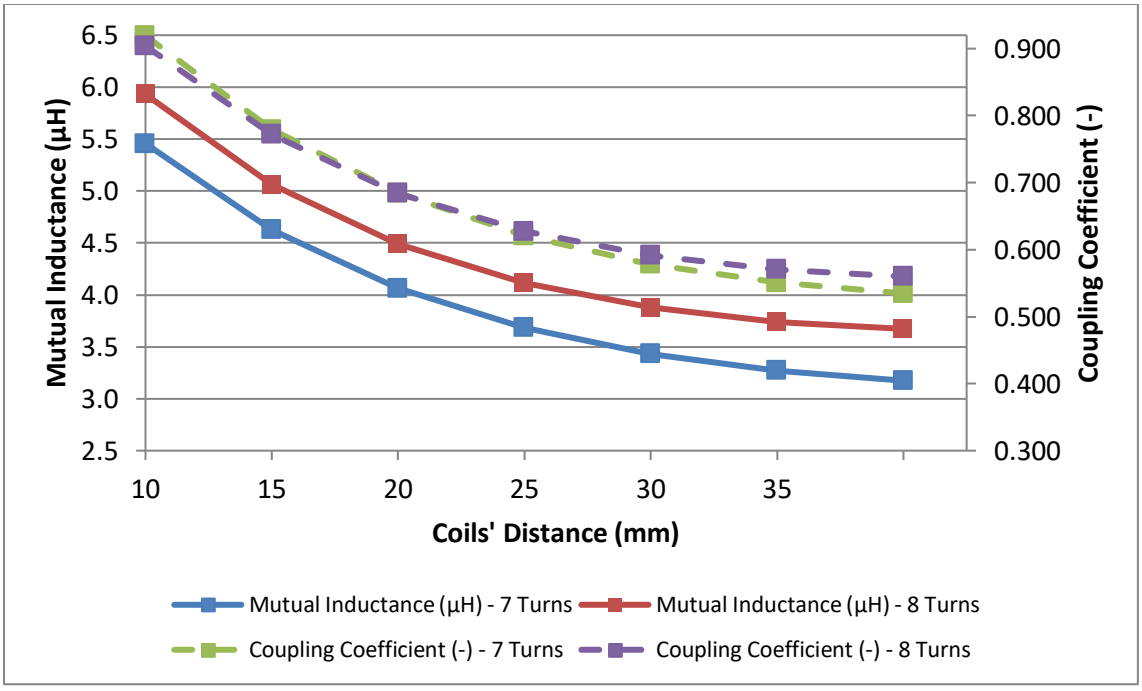

Figure 4.2: Rectangular Coils – Mutual Inductance & Coupling Coefficient vs. Coils' Distance (d_{out} = 120 mm, w = 4 mm & s = 1 mm)

This is logical, since based on equation (3.31) when the distance between the coils increases, the geometric factor (g) of the elliptic integrals of first and second kind ($K(g)$, $E(g)$) decreases and thus the mutual inductance decreases. The reduction of the mutual inductance leads to the reduction of the coupling coefficient too, according to equation (3.20).

So, for a range of distances between 10 and 40 mm, the most ideal distance between the coils seems to be the distance of 10 mm, for which both types of coils have the best values of mutual inductance and coupling coefficient. Therefore, this is the value of distance that was used for the analysis of the systems. (See also Appendix B, Tables B.1 – B.4)

However, the distance between the coils does not affect the self-inductances of the coils, since they remain constant. This happens, because the main parameters that affect their self-inductances are parameters, such as the diameters of the coils (d_{in}, d_{out}) and the number of turns and not the distance between them.

Furthermore, from Figures 4.1 & 4.2, it is also clear that the coupling coefficient is higher for lower number of turns (7 turns) at low distance (10 mm) and for higher number of turns (8 turns) at higher distance (40 mm). This happens, because according to equations (3.21) and (3.24) when the number of turns increases, the self-inductances increase too. The same happens with the mutual inductance. However, when the coil's distance rises, the mutual inductance decreases, but the self-inductances remain constant. So, based on equation (3.20) the main reason that k_{12} behaves like this, is the interaction between L_1, L_2 and M_{12}, when N and d change.

As far as the turn spacing is concerned, from Figures 4.3 & 4.4, it can be seen that for coils, of circular or rectangular shape, with number of turns equal to 7 and 8, with turn width equal to 4 mm and a distance between the coils of 10 mm, the increase of the turn spacing results in the reduction of the mutual inductance and the increase of the coupling coefficient.

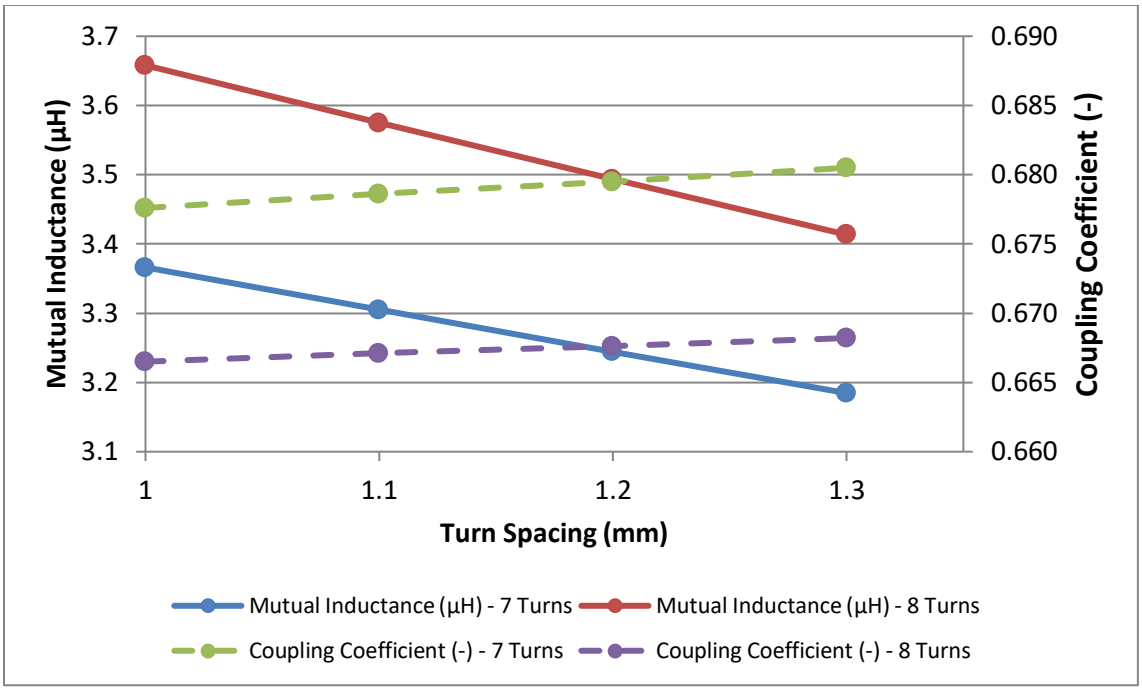

Figure 4.3: Circular Coils – Mutual Inductance & Coupling Coefficient vs. Turn Spacing (d_{out} = 120 mm, w = 4 mm & d = 10 mm)

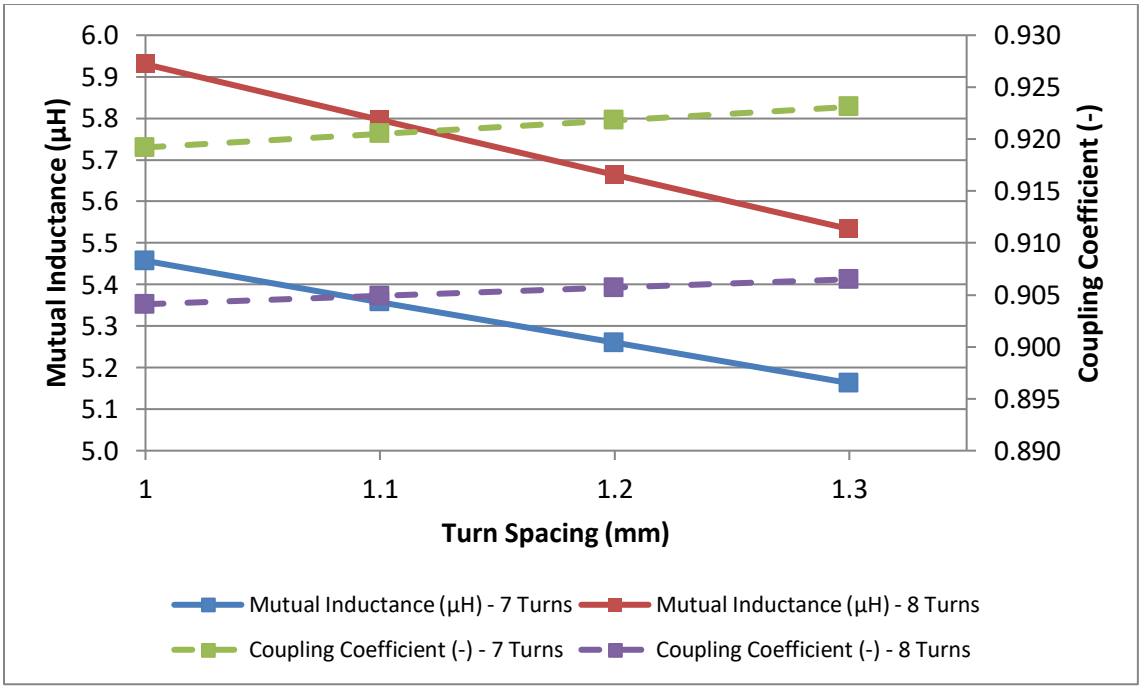

Figure 4.4: Rectangular Coils – Mutual Inductance & Coupling Coefficient vs. Turn Spacing (d_{out} = 120 mm, w = 4 mm & d = 10 mm)

In Figure 4.5, it can be observed that the increase of the turn spacing, for a range between 1 and 1.3 mm, results in the reduction of the self-inductances too. All these happen, because when the turn spacing increases, the internal diameters of the coils decrease and this leads to the reduction of both self-inductances and mutual inductance.

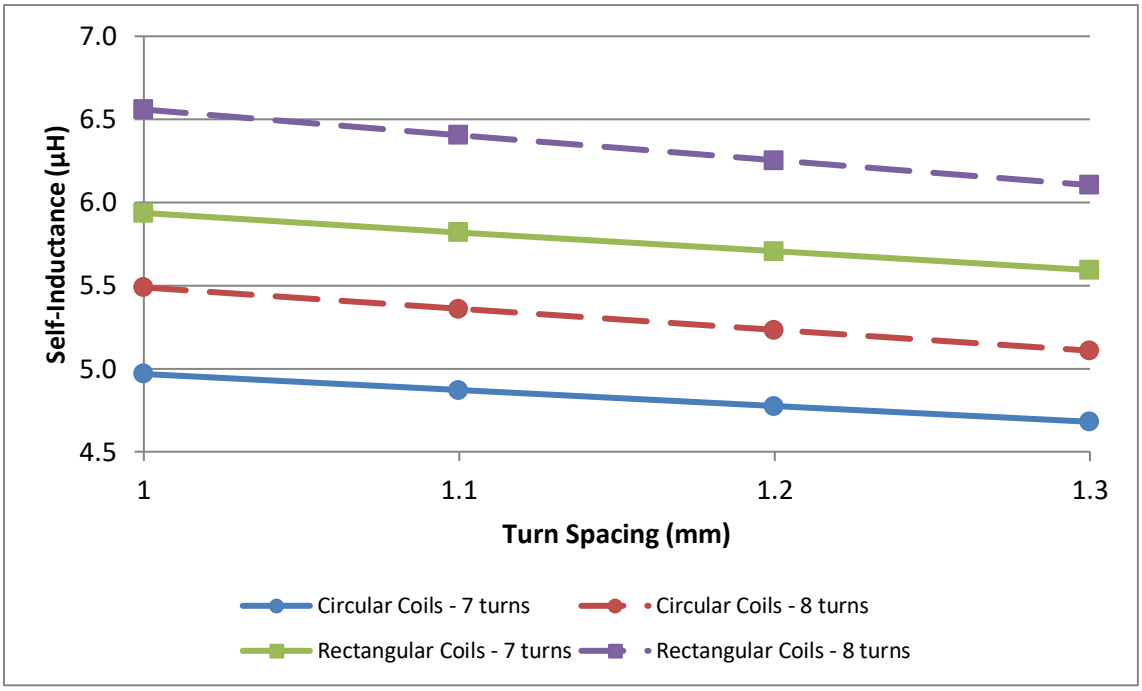

Figure 4.5: Circular & Rectangular Coils – Self-Inductance vs. Turn Spacing (d_{out} = 120 mm, w = 4 mm & d = 10 mm)

However, the turn spacing affects slightly more the self-inductances of the coils, rather than their mutual inductance. Namely, the reduction of the first is slightly higher and thus the coupling coefficient increases at a small level. So, the turn spacing was chosen to be equal to 1 mm, since this value provides better self-inductances and mutual inductance. (See also Appendix B, Tables B.5 – B.8)

Furthermore, from Figures 4.6 – 4.8, it can be seen that the increment of the turn width results in the reduction of the self-inductances and the mutual inductance of both circular and rectangular coils, with number of turns equal to 7 and 8, with turn spacing equal to 1 mm and a distance between the coils of 10 mm, as well as in the reduction of the coupling coefficient.

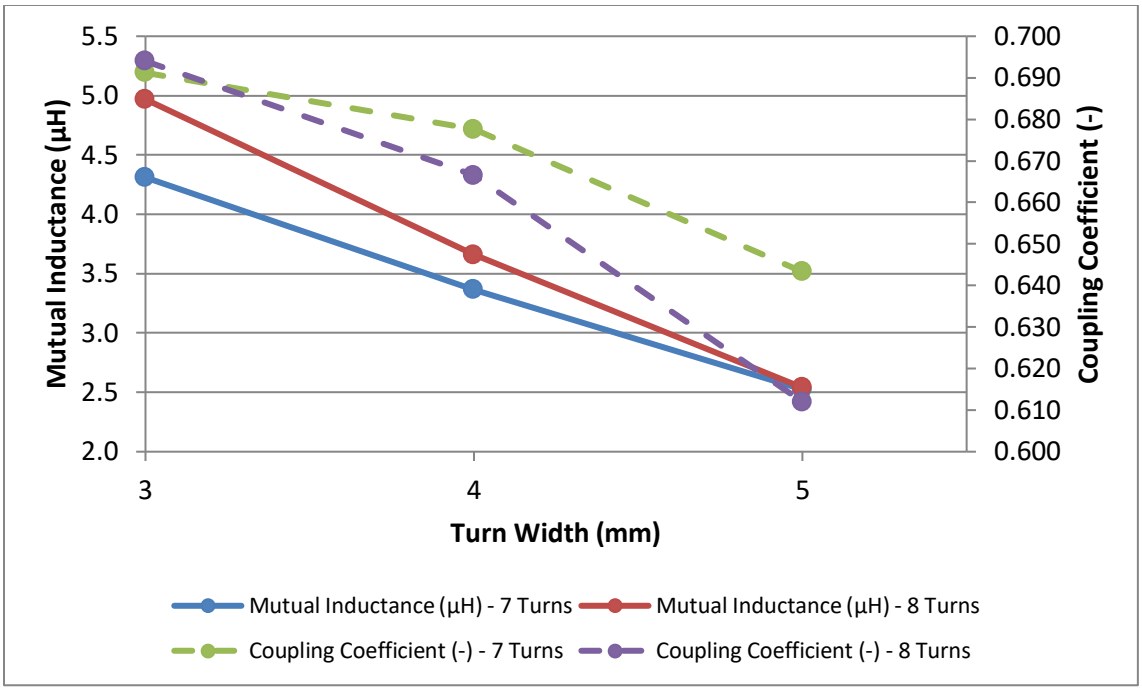

Figure 4.6: Circular Coils – Mutual Inductance & Coupling Coefficient vs. Turn Width (d_{out} = 120 mm, s = 1 mm & d = 10 mm)

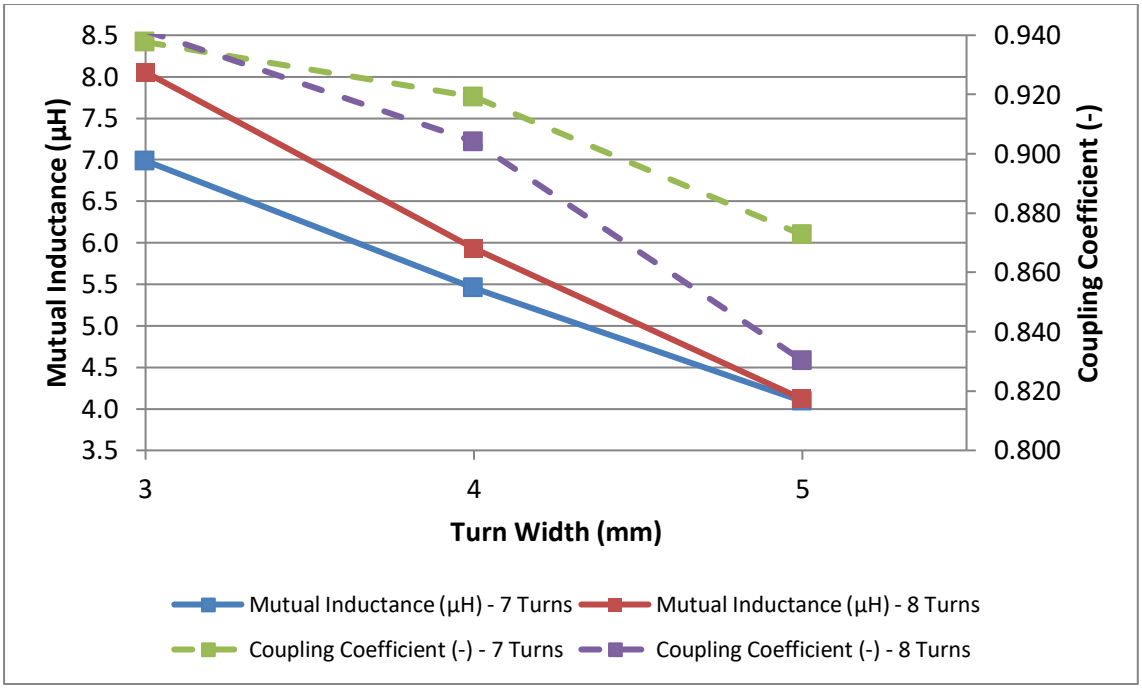

Figure 4.7: Rectangular Coils – Mutual Inductance & Coupling Coefficient vs. Turn Width (d_{out} = 120 mm, s = 1 mm & d = 10 mm)

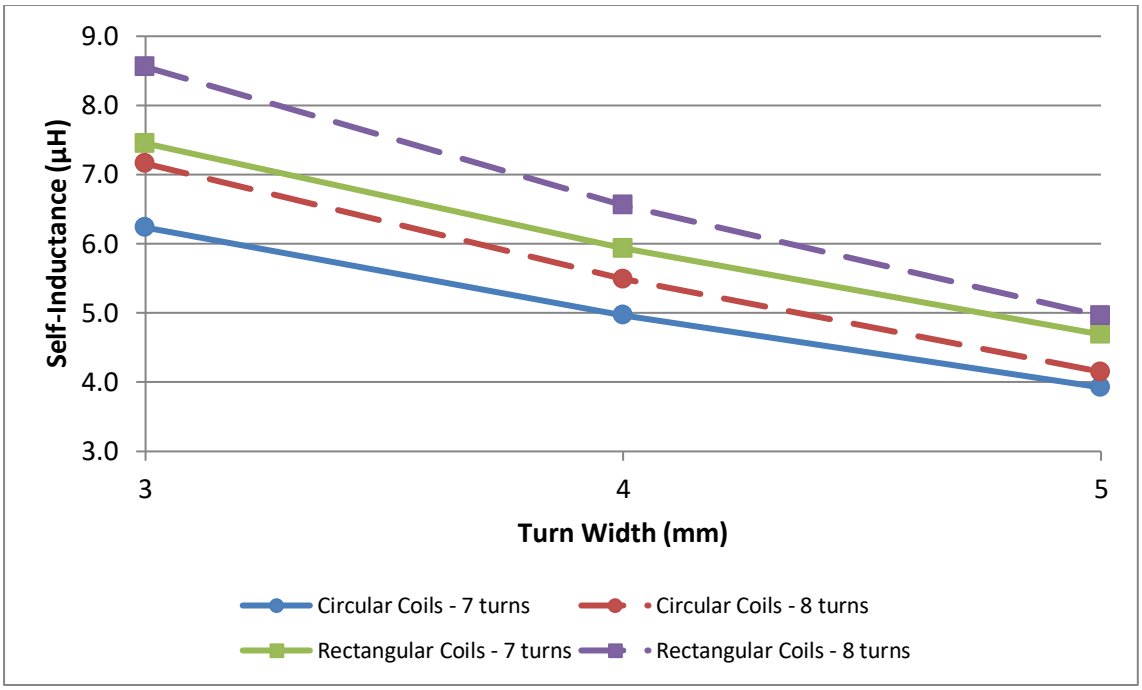

Figure 4.8: Circular & Rectangular Coils – Self-Inductance vs. Turn Width (d_{out} = 120 mm, s = 1 mm & d = 10 mm)

Someone could expect that since the rise of the turn spacing led to lower inductances and higher coupling coefficients, the same would happen with the rise of turn width too. However, it seems that the turn width has a stronger impact to the inductances and the coupling coefficient, in comparison to the turn spacing, since the increase of it causes higher reduction of them. This is logical, due to the fact that the values of turn spacing that are tested have a difference of 0.1 mm, but the values of turn width have a difference of 1 mm.

So, it appears that the turn width influence the diameters of the coils, and thus the inductances and the coupling coefficient, in higher level than the turn spacing, due to higher difference between the values of it. If the values that were tested had the same difference with the values of the turn spacing (0.1 mm), then the impact to the inductances and the coupling coefficient might was the same. (See also Appendix B, Tables B.9 – B.12)

Based on the results in Figures 4.6 – 4.8, someone could say that the most ideal value of turn width for both types of coils would be equal to 3 mm. However, it

should be mentioned that the turn width affects the cross-sections (A_{cs}) of the coils and by extension their parasitic resistances too.

This effect can be seen in Figure 4.9, where the coil resistance as a function of the turn width is shown for coils with circular and rectangular cross-section, respectively. As expected, for lower values of turn width the coil resistances are higher, which means that the systems might have higher losses.

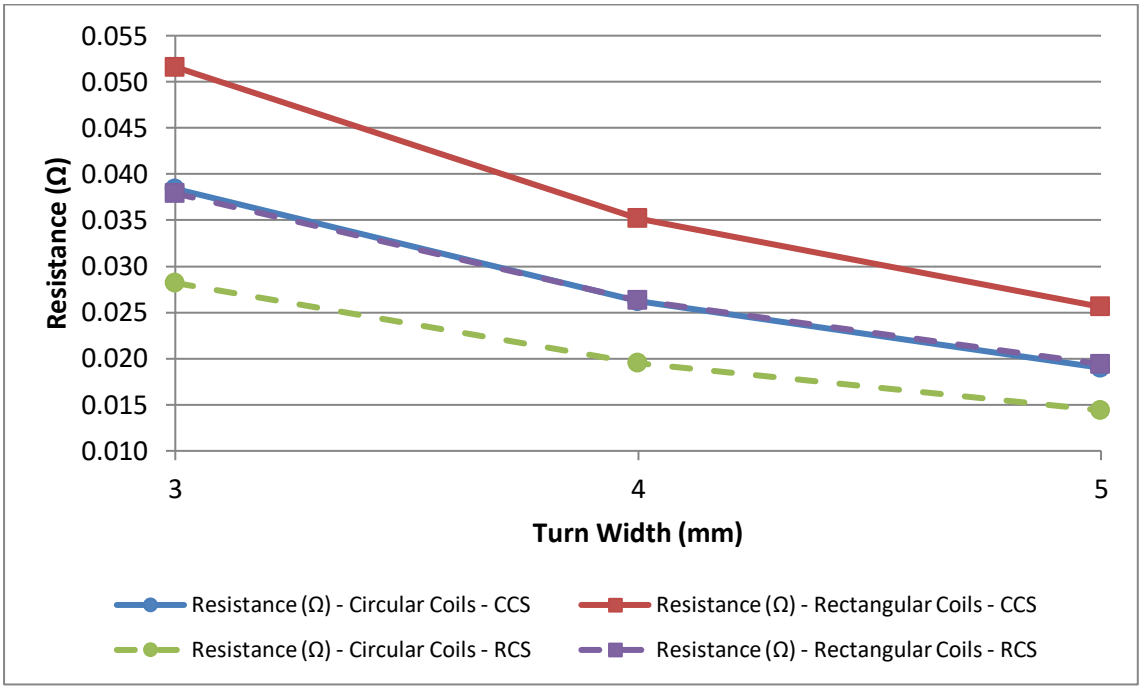

Figure 4.9: Circular & Rectangular Coils with Circular & Rectangular Cross-Section – Resistance vs. Turn Width (d_{out} = 120 mm, N = 7 turns, s = 1 mm, d = 10 mm & f_o = 100 kHz)

In Figure 4.9, there is another parameter that appears and this is the resonant frequency (f_o) of the systems. As mentioned in Chapter 3, AC resistance of a coil is also a function of the operating frequency, due to the skin effect. However, more details on the role of the resonant frequency on the system performance are given in the following sections.

In general, the most ideal case scenario would be to have systems with coils of low turn width and at the same time with low values of parasitic resistances, but something like that is not possible for solid type coils.

On the other hand, litz-wire coils could be a good option to minimize the AC resistances and the eddy-current losses. The main cause of these losses is the skin and the proximity effects, which can be reduced with the use of litz-wires of high frequency [24],[46].

According to the information above, the litz-wire coils could be a better option in comparison to the solid coils. However, it would be difficult to be adjusted on the surface of a solar cell, due to the fact that they consist of multiple thin strands, the number and the thickness of which depend on the amount of current and the frequency that the system is designed for [24],[46].

The use of litz-wire coils had been not considered in this project. However, further research on their use for PV cells and Wireless Power Transfer is recommended for future projects.

So, a value of turn width that balances the coupling capabilities and the parasitic resistances of the coils should be found. To do that, simulations of the whole system should be run for the different case scenarios of turn width. In this way, its optimal value, namely the value that will maximize the system's efficiency, will be identified. The identification will be held by running simulations in Simulink.

Finally, in Figures 4.10 – 4.12, it can be observed that the rise of the number of turns of the coils, of circular and rectangular shape, with turn widths of 4 and 5 mm, turn spacing of 1 mm and distance between the coils of 10 mm, lead to the increase of the self-inductances and the mutual inductance.

The increase of the number of turns results in the decrease of the internal diameters of the coils, since their external diameter should be maintained at 120 mm. Therefore, the self-inductances and the mutual inductance that depend on the internal diameters, increase when the values of turn width and turn spacing remain constant.

On the other hand, for the circular and rectangular coils of turn width equal to 4 mm, the rise of the number of turns leads to fluctuations of the coupling

coefficient and for coils with turn width equal to 5 mm the increase of the number of turns results in the reduction of the coupling coefficient. The fluctuations happen, because for both types of coils, when the turn width is equal to 4 mm and the number of turns rises from 5 to 6, the increase of the mutual inductance, which rose by 23.6%, is bigger than the increase of the self-inductances (22.76%).

So, based on equation (3.20), the coupling coefficient is smaller in comparison to the cases for which the rise of turns (from 6 to 7) leads to higher increase of the self-inductances, than the increase of the mutual inductance. (See also Appendix B, Tables B.13 – B.16)

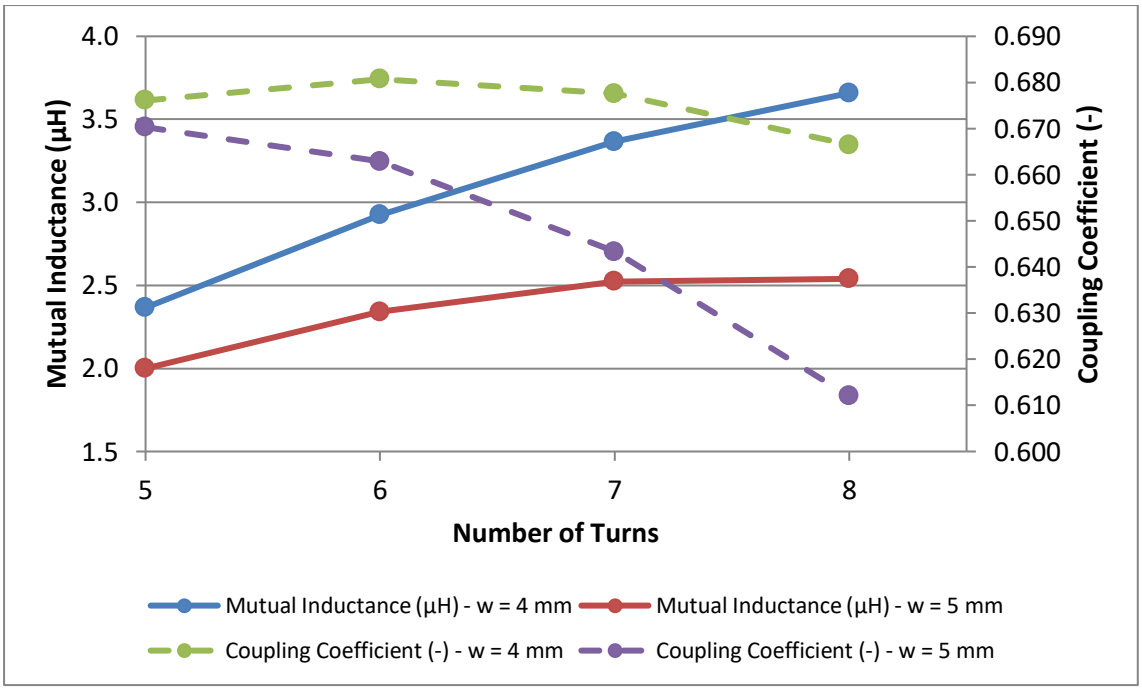

Figure 4.10: Circular Coils – Mutual Inductance & Coupling Coefficient vs. Number of Turns (d_{out} = 120 mm, s = 1 mm & d = 10 mm)

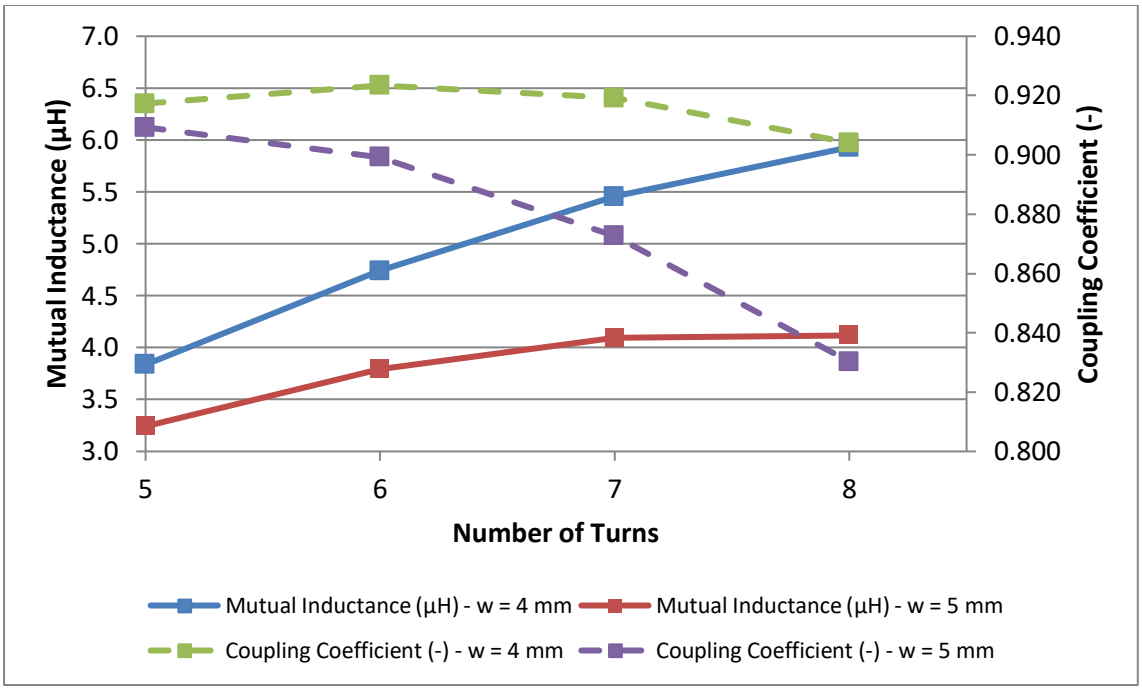

Figure 4.11: Rectangular Coils – Mutual Inductance & Coupling Coefficient vs. Number of Turns (d_{out} = 120 mm, s = 1 mm & d = 10 mm)

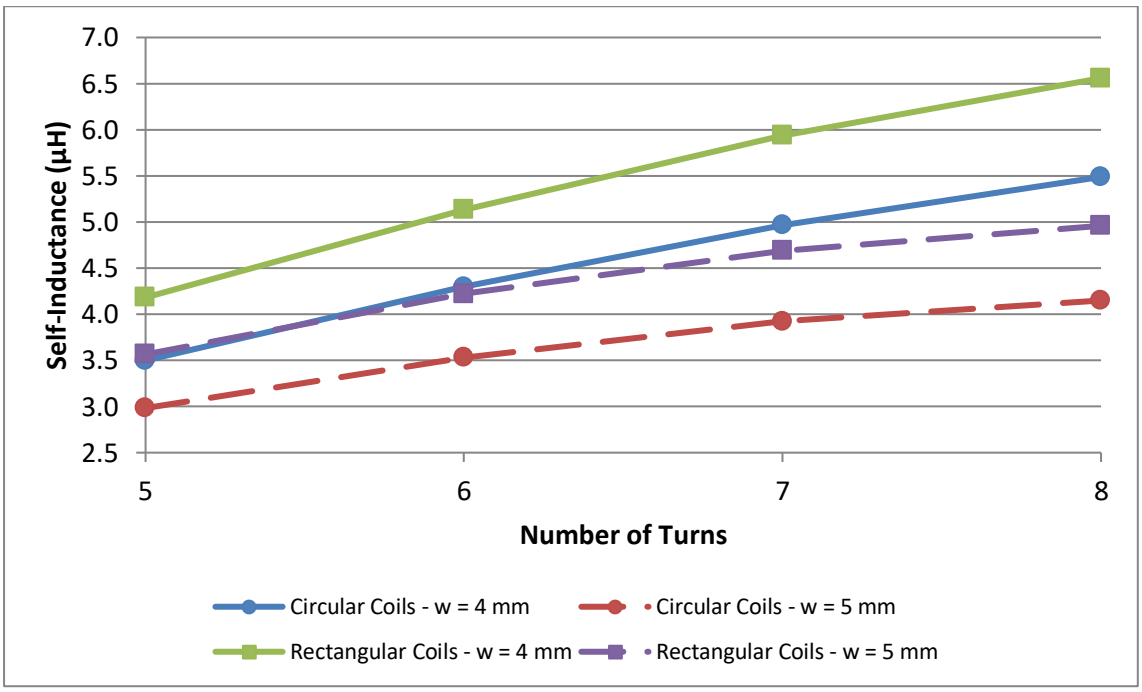

Figure 4.12: Circular & Rectangular Coils – Self-Inductance vs. Number of Turns (d_{out} = 120 mm, s = 1 mm & d = 10 mm)

The number of turns affects the parasitic resistances of the coils too. This effect can be seen in Figure 4.13, where the coil resistance as a function of the number of turns is shown for coils with circular and rectangular cross-section, respectively. As expected, for higher number of turns the coil resistances get higher too, since the length of the coils (*l*) rises. This means that the losses of the systems might be higher.

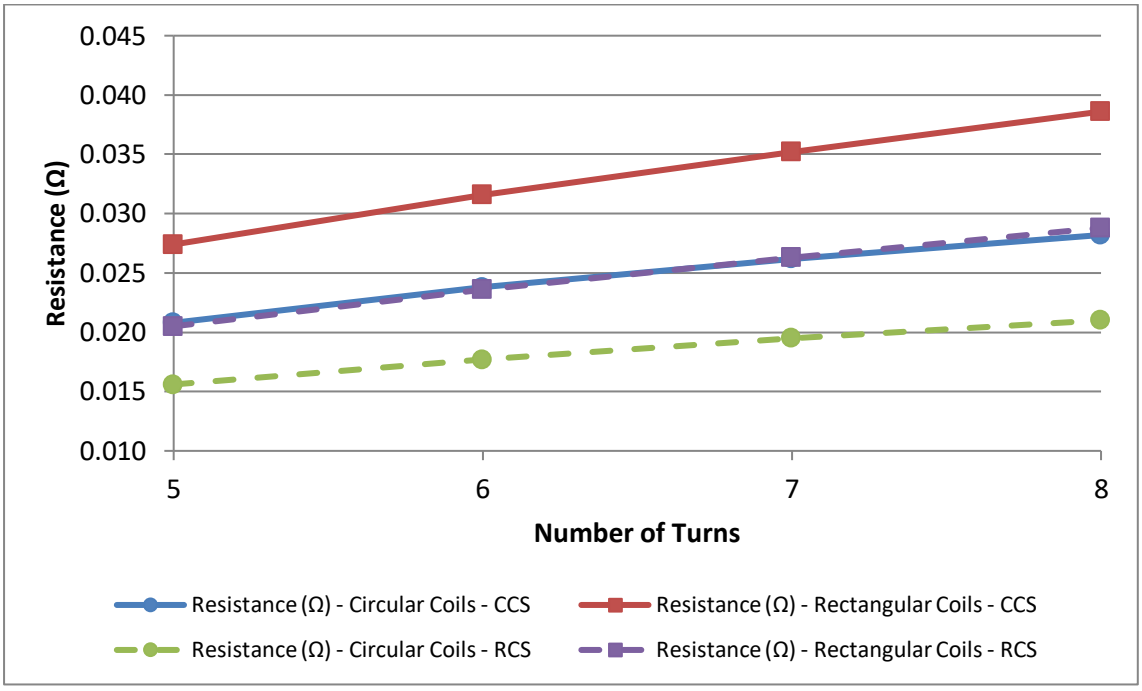

Figure 4.13: Circular & Rectangular Coils with Circular or Rectangular Cross-Section – Resistance vs. Number of Turns (d_{out} = 120 mm, w = 4 mm, s = 1 mm & d = 10 mm)

So, a number of turns that balances the coupling capabilities and the parasitic resistances of the coils should be found too.

4.1.2 Shape of Coils

As far as the shape of the coils is concerned, from Figures 4.14 – 4.17, it is clear that in every case scenario the rectangular coils develop better mutual inductances and coupling coefficients than the circular ones, as expected from the models presented in Section 3.2.2.

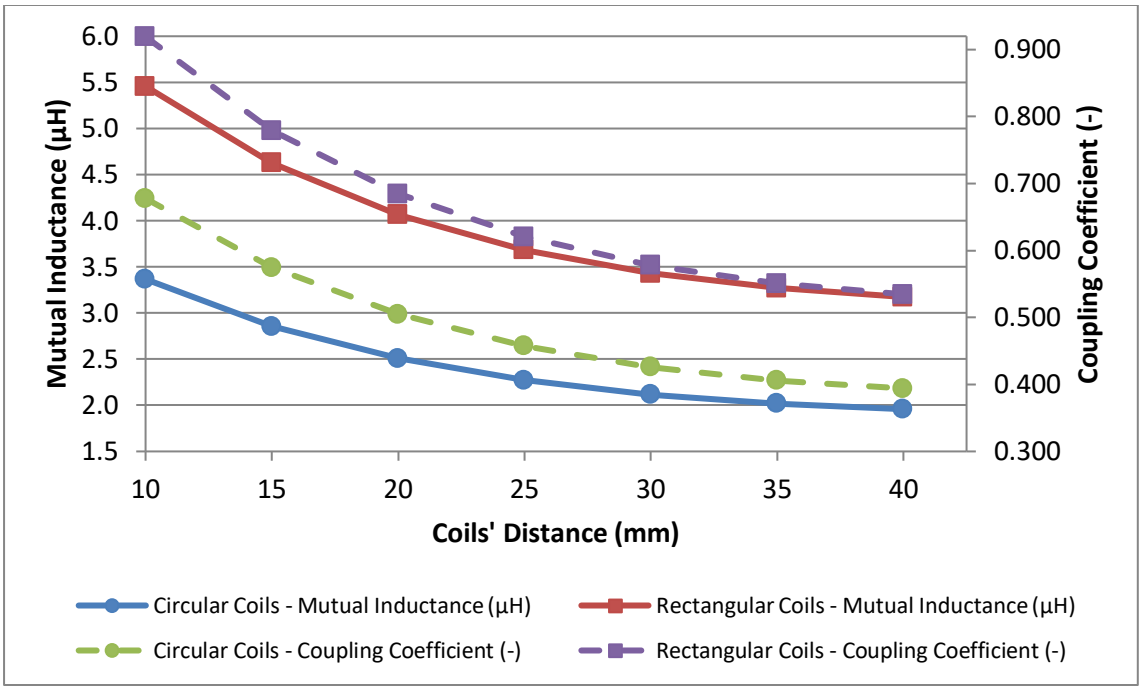

Figure 4.14: Circular vs. Rectangular Coils – Mutual Inductance & Coupling Coefficient vs. Coils' Distance (d_{out} = 120 mm, N = 7 turns, w = 4 mm & s = 1 mm)

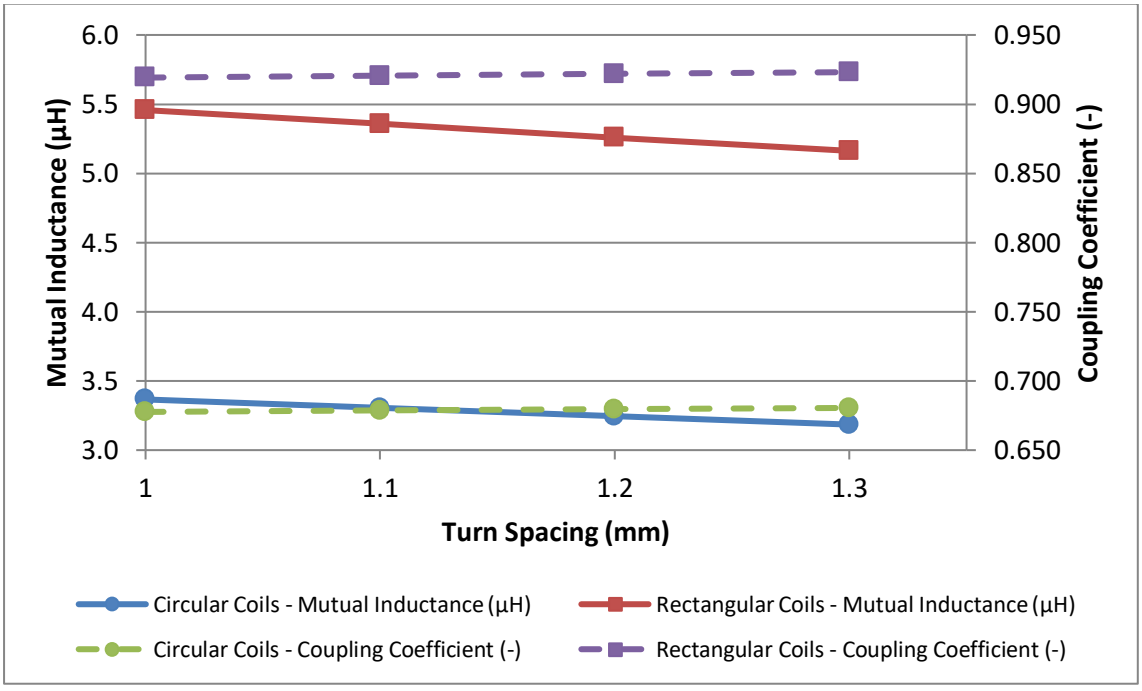

Figure 4.15: Circular vs. Rectangular Coils – Mutual Inductance & Coupling Coefficient vs. Turn Spacing (d_{out} = 120 mm, N = 7 turns, w = 4 mm & d = 10 mm)

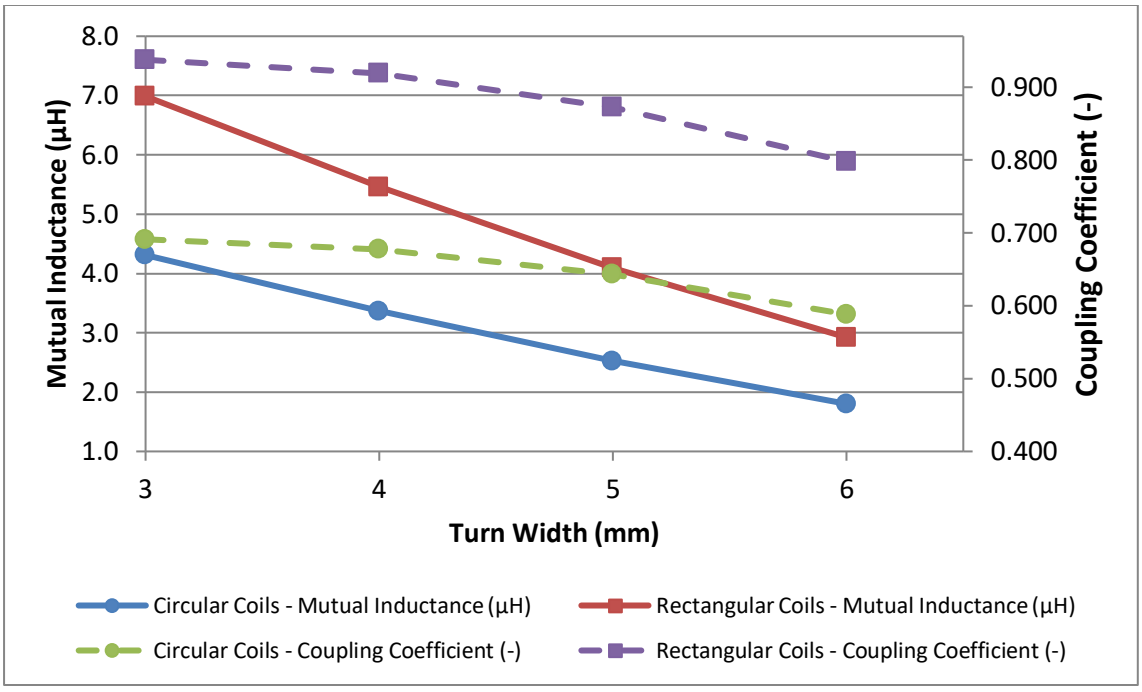

Figure 4.16: Circular vs. Rectangular Coils – Mutual Inductance & Coupling Coefficient vs. Turn Width (d_{out} = 120 mm, N = 7 turns, s = 1 mm & d = 10 mm)

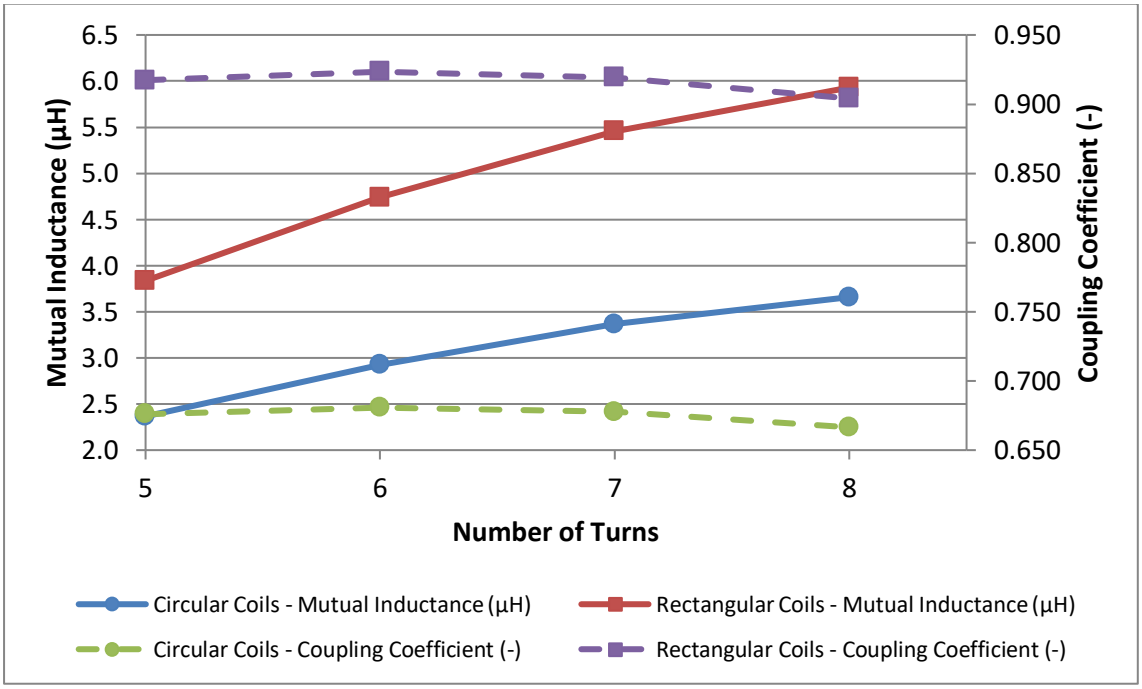

Figure 4.17: Circular vs. Rectangular Coils – Mutual Inductance & Coupling Coefficient vs. Number of Turns (d_{out} = 120 mm, w = 4 mm, s = 1 mm & d = 10 mm)

Also, as mentioned in Chapter 3 and in the introduction of Chapter 4, the range of the coupling coefficient is between 0 and 1. If the coupling coefficient is higher than 0.5, it means that the coils are tightly-coupled and if the coupling coefficient is lower than 0.5 the coils are loosely-coupled [19].

The only type of coils that develops coupling coefficients with values lower than 0.5 are the circular ones, when the distance between the coils increases, for a range of 10 to 40 mm. This does not happen for the rectangular coils, which always develop coupling coefficients with values higher than 0.5. The main reason for this is that the rectangular coils develop much higher values of self-inductances and mutual inductance in comparison to the circular ones, and thus higher ratios between the mutual inductance and the square root of the self-inductances.

So, it is obvious that by using rectangular coils, there will be tighter bonds between the circuits; hence more power will be transferred wirelessly from the primary circuit to the secondary one.

However, in the next chapter, the values of the parasitic resistances are presented and it is shown that the rectangular coils have higher parasitic resistances than the circular ones. This was expected, since for the same values of the different parameters, such as the number of turns, the external diameter, the turn width and the turn spacing, the overall length of the coils is larger for planar coils of rectangular shape.

So, the shape of coils that balances the coupling capabilities and the parasitic resistances should be found too, by running simulations in Simulink.

4.1.3 Cross-Section of the Coils

In this section, the effect of the coil's cross-section on the parasitic resistance is studied. The effect of both the cross-section's shape and size are considered.

Generally, to decrease the power losses of the transferred power from the primary circuit to the secondary one, the parasitic resistances of the coils should

be reduced. The most effective way to do that, for both circular and rectangular coils, is by increasing their cross-section.

For coils with circular cross-section (CCS), the increase of the width of the cross-section, which is equal to the turn width of the coils, leads to the increase of the radius of the cross-section ($r = \frac{w}{2}$) and thus the increase of the cross-section. This has as a result the decrease of the parasitic resistances of the coils, as can be seen in Figure 4.18. (See also Appendix B, Tables B.17 & B.18)

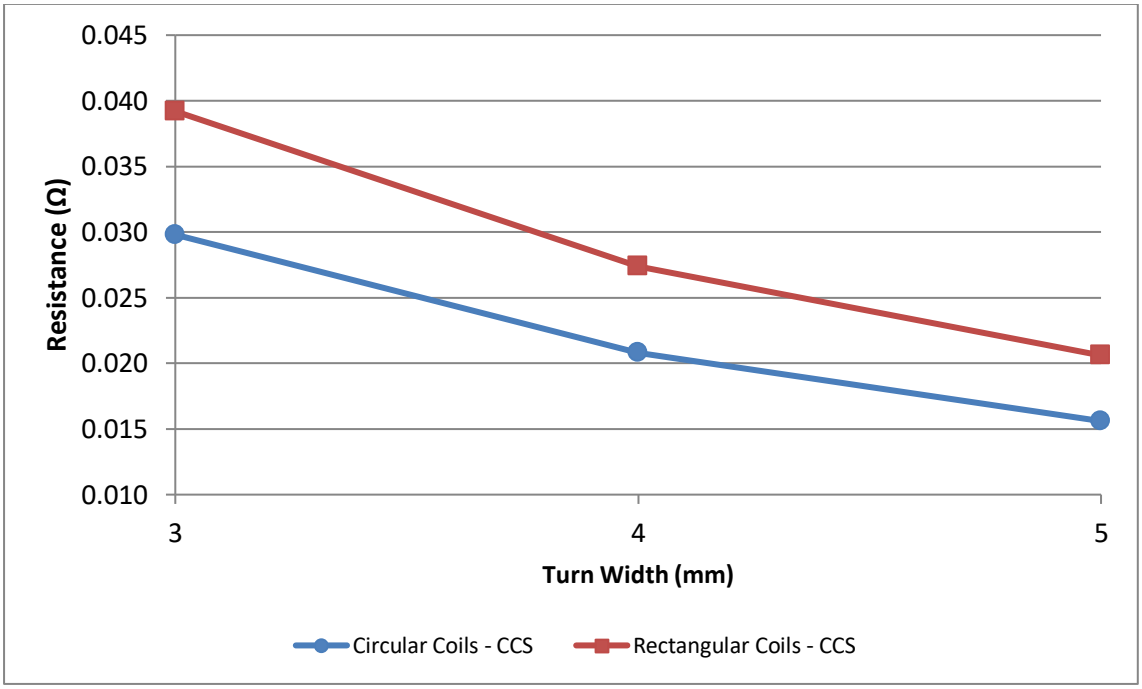

Figure 4.18: Circular & Rectangular Coils with Circular Cross-Section – Resistance vs. Turn Width (d_{out} = 120 mm, N = 5 turns, s = 1 mm, d = 10 mm & f_o = 100 kHz)

It should be mentioned that for structural reasons, only half of the circular cross-sections ($\frac{A_{cs}}{2}$) are taken into account in the calculations of the parasitic resistances (Figure 4.19).

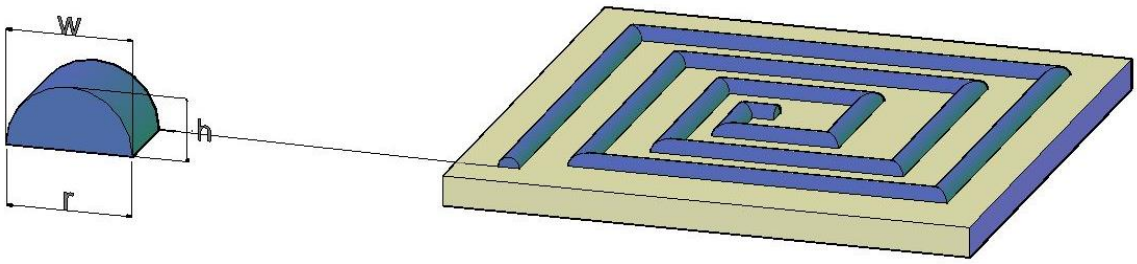

Figure 4.19: Circular Cross-Section on the Surface of a Solar Cell

On the other hand, for coils with rectangular cross-section (RCS), the whole surface of the cross-section was used for the calculations (Figure 4.20).

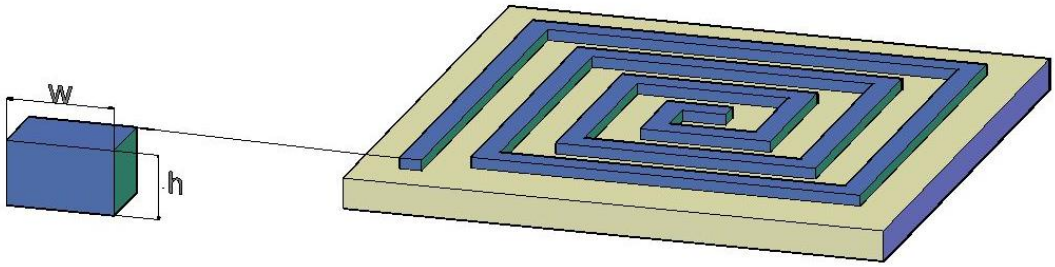

Figure 4.20: Rectangular Cross-Section on the Surface of a Solar Cell

For coils with rectangular cross-section, the increase of the width leads to the increase of the cross-section. However, in the case of a rectangular cross-section, the thickness or height of the conductor (*h*) affects the rectangular cross-section too. The height of the rectangular cross-section is not related to the width by any geometrical reasons, as in circular cross-section, where the radius is related to the width (Figures 4.19 & 4.20). Therefore, the cross-section can be varied by directly changing the height.

When the width remains the same and the thickness increases, the cross-section increases, but the parasitic resistances are not affected as can be seen in Figure 4.21. This shows that for heights between 1.5 and 2.5 mm, the skin effect is dominant and the conduction losses depend mainly on it. However, in Figure 4.22 it can be seen that for heights less than 1 mm, the effect of skin effect decreases, since there is a fluctuation of the AC resistances. (See also Appendix B, Tables B.19 & B.20)

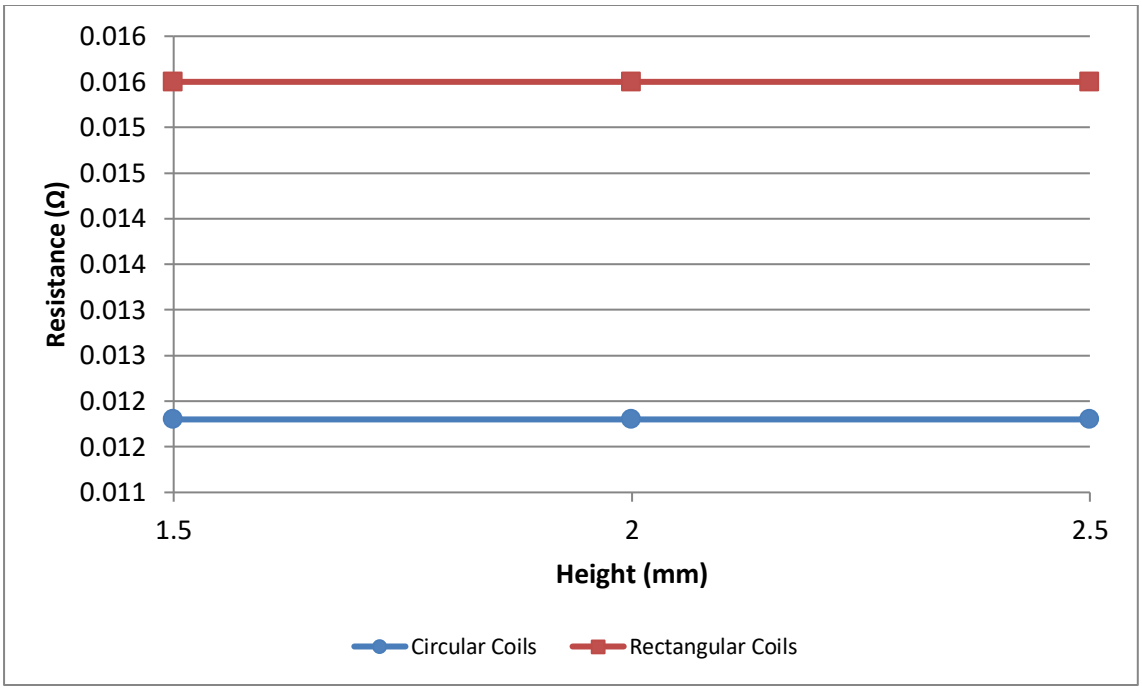

Figure 4.21: Circular & Rectangular Coils with Rectangular Cross-Section – Resistance vs. Height of the Conductor (d_{out} = 120 mm, N = 5 turns, w = 5 mm, s = 1 mm, d = 10 mm & f_o = 100 kHz)

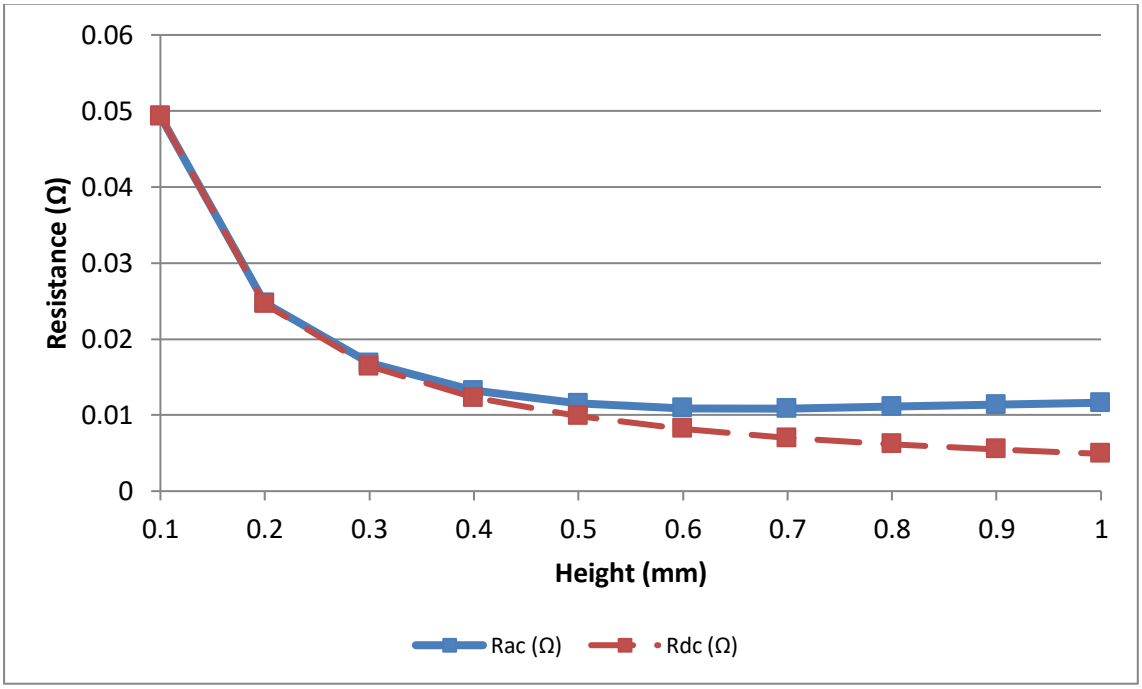

Figure 4.22: Circular Coils with Rectangular Cross-Section – Resistance vs. Height of the Conductor (d_{out} = 120 mm, N = 5 turns, w = 5 mm, s = 1 mm, d = 10 mm & f_o = 100 kHz)

This might happen, because for a range between 0.1 and 1 mm the reduction of the DC resistance (R_{DC}) is more significant than the skin effect. Therefore, to reduce the parasitic resistances of coils with rectangular cross-section, the area of the cross-section should be increased, by increasing the width and not the thickness of the conductor, since for the values of thickness that the systems are studied (1.5 – 2.5 mm) the skin effect is dominant (Figure 4.23).

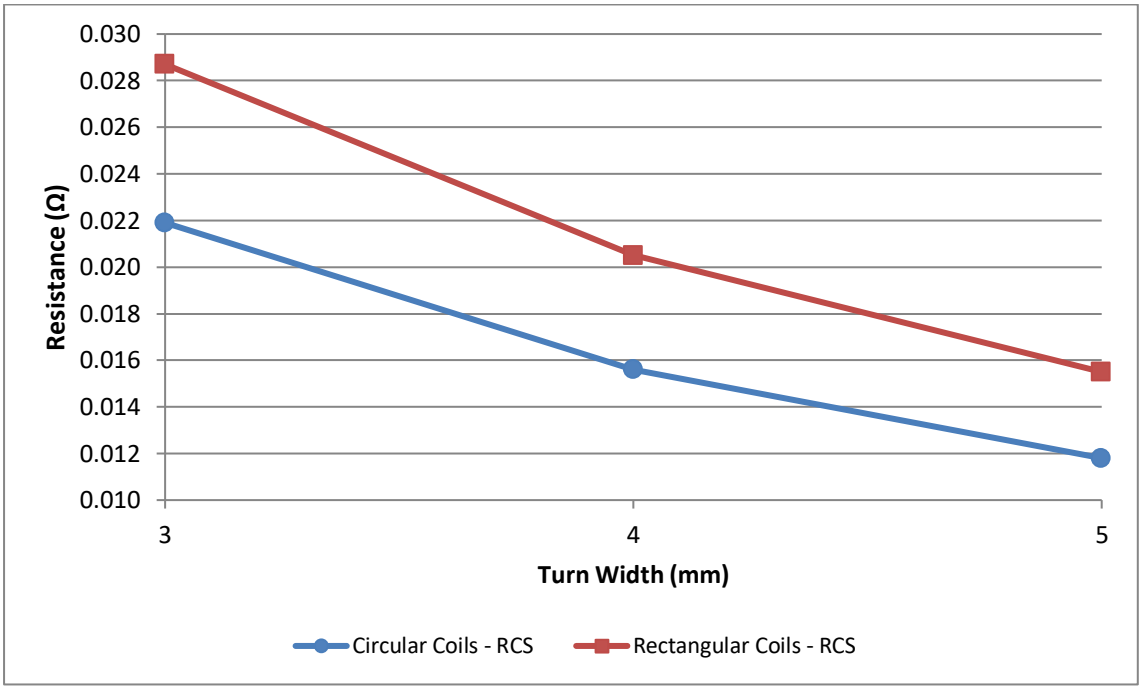

Figure 4.23: Circular & Rectangular Coils with Rectangular Cross-Section – Resistance vs. Turn Width (d_{out} = 120 mm, N = 5 turns, s = 1 mm, d = 10 mm & f_o = 100 kHz)

Based on these results, it seems that the best option of turn width would be a turn width equal to 5 mm. However, as it has been discussed in Section 4.1.1 for smaller values of turn width the coils develop better mutual inductances and coupling coefficients and thus a value of turn width that balances the coupling capabilities and the parasitic resistances of the coils should be found.

As far as the skin depth (δ) is concerned, according to equation (3.47) from Section 3.2.4, the main parameters that define it are the permeability of the vacuum (μ_o), the relative permeability of the conductor (μ_r), the conductivity of the conductor (σ) and the frequency.

Due to high conductivity and consequently lower resistance, in comparison to other materials, such as aluminum, copper has been chosen as the main material of the coils. For coils made from copper μ_r is equal to 0.999991 and σ is equal to $5.8 \cdot 10^7$ $^{S}/_{m}$. The permeability of the vacuum is equal to $4 \cdot \pi \cdot 10^{-7}$ $^{H}/_{m}$. So, since these parameters are constant, the only parameter that can be changed is the frequency [31].

In Figure 4.24, it can be observed that for any type of coils, the increase of the frequency leads to higher parasitic resistances. This happens, because by increasing the frequency, the skin depth decreases (Figure 4.25), the skin ratio (F_{skin}) increases and consequently the skin resistance (R_{skin}) increases. (See also Appendix B, Tables B.21 – B.24)

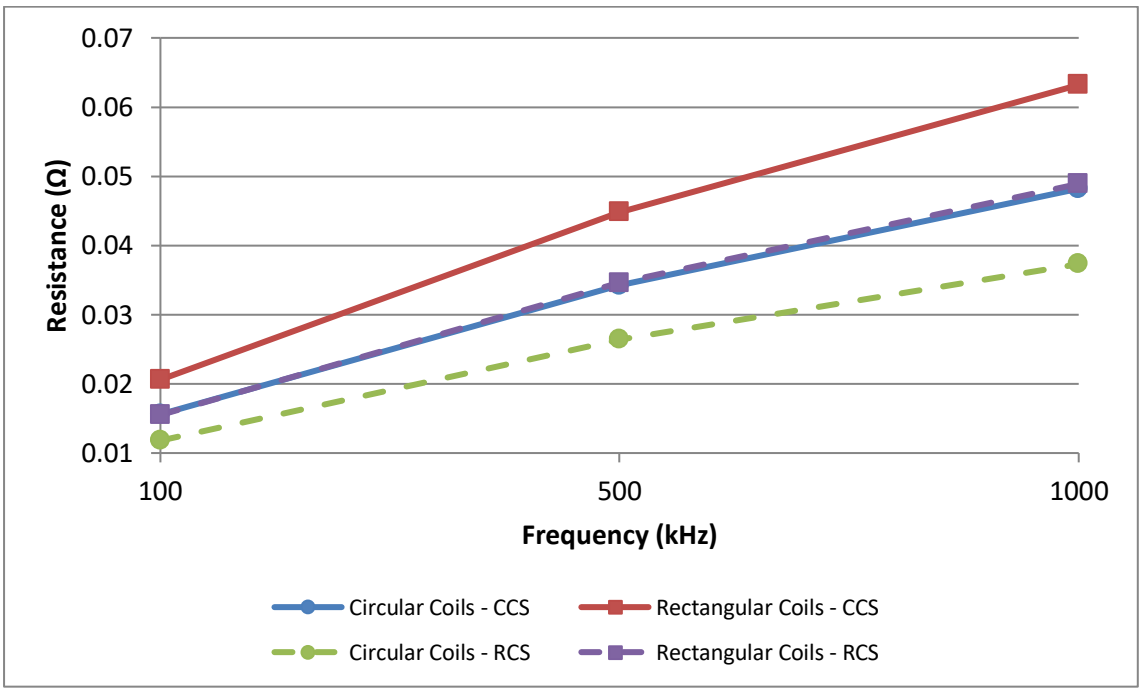

Figure 4.24: Resistance vs. Frequency (d_{out} = 120 mm, N = 5 turns, w = 5 mm, s = 1 mm & d = 10 mm)

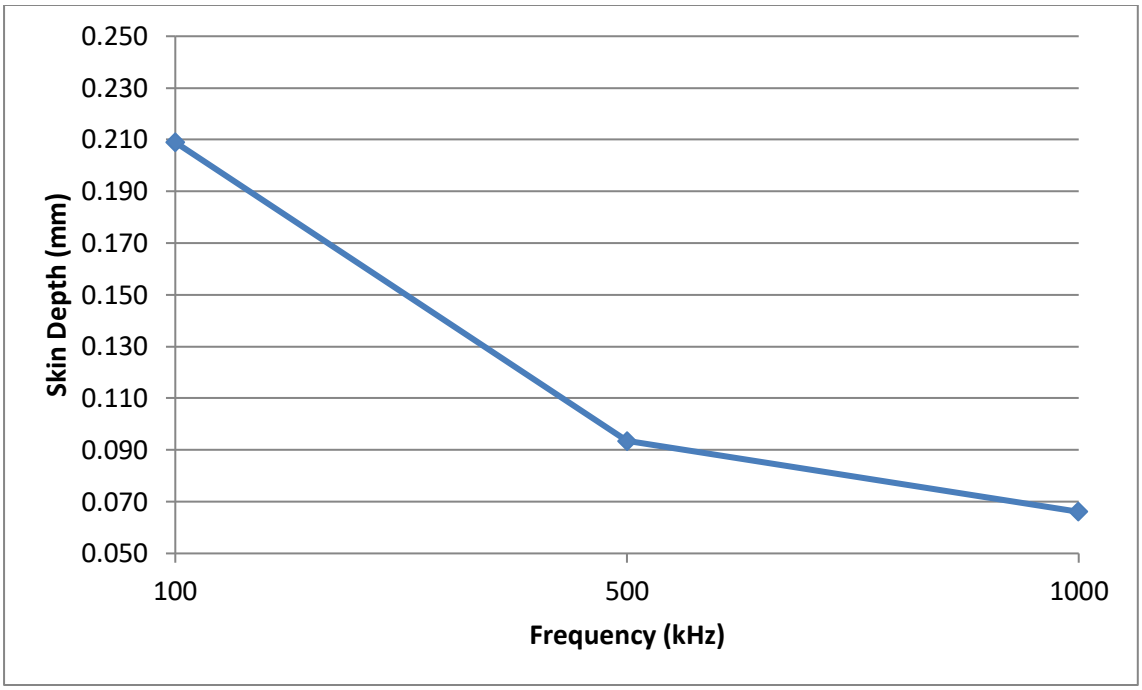

Figure 4.25: Skin Depth vs. Frequency

Finally, from Figure 4.24, it can be observed that the coils with rectangular shape and rectangular cross-section develop lower parasitic resistances than the rectangular coils with circular cross-section. The same goes for the circular coils with rectangular cross-section that develop lower parasitic resistances than the circular coils with circular cross-section.

However, from the same figure (Figure 4.24), it can be seen that the circular coils with circular cross-section develop slightly lower parasitic resistances, than the rectangular coils with rectangular cross-section. The difference of these values is between 0.6 and 1.5%.

So, the rectangular cross-section seems to be the most ideal cross-section for both types of coils. Nonetheless, simulations of the whole system should be run for both types of cross-sections to see which one will help the systems develop higher efficiencies.

4.1.4 Compensation Capacitances

As mentioned in Section 2.4.3, in order to have magnetic resonant coupling, capacitors should be implemented in the primary and the secondary circuits. The position of the capacitors depends on the compensation topology. For example, in Series-Series topology, in both circuits the capacitors are connected in series with the rest of the components (coils), but in Series-Parallel topology, the capacitor of the secondary circuit is connected in parallel with the receiver coil and the load (Figures 3.1 & 3.2).

Based on the equations of Table 3.2 in Section 3.2.3, it is clear that the main parameters that affect the capacitances of the circuits are the self-inductances, the mutual inductance and the resonant frequency. So, for both circular and rectangular coils, with turn spacing equal to 1 mm and a distance between the coils of 10 mm, the capacitances of the primary and the secondary circuits were calculated for all the types of topologies.

First, the capacitances were calculated for coils with different number of turns and for different frequencies and then, by changing the value of turn width and for different frequencies.

4.1.4.1 Capacitances vs. Number of Turns

In Figures 4.26 – 4.29, it can be observed that for the circular coils the increase of the number of turns results in lower capacitances. This is logical, since in higher number of turns, the self-inductances and the mutual inductance of the coils are higher and thus the capacitances will be lower in every frequency, based on the mathematical models of Table 3.2.

Also, in higher frequencies, such as 500 and 1000 kHz, the capacitances are extremely low, in comparison to the capacitances at 100 kHz. This was expected too, since the capacitances and the frequency are inversely proportional. (See also Appendix B, Tables B.25 – B.28)

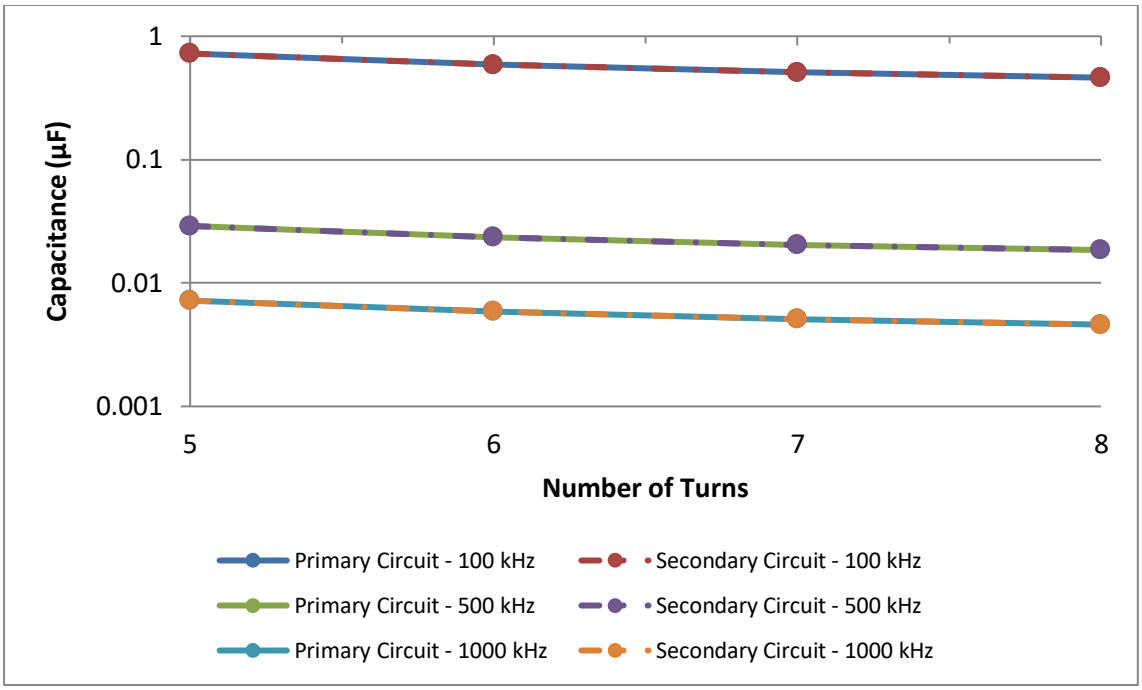

Figure 4.26: Series-Series Topology – Circular Coils – Capacitance (Logarithmic Scale) vs. Number of Turns (d_{out} = 120 mm, w = 4 mm, s = 1 mm & d = 10 mm)

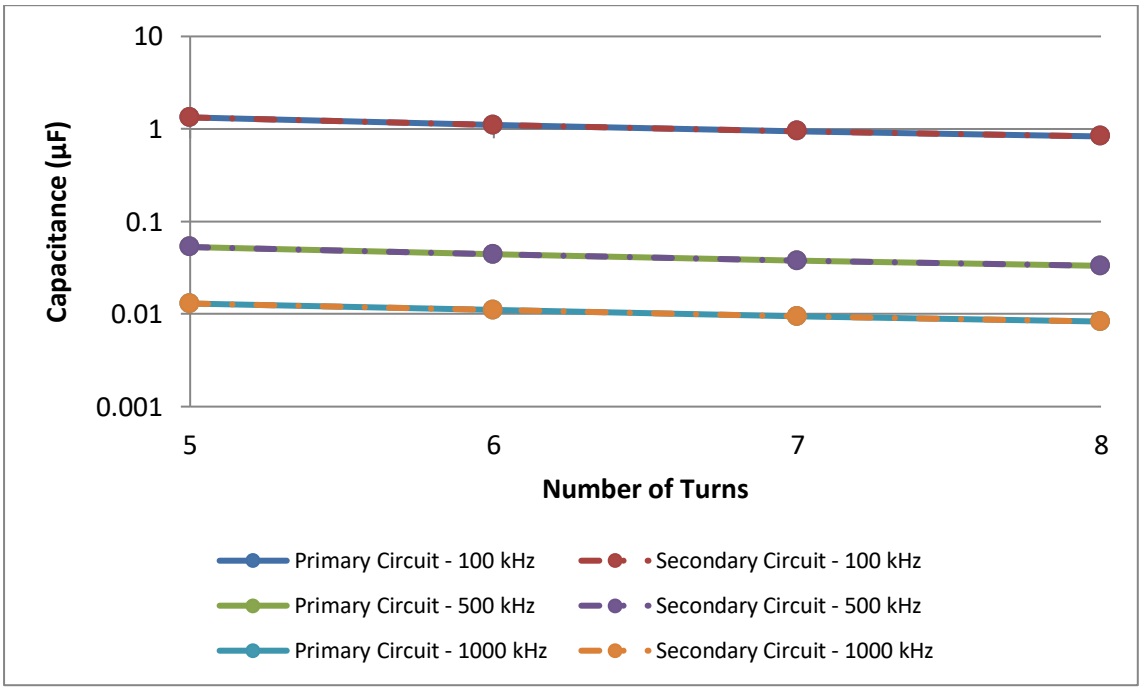

Figure 4.27: Parallel-Parallel Topology – Circular Coils – Capacitance (Logarithmic Scale) vs. Number of Turns (d_{out} = 120 mm, w = 4 mm, s = 1 mm & d = 10 mm)

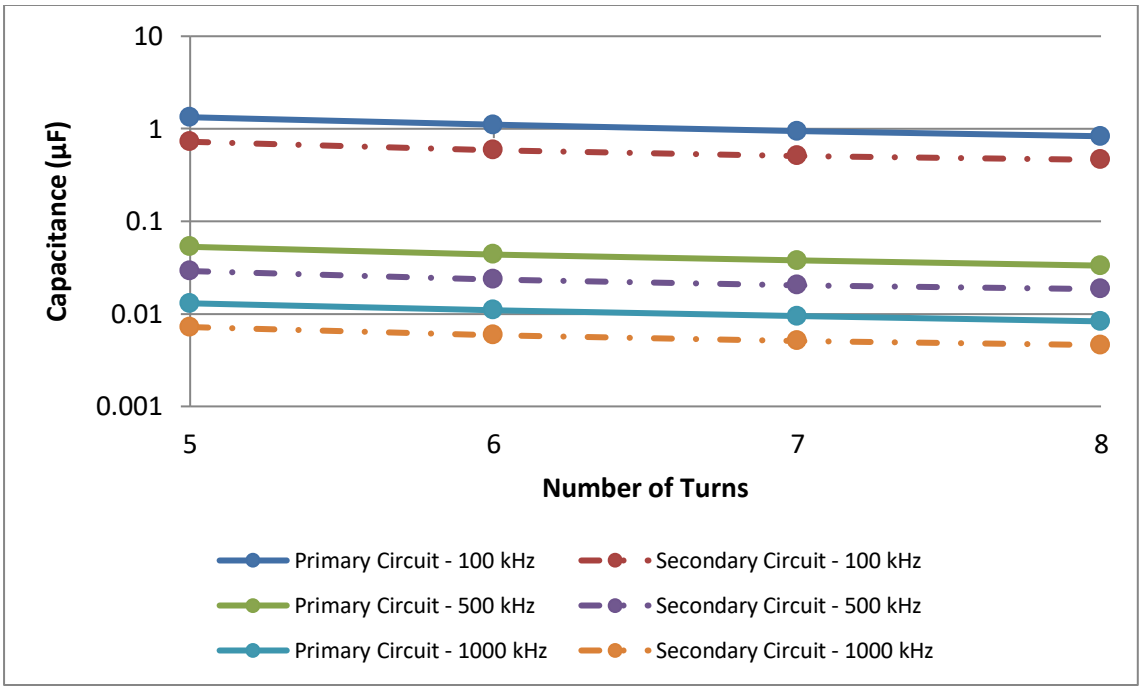

Figure 4.28: Series-Parallel Topology – Circular Coils – Capacitance (Logarithmic Scale) vs. Number of Turns (d_{out} = 120 mm, w = 4 mm, s = 1 mm & d = 10 mm)

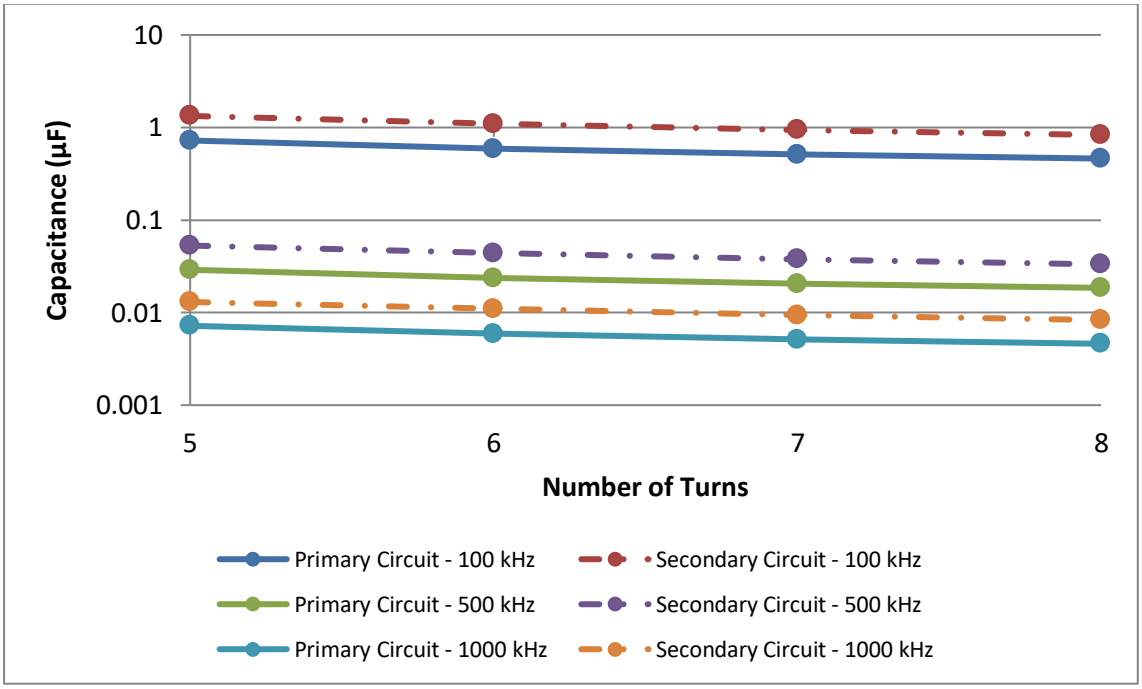

Figure 4.29: Parallel-Series Topology – Circular Coils – Capacitance (Logarithmic Scale) vs. Number of Turns (d_{out} = 120 mm, w = 4 mm, s = 1 mm & d = 10 mm)

Furthermore, in Series-Series topology the capacitances have lower values in comparison to the ones in Parallel-Parallel topology. This was expected, since in Series-Series topology the main parameters that affect the capacitances of the primary and the secondary circuits are the self-inductances of the coils of the primary and the secondary circuits, respectively (Table 3.2).

On the other hand, in Parallel-Parallel topology, the capacitances of both circuits are affected by both the self-inductances of the coils and the mutual inductance (Table 3.2). Therefore, the systems in Parallel-Parallel topology require higher capacitances in comparison to the ones in Series-Series topology.

For the exact same reasons and based on the mathematical models of Table 3.2, in Series-Parallel and in Parallel-Series topologies, the capacitors that are connected in parallel could be smaller, since lower capacitances were obtained, in comparison to the capacitors that are connected in series.

In general, capacitors are components with the ability to store electrical energy. There are many different types of capacitors, but in their basic form consist of two parallel metal plates, that are not connected. The capacitance is the ability of the capacitors to store electrical charge in the form of an electrostatic field between their plates and it depends on three main factors, the surface area of the plates, the distance between the plates and the dielectric material. For plates with larger surface areas (bigger capacitors) and smaller distances between them, greater capacitances can be stored [49].

So, it is clear that for PV cells that are connected with circuits in Series-Series topology smaller capacitors could be used, in comparison to the capacitors that could be used in circuits in Parallel-Parallel topology. Also, in Series-Parallel and in Parallel-Series topologies smaller capacitors could be used when they are connected in parallel, rather than when they are connected in series.

For the rectangular coils similar trends are obtained. In other words, for higher number of turns and for higher frequencies the systems require lower capacitances too. (See also Appendix B, Tables B.29 – B.32)

Finally, after a comparison between the capacitors that are connected with circular coils and the ones that are connected with coils of rectangular shape, it should be mentioned that for coils of circular shape in Series-Series topology, bigger capacitors should be used, since higher capacitances were obtained, in comparison to coils of rectangular shape (Figure 4.30).

The main reason for this is that the rectangular coils, due to their shape, develop higher self-inductances and mutual inductance, in comparison to the circular ones. So, according to the mathematical models of Table 3.2, it was expected that smaller capacitors could be used, since lower capacitances were obtained.

On the other hand, in Parallel-Parallel topology, the systems with rectangular coils require larger capacitors, since higher capacitances were obtained, than the systems that are connected with circular coils (Figure 4.31).

This was expected too, since from Table 3.2, it can be seen that the mathematical models that are used in Parallel-Parallel topology include both the self-inductances and the mutual inductance, as mentioned before. In other words, C_1 and C_2 are affected by the difference between the self-inductance of the one circuit and the ratio of the mutual inductance and the self-inductance of the other circuit. The lower this difference is, the higher the capacitances become.

As far as the Series-Parallel topology is concerned, for the exact same reasons, the capacitor of the primary circuit that is connected in series with the rectangular coil need to be larger than the one that is connected in series with the circular coil, since higher capacitances were obtained. In contrary, the capacitor of the secondary circuit that is connected in parallel with the rectangular coil could be smaller than the one that is connected in parallel with the circular coil, since slightly lower capacitances were obtained (Figure 4.32).

In Figure 4.33, it is shown that the exact opposite applies for the capacitors and the capacitances of the Parallel-Series topology.

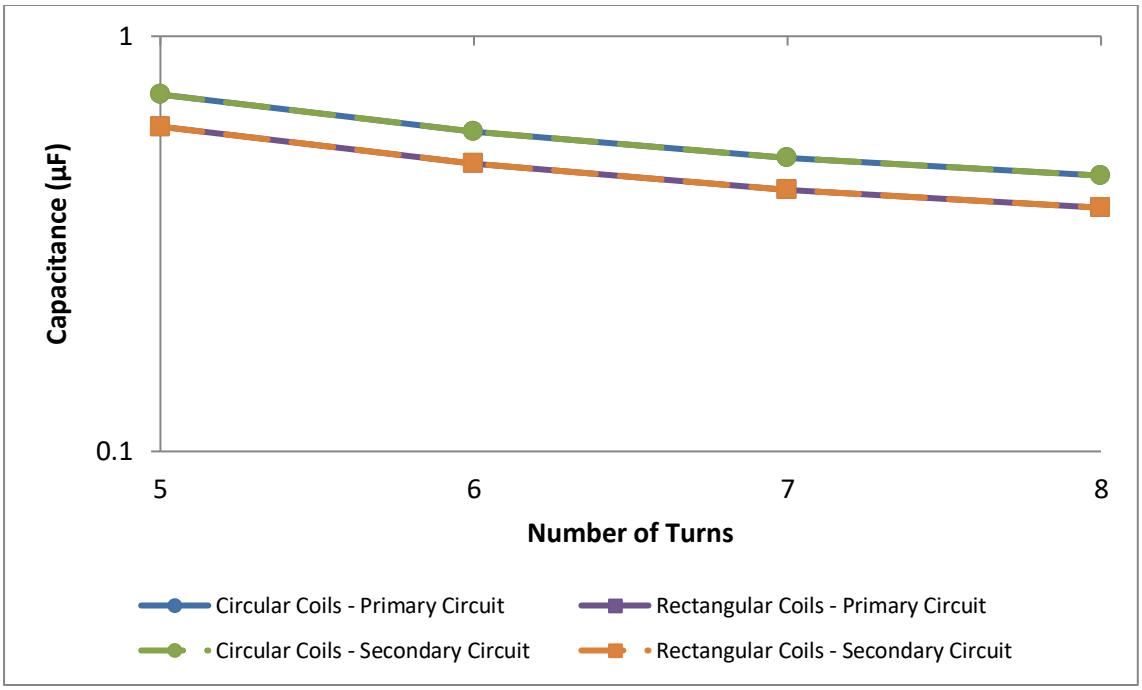

Figure 4.30: Series-Series Topology – Circular vs. Rectangular Coils – Capacitance (Logarithmic Scale) vs. Number of Turns (d_{out} = 120 mm, w = 4 mm, s = 1 mm, d = 10 mm & f_o = 100 kHz)

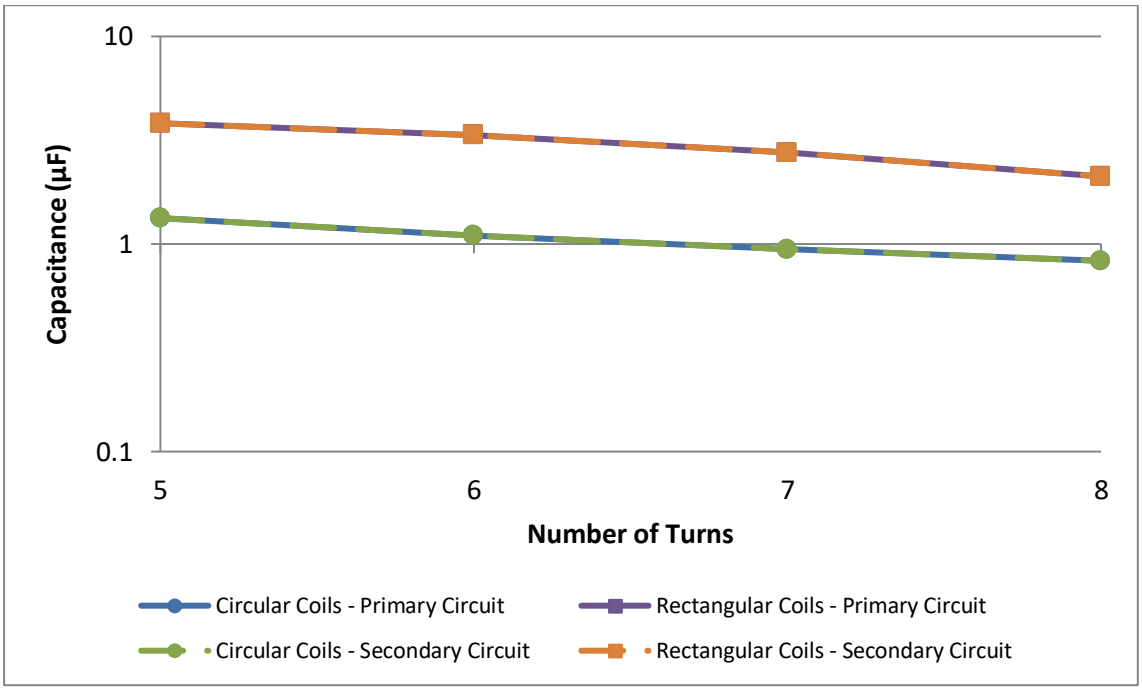

Figure 4.31: Parallel-Parallel Topology – Circular vs. Rectangular Coils – Capacitance (Logarithmic Scale) vs. Number of Turns (d_{out} = 120 mm, w = 4 mm, s = 1 mm, d = 10 mm & f_o = 100 kHz)

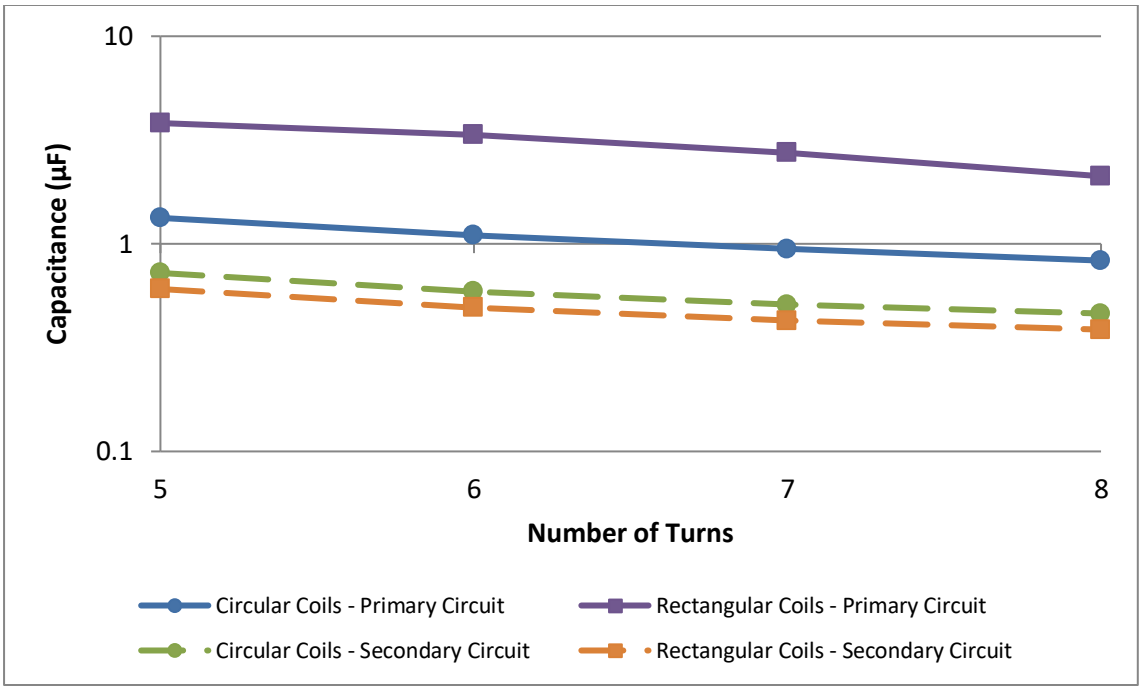

Figure 4.32: Series-Parallel Topology – Circular vs. Rectangular Coils – Capacitance (Logarithmic Scale) vs. Number of Turns (d_{out} = 120 mm, w = 4 mm, s = 1 mm, d = 10 mm & f_o = 100 kHz)

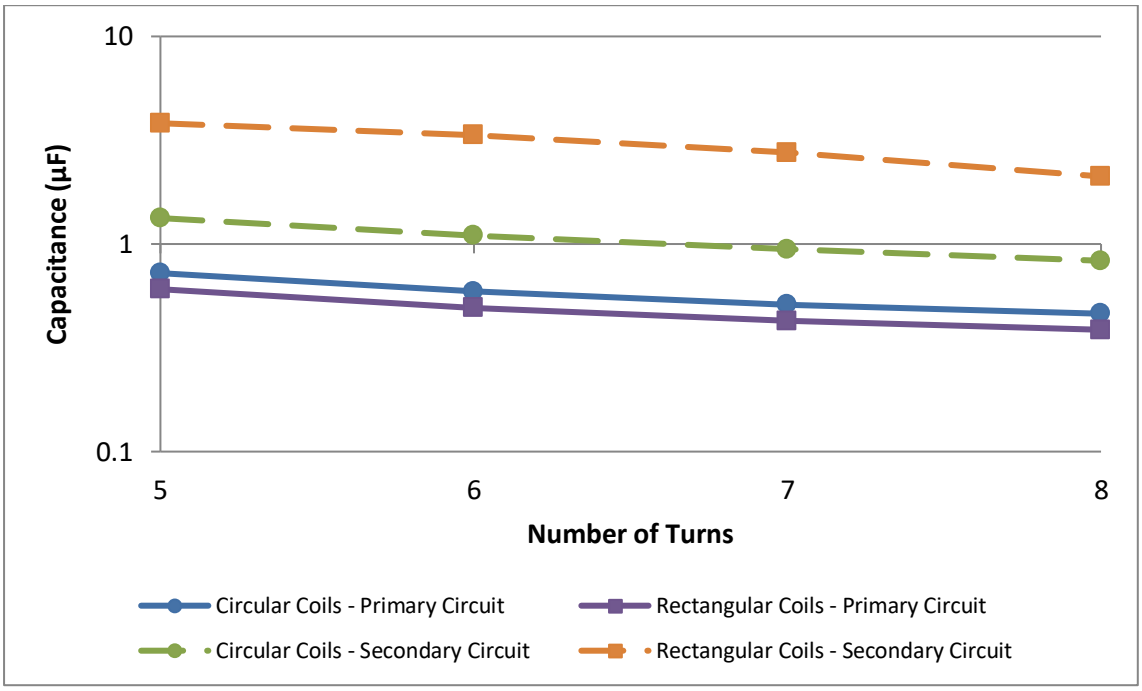

Figure 4.33: Parallel-Series Topology – Circular vs. Rectangular Coils – Capacitance (Logarithmic Scale) vs. Number of Turns (d_{out} = 120 mm, w = 4 mm, s = 1 mm, d = 10 mm & f_o = 100 kHz)

4.1.4.2 Capacitances vs. Turn Width

Since the capacitances for different number of turns were presented, the effect of the turn width on the compensation capacitances will be presented too, for a range between 3 and 5 mm.

In Figures 4.34 – 4.37, it can be seen, that in Series-Series and in Parallel-Parallel topologies, in circuits with circular or rectangular coils of 5 turns, the increment of turn width results in higher capacitances for a frequency range between 100 and 1000 kHz.

This is logical, since as have been analyzed in previous sections, the rise of the turn width results in lower values of self-inductances and thus to higher values of capacitances. (See also Appendix B, Tables B.33 – B.40)

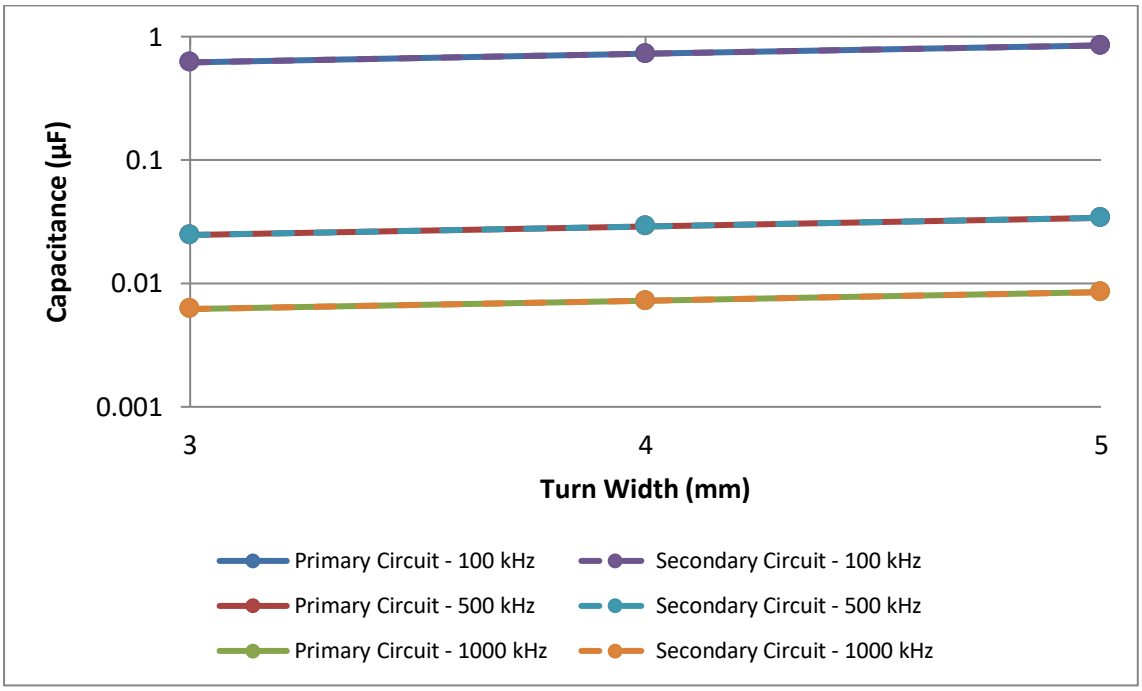

Figure 4.34: Series-Series Topology – Circular Coils – Capacitance (Logarithmic Scale) vs. Turn Width (d_{out} = 120 mm, N = 5 turns, s = 1 mm & d = 10 mm)

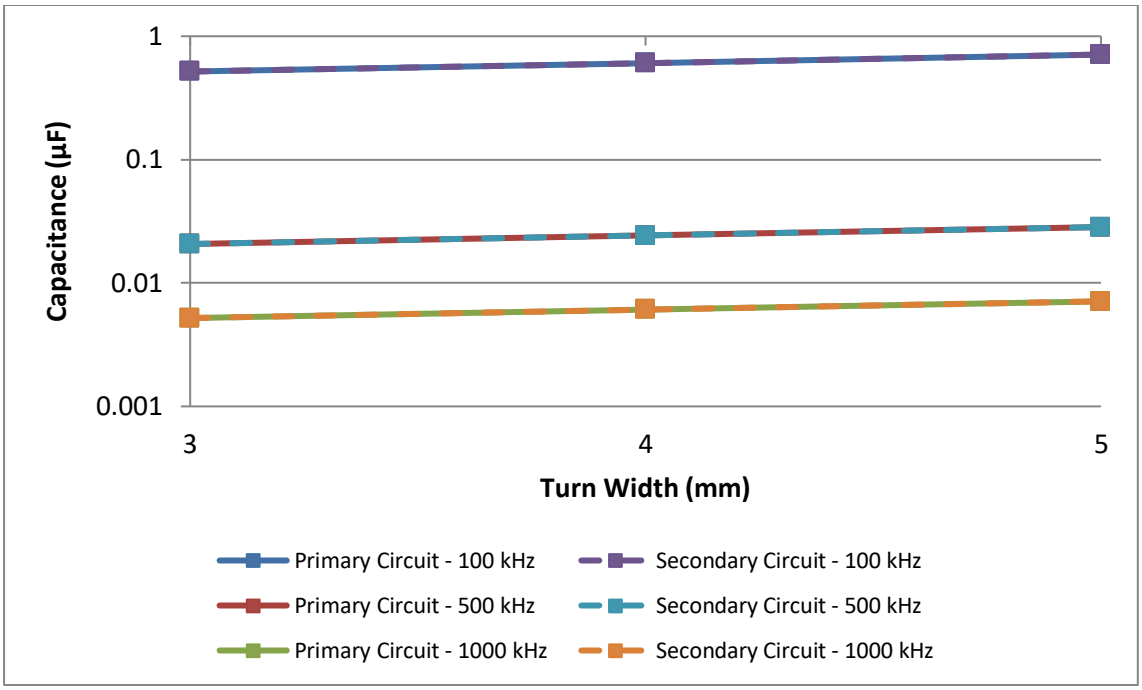

Figure 4.35: Series-Series Topology – Rectangular Coils – Capacitance (Logarithmic Scale) vs. Turn Width (d_{out} = 120 mm, N = 5 turns, s = 1 mm & d = 10 mm)

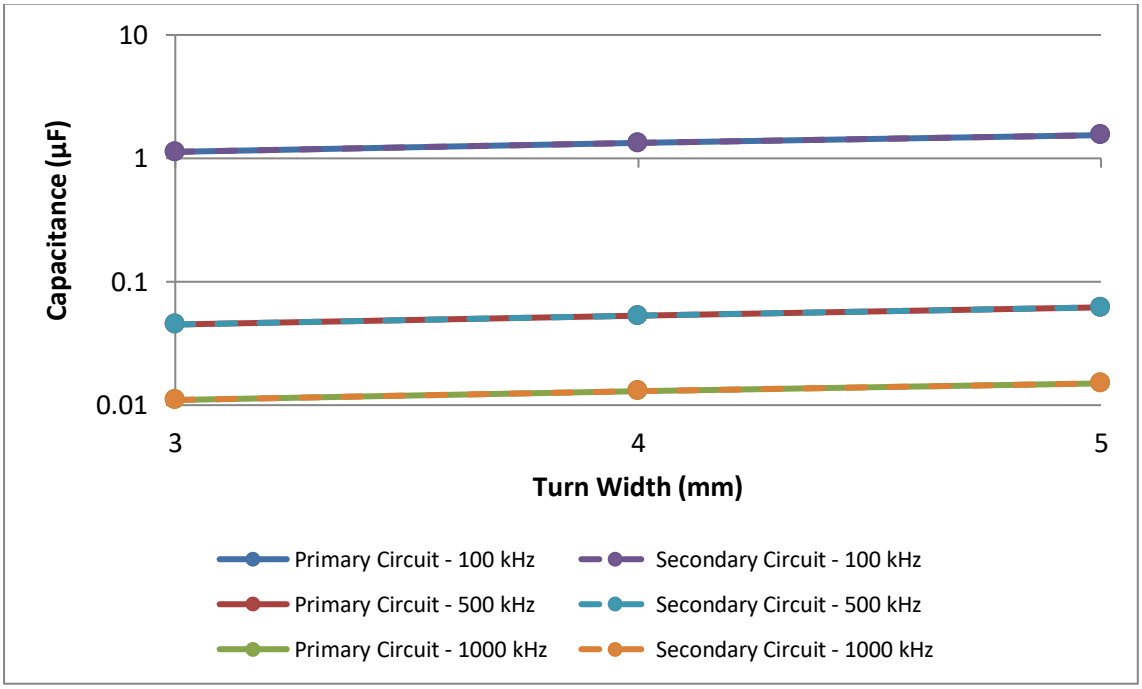

Figure 4.36: Parallel-Parallel Topology – Circular Coils – Capacitance (Logarithmic Scale) vs. Turn Width (d_{out} = 120 mm, N = 5 turns, s = 1 mm & d = 10 mm)

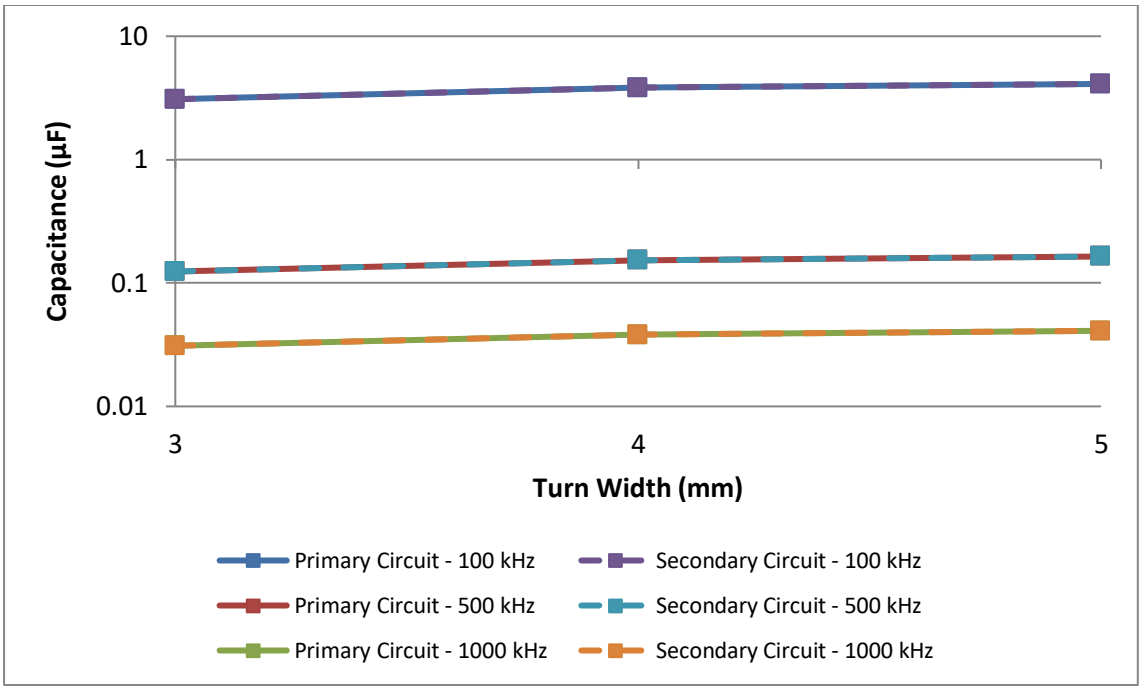

Figure 4.37: Parallel-Parallel Topology – Rectangular Coils – Capacitance (Logarithmic Scale) vs. Turn Width (d_{out} = 120 mm, N = 5 turns, s = 1 mm & d = 10 mm)

For the exact same reasons, according to Figures 4.38 – 4.41, in Series-Parallel and in Parallel-Series topologies similar trends can be observed. Namely, it seems that in both primary and secondary circuits with capacitors connected with coils of circular or rectangular shape, when the value of the turn width increases, for a range between 3 and 5 mm, the values of the capacitances increase too.

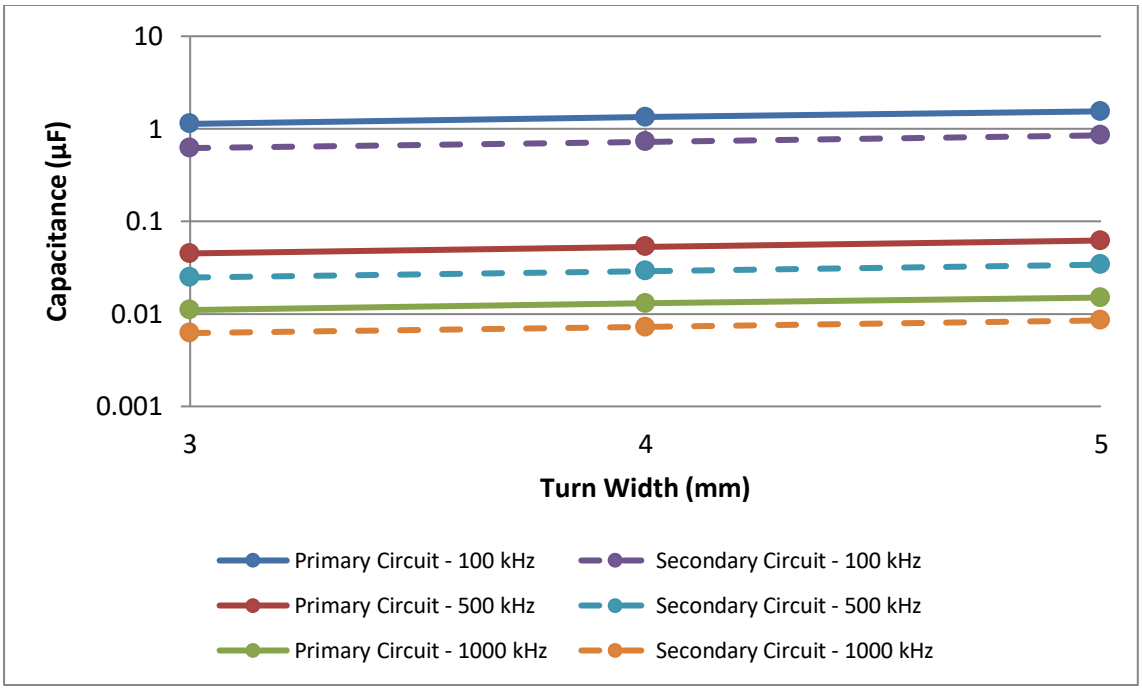

Figure 4.38: Series-Parallel Topology – Circular Coils – Capacitance (Logarithmic Scale) vs. Turn Width (d_{out} = 120 mm, N = 5 turns, s = 1 mm & d = 10 mm)

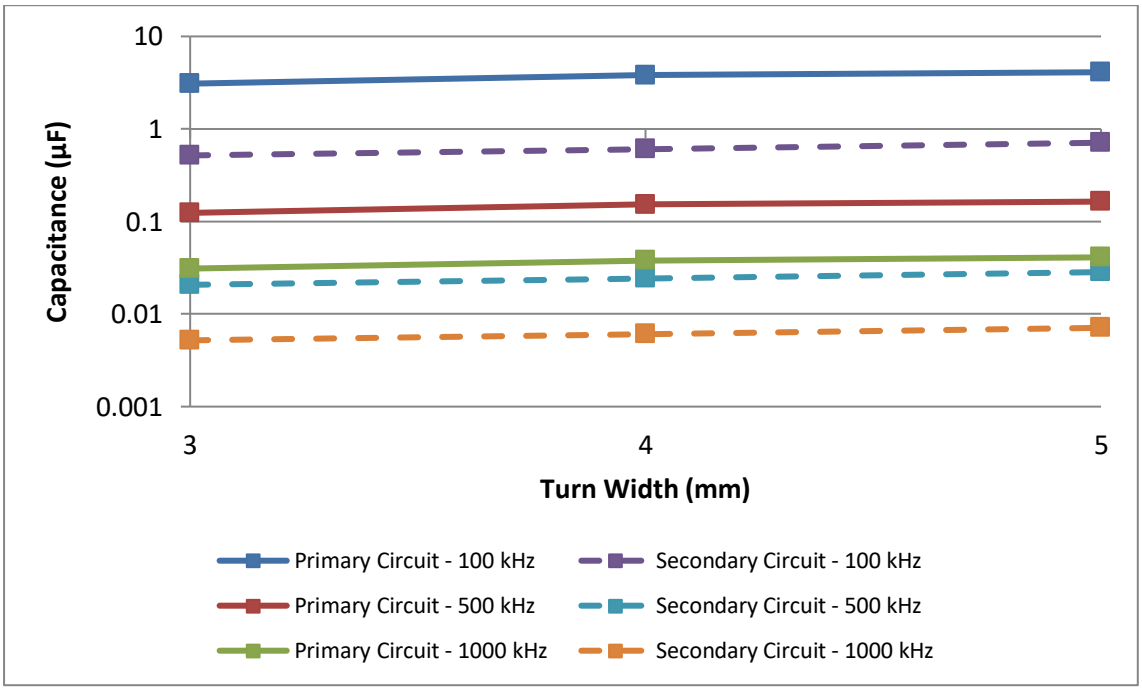

Figure 4.39: Series-Parallel Topology – Rectangular Coils – Capacitance (Logarithmic Scale) vs. Turn Width (d_{out} = 120 mm, N = 5 turns, s = 1 mm & d = 10 mm)

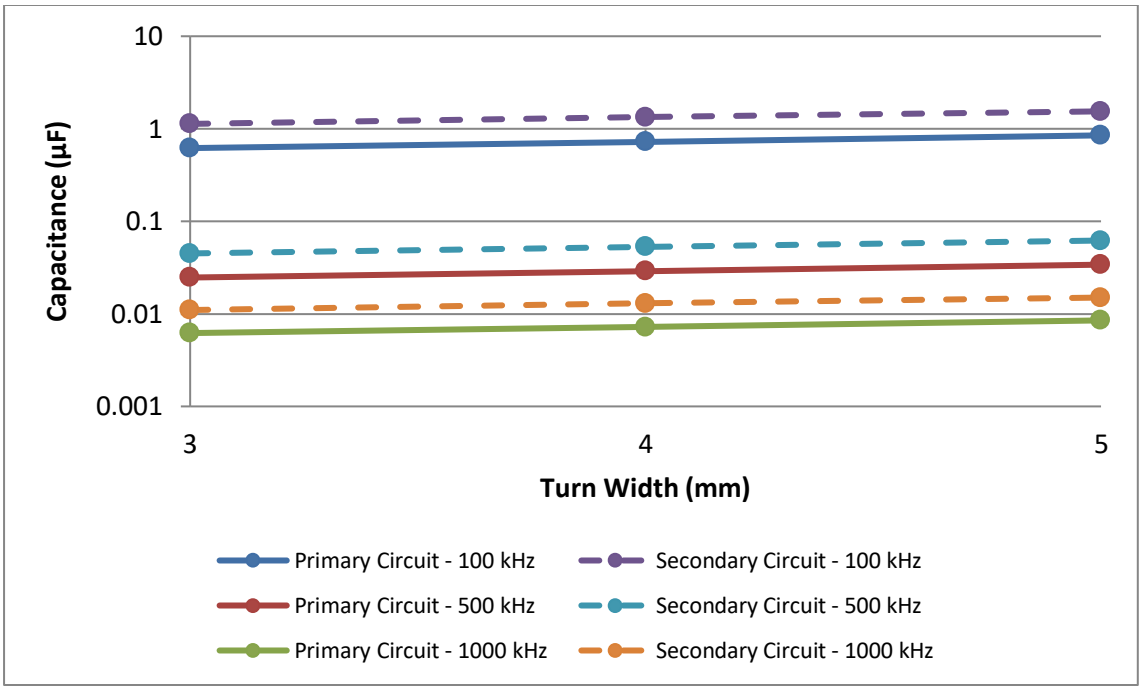

Figure 4.40: Parallel-Series Topology – Circular Coils – Capacitance (Logarithmic Scale) vs. Turn Width (d_{out} = 120 mm, N = 5 turns, s = 1 mm & d = 10 mm)

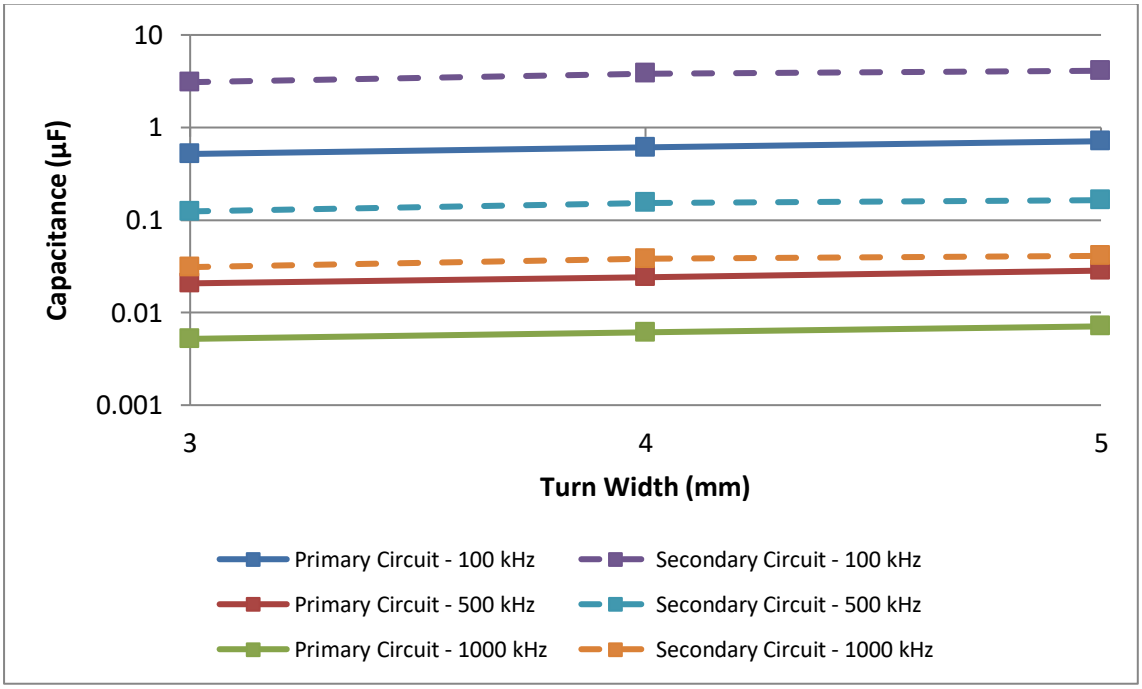

Figure 4.41: Parallel-Series Topology – Rectangular Coils – Capacitance (Logarithmic Scale) vs. Turn Width (d_{out} = 120 mm, N = 5 turns, s = 1 mm & d = 10 mm)

Another point that arises from Figures 4.38 – 4.41 is that in Series-Parallel and in Parallel-Series topologies, the capacitors that are connected in series should be bigger than the ones that are connected in parallel, since higher capacitances were obtained.

This was expected, since according to the mathematical models in Table 3.2 in Section 3.2.3, in systems that are connected wirelessly, when in one of the circuits the capacitor is connected in parallel, the capacitance of the capacitor of the other circuit that is connected in series is affected by both the self-inductances and the mutual inductance of the coils. So, for reasons that were mentioned before, the capacitors of these systems should be big enough to handle the obtained capacitances.

Finally, four extra figures (Figures 4.42 – 4.45) were created, to make the comparison of the capacitances between the systems that use circular coils and the systems that use rectangular coils easier to be seen. For the comparison, coils of number of turns equal to 5 and turn spacing equal to 1 mm were used. The distance between the coils is equal to 10 mm and each topology works at a resonant frequency of 100 kHz.

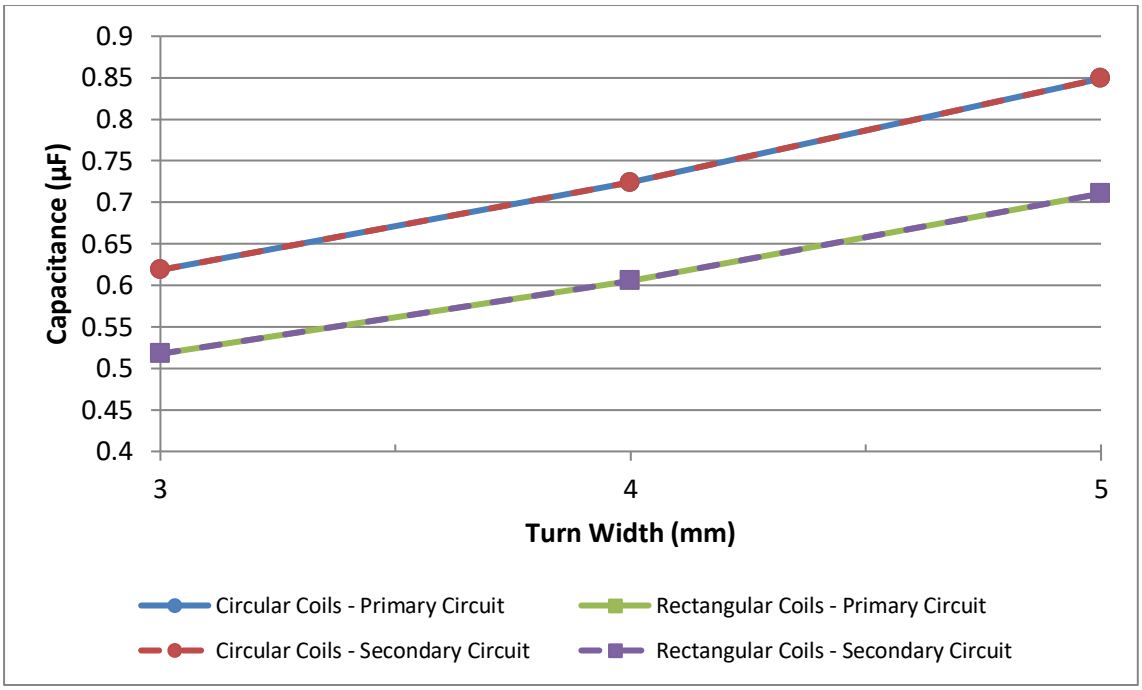

Figure 4.42: Series-Series Topology – Circular vs. Rectangular Coils – Capacitance vs. Turn Width (d_{out} = 120 mm, N = 5 turns, s = 1 mm, d = 10 mm & f_o = 100 kHz)

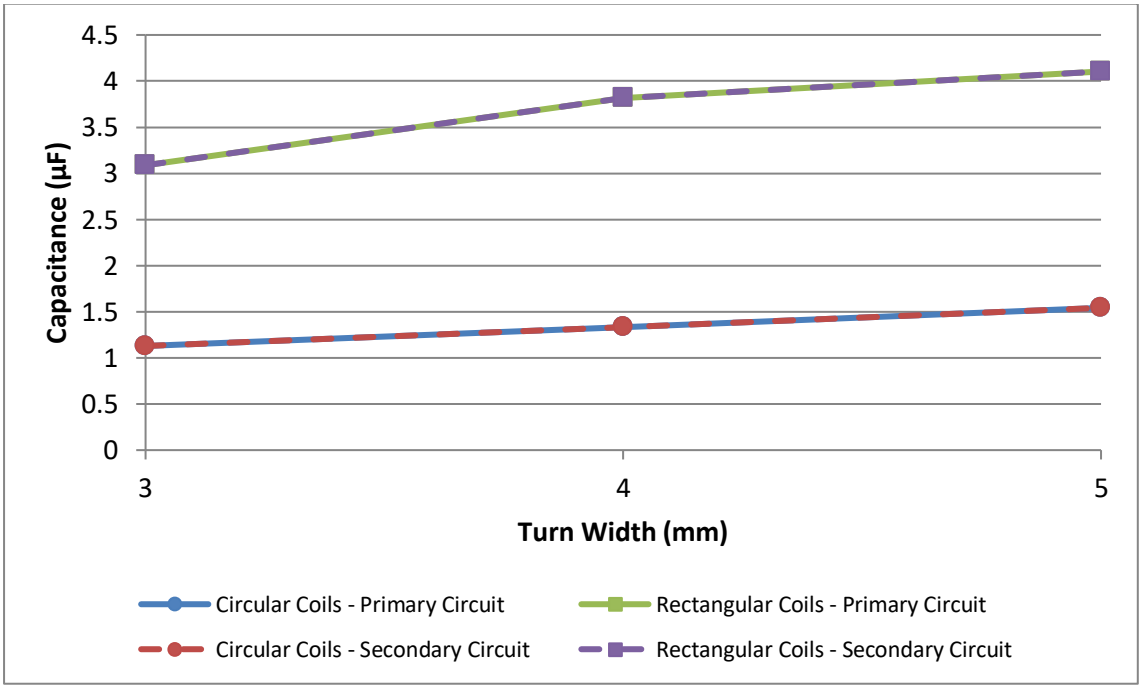

Figure 4.43: Parallel-Parallel Topology – Circular vs. Rectangular Coils – Capacitance vs. Turn Width (d_{out} = 120 mm, N = 5 turns, s = 1 mm, d = 10 mm & f_o = 100 kHz)

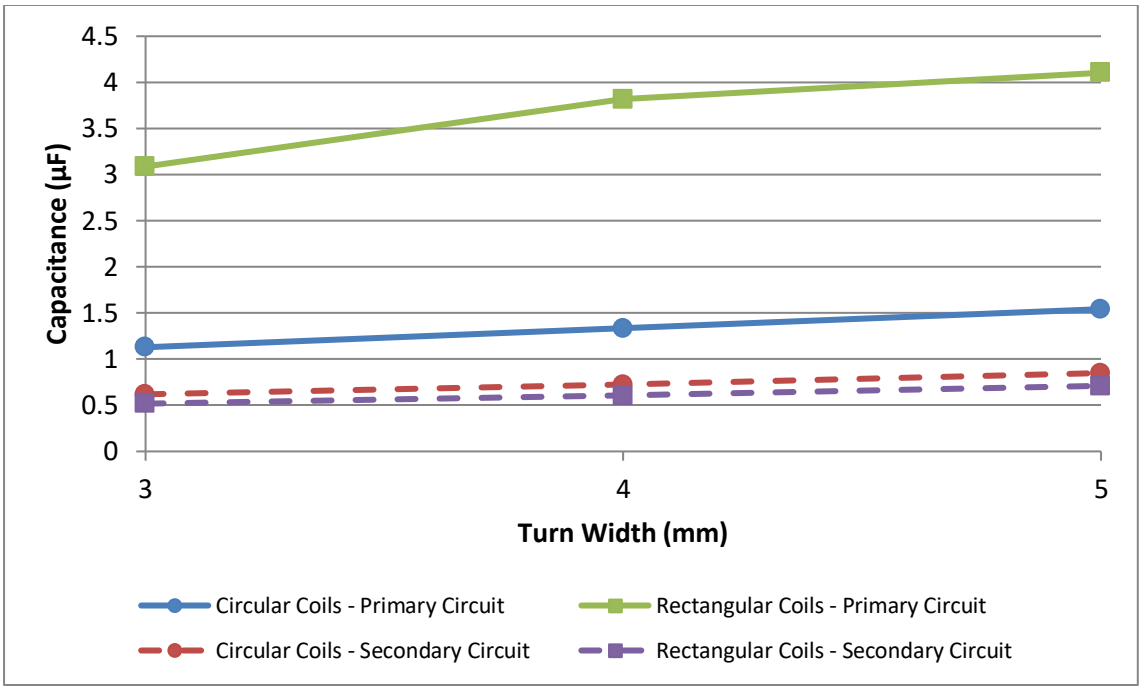

Figure 4.44: Series-Parallel Topology – Circular vs. Rectangular Coils – Capacitance vs. Turn Width (d_{out} = 120 mm, N = 5 turns, s = 1 mm, d = 10 mm & f_o = 100 kHz)

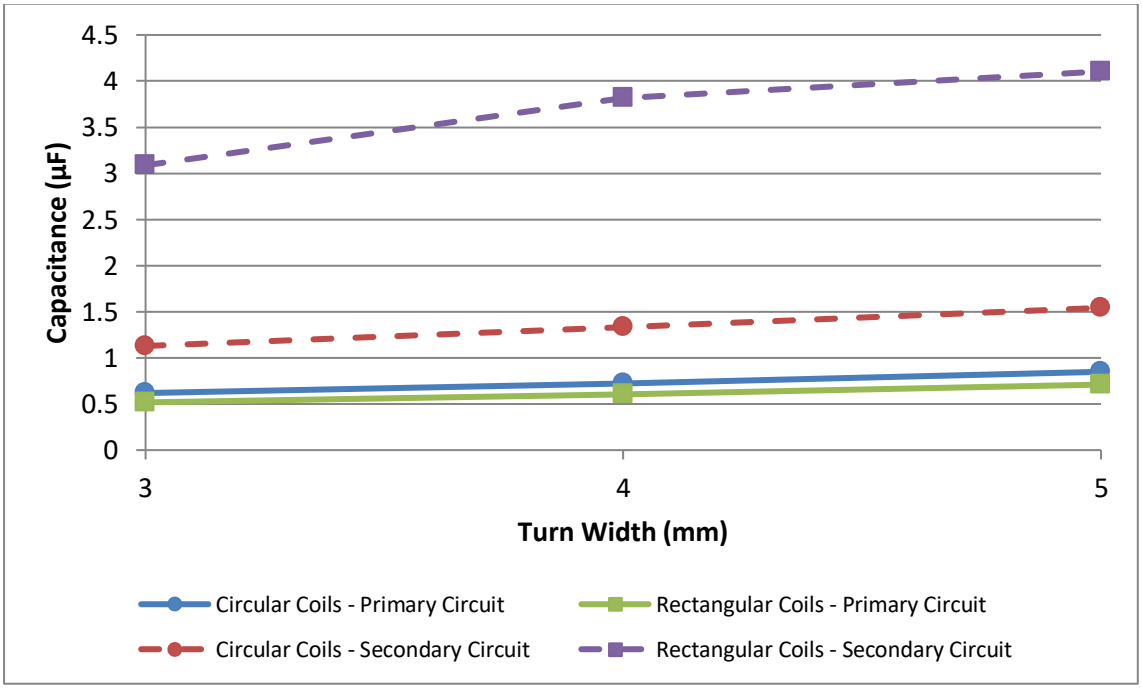

Figure 4.45: Parallel-Series Topology – Circular vs. Rectangular Coils – Capacitance vs. Turn Width (d_{out} = 120 mm, N = 5 turns, s = 1 mm, d = 10 mm & f_o = 100 kHz)

4.2 Efficiency of the Wireless Power Transfer Systems

As mentioned in the introduction chapter of the report, PV panels are one of the most advantageous ways to generate energy. However, the power that is produced from a PV panel is not constant and depends on the environmental conditions, as well as on its operating point. So, there is a need for each PV cell to work at its maximum power, and thus achieve the maximum efficiency, regardless of the standard or the varying ambient conditions [50],[51].

The Maximum Power Point (MPP) depends on the climatic and irradiation conditions. However, in this thesis project, systems that work under standard test conditions (STC) were considered. STC are the industrial test conditions under which a solar panel is tested and these are 25°C of cell temperature, 1000 $^{W}/_{m^2}$ of solar irradiance and 1.5 AM. Despite the fact that operation under varying environmental conditions has not been considered, they are relevant and deserve further study, discussion and development [50],[51].

At first, the results for systems that are connected with one IBC solar cell that works at maximum power point, with voltage (V_{mpp}) of 0.6 V and current (I_{mpp}) of 5.9 A, will be presented. Afterwards, results for the case of 16 series-connected solar cells will be presented as well. All these results come from simulations that were held using Simulink. In these simulations, ideal DC/AC conversion has been assumed and the load resistance that makes the generator work at its MPP is calculated through the mathematical models that have been developed in Chapter 3. An example of one of the Simulink models that were developed and used for the simulations it can be seen in Figure 4.46.

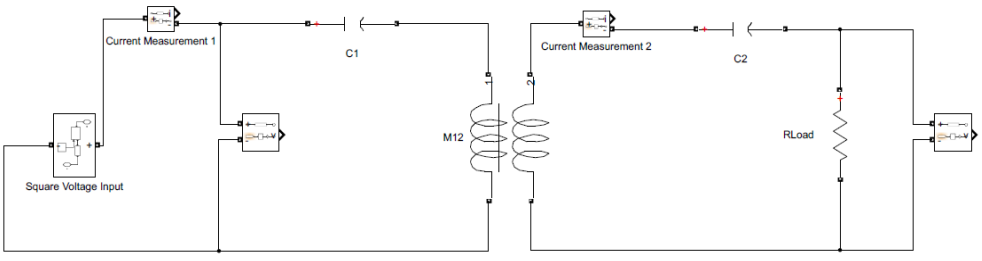

Figure 4.46: Simulink Model of the Series-Series Compensation Topology

4.2.1 Effect of the Cross-Section of Coils on System's Efficiency – 1 Solar Cell

In Figures 4.47 & 4.48, in Series-Series topology, both circular and rectangular planar coils, at a resonant frequency of 100 kHz, with a range of turn width between 3 and 5 mm, with number of turns between 5 and 8 and with rectangular cross-section, help the systems develop higher efficiencies, in comparison to the systems with coils with circular cross-section.

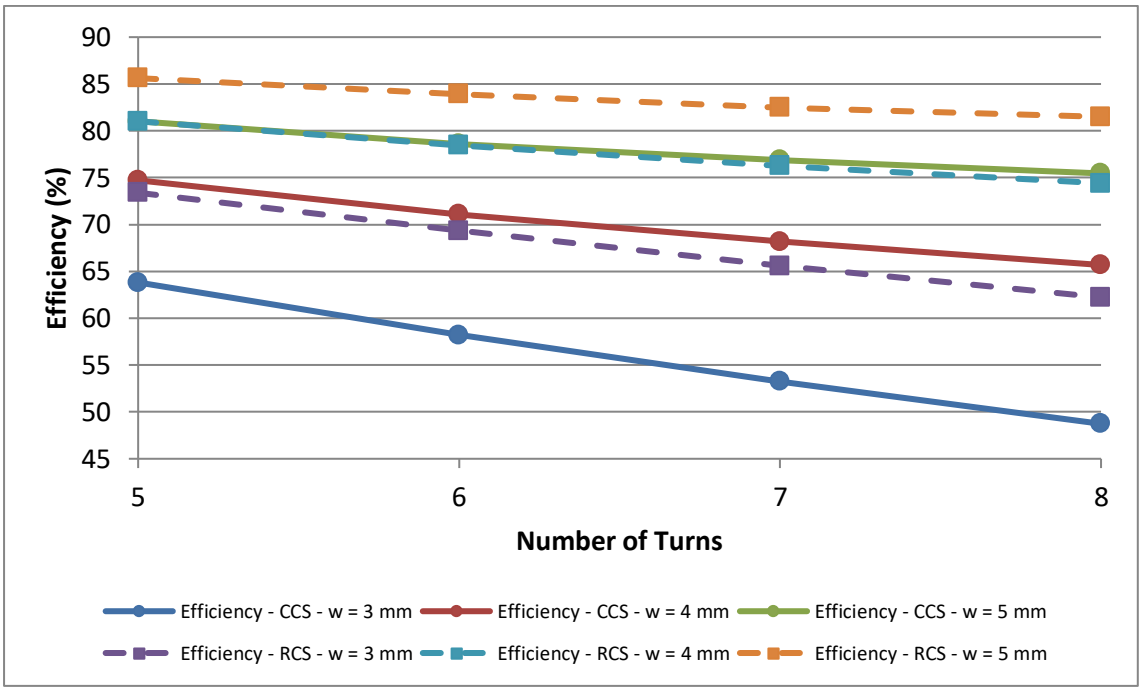

Figure 4.47: Series-Series – Circular Coils – Circular vs. Rectangular Cross-Section – Efficiency vs. Number of Turns (d_{out} = 120 mm, s = 1 mm, d = 10 mm & f_o = 100 kHz)

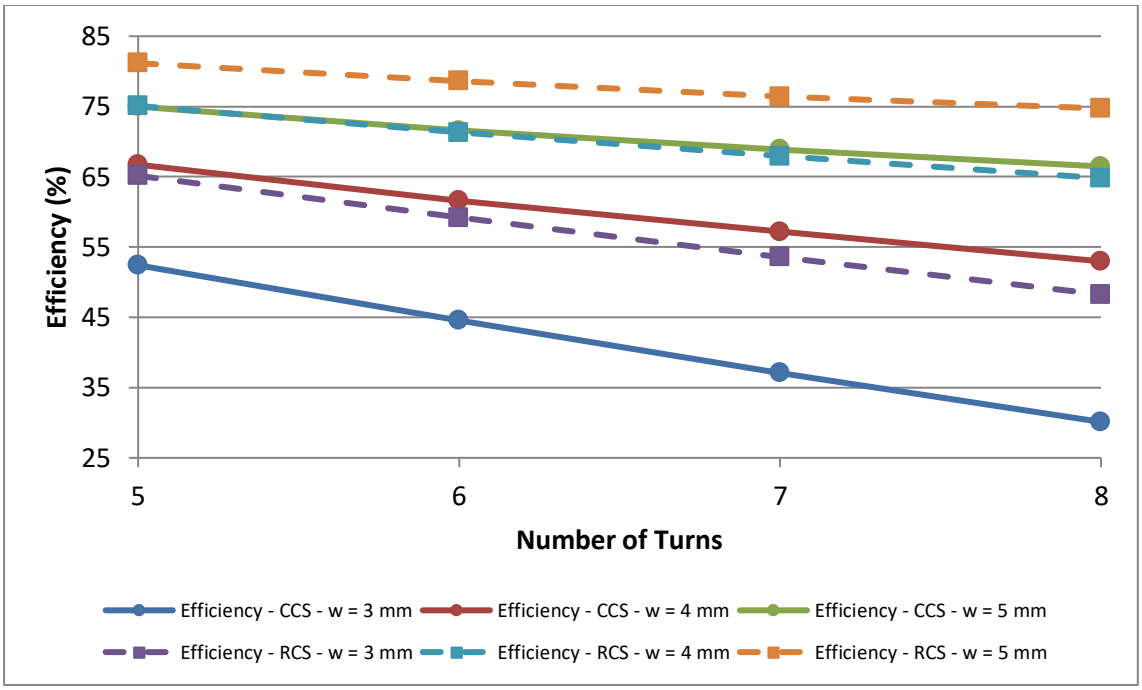

Figure 4.48: Series-Series – Rectangular Coils – Circular vs. Rectangular Cross-Section – Efficiency vs. Number of Turns (d_{out} = 120 mm, s = 1 mm, d = 10 mm & f_o = 100 kHz)

This happens, since the coils with rectangular cross-section develop lower parasitic resistances than the coils with circular cross-section, due to the fact that the surface of the rectangular cross-section is bigger than the surface of the circular one and the skin effect is less significant. (See also Appendix B, Tables B.65 – B.68)

For the exact same reasons, in Figures 4.49 & 4.50, it is clear that in Series-Parallel topology the coils with rectangular cross-section help the systems to develop better efficiencies too, in comparison to the ones with circular cross-section.

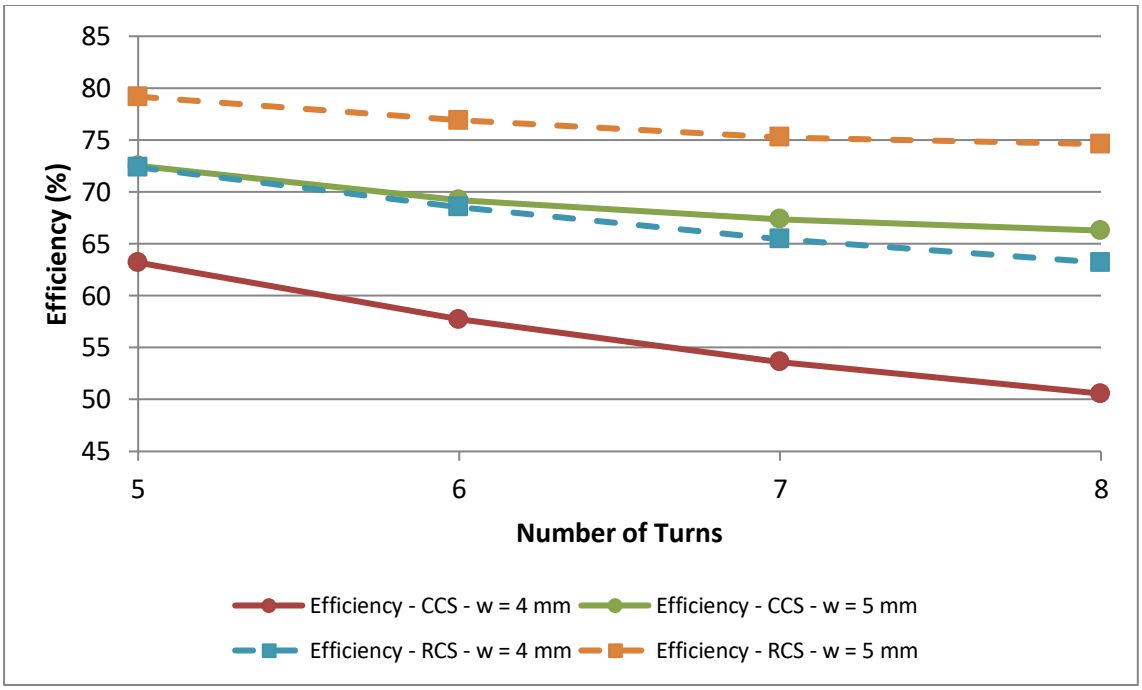

Figure 4.49: Series-Parallel – Circular Coils – Circular vs. Rectangular Cross-Section – Efficiency vs. Number of Turns (d_{out} = 120 mm, s = 1 mm, d = 10 mm & f_o = 100 kHz)

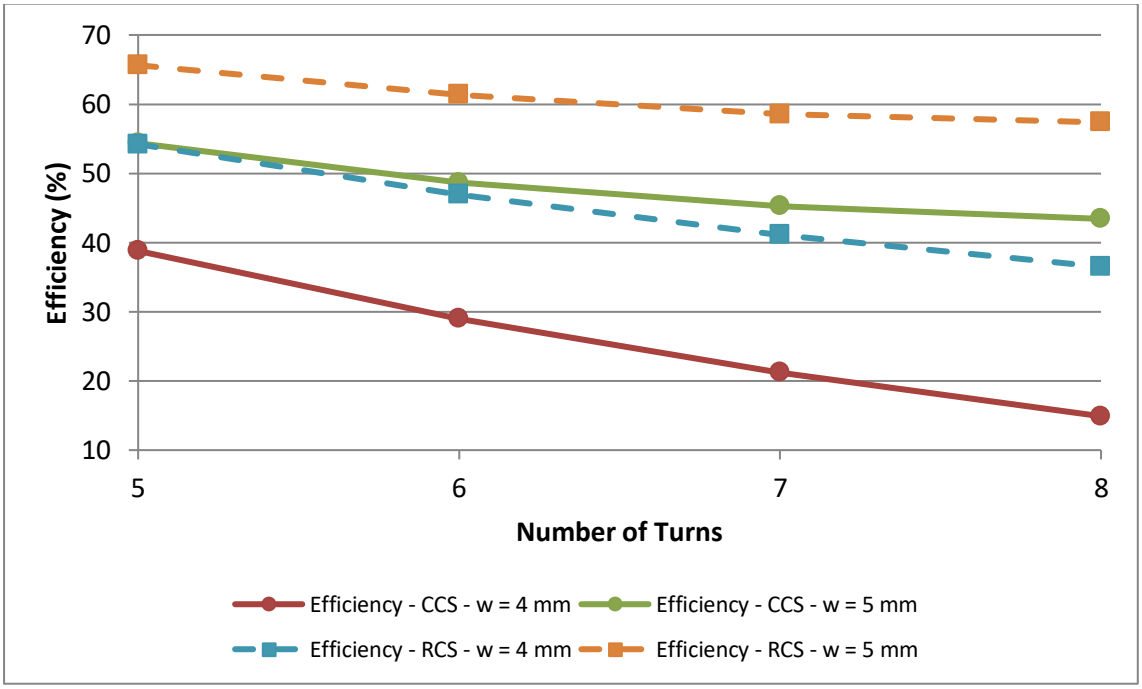

Figure 4.50: Series-Parallel – Rectangular Coils – Circular vs. Rectangular Cross-Section – Efficiency vs. Number of Turns (d_{out} = 120 mm, s = 1 mm, d = 10 mm & f_o = 100 kHz)

However, in Figures 4.49 & 4.50, there are only cases of coils with turn widths equal to 4 and 5 mm. This is the case, since in Series-Parallel topology, for rectangular coils with circular cross-section, turn width equal to 3 mm and a range of 6 to 8 turns, the IBC solar cell could not operate at MPP and the main reason might be that the losses were too high. (See also Appendix B, Tables B.69 – B.72)

Lastly, in Figures 4.51 & 4.52, it can be seen, for once again, that in Parallel-Series and in Parallel-Parallel topologies the systems with coils with rectangular cross-section have better efficiencies, than those with coils with circular cross-section.

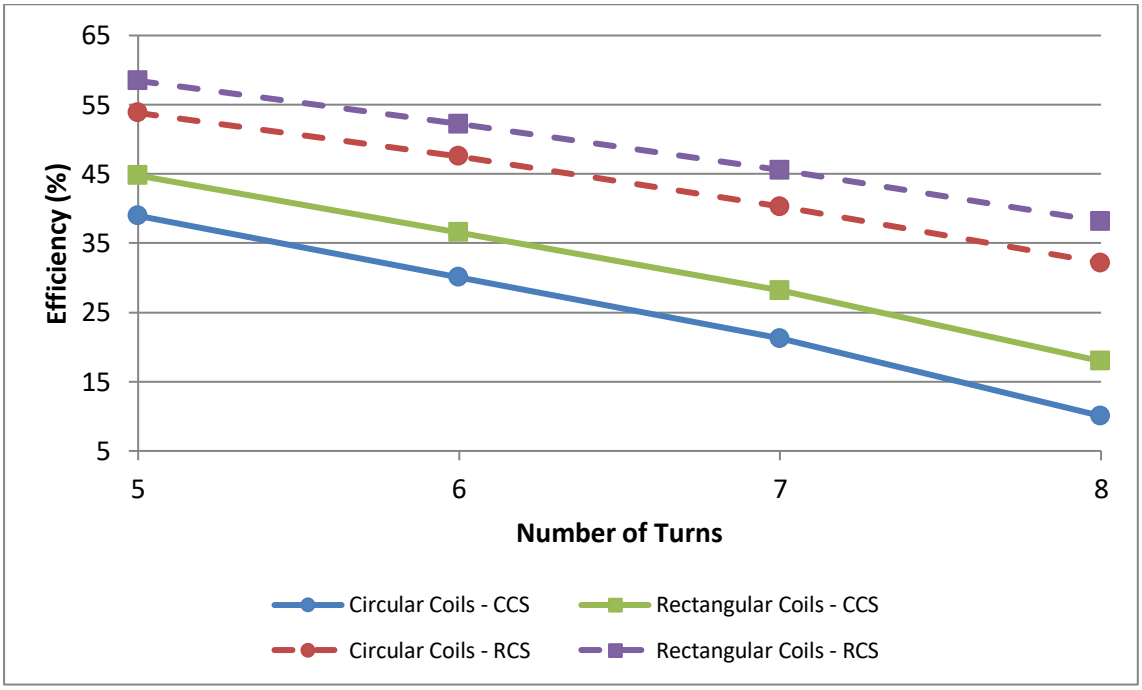

Figure 4.51: Parallel-Series – Circular & Rectangular Coils – Circular vs. Rectangular Cross-Section – Efficiency (%) vs. Number of Turns (d_{out} = 120 mm, w = 5 mm, s = 1 mm, d = 10 mm & f_o = 100 kHz)

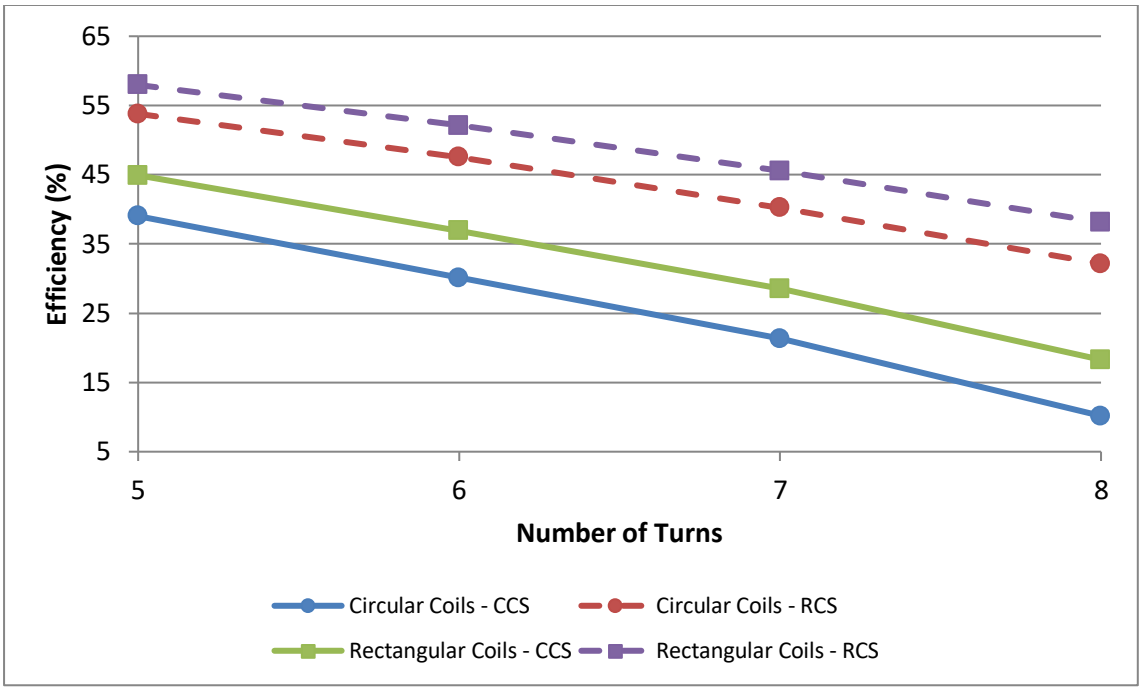

Figure 4.52: Parallel-Parallel – Circular & Rectangular Coils – Circular vs. Rectangular Cross-Section – Efficiency (%) vs. Number of Turns (d_{out} = 120 mm, w = 5 mm, s = 1 mm, d = 10 mm & f_o = 100 kHz)

However, in these topologies, only the systems with coils of 5 mm turn width were studied, because for coils with lower values of turn width (3 and 4 mm), in some cases, the solar cell could not operate at its MPP, probably due to high losses. (See also Appendix B, Tables B.73 – B.80)

In conclusion, from Figures 4.47 – 4.52 and as mentioned in the previous sections, the best option of coils to help the systems transfer power wirelessly in a more efficient way and develop high efficiencies is coils with rectangular cross-section.

4.2.2 Effect of the Shape of Coils on System's Efficiency – 1 Solar Cell

As far as the shape of planar coils is concerned, from Figures 4.53 & 4.54, it can be seen that in Series-Series and in Series-Parallel topologies, in every case scenario of turn width and number of turns, the circular planar coils with rectangular cross-section seems to be the most ideal option for the development of higher efficiencies, compared to the rectangular coils with rectangular cross-section.

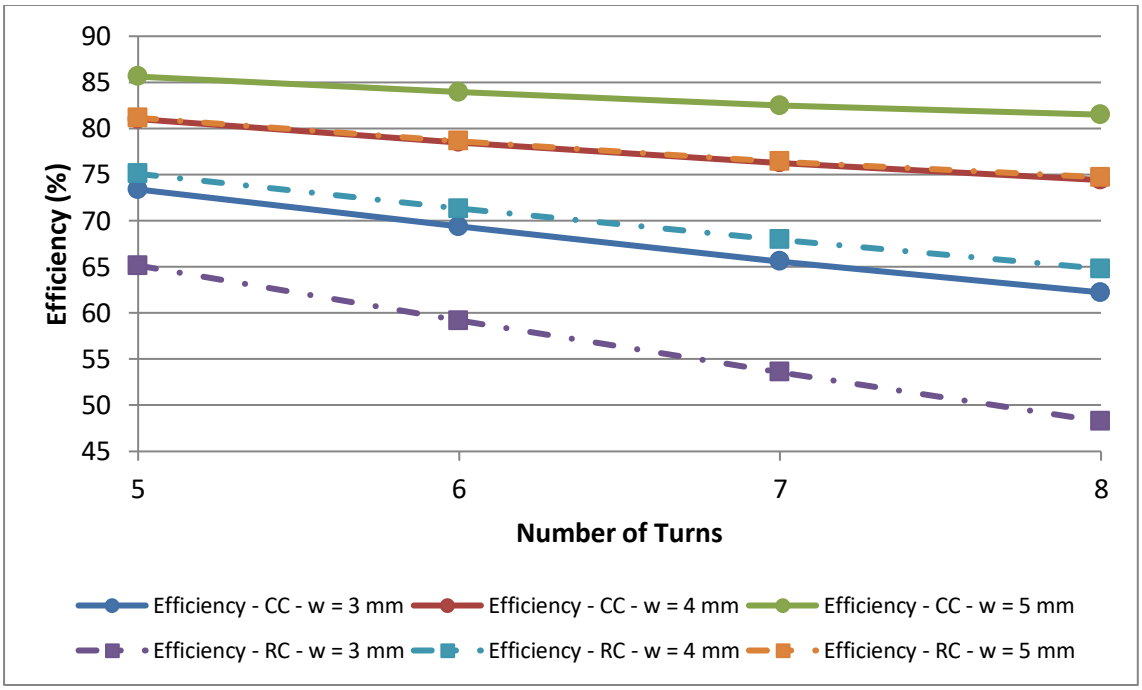

Figure 4.53: Series-Series – Circular vs. Rectangular Coils – Rectangular Cross-Section – Efficiency (%) vs. Number of Turns (d_{out} = 120 mm, s = 1 mm, d = 10 mm & f_o = 100 kHz)

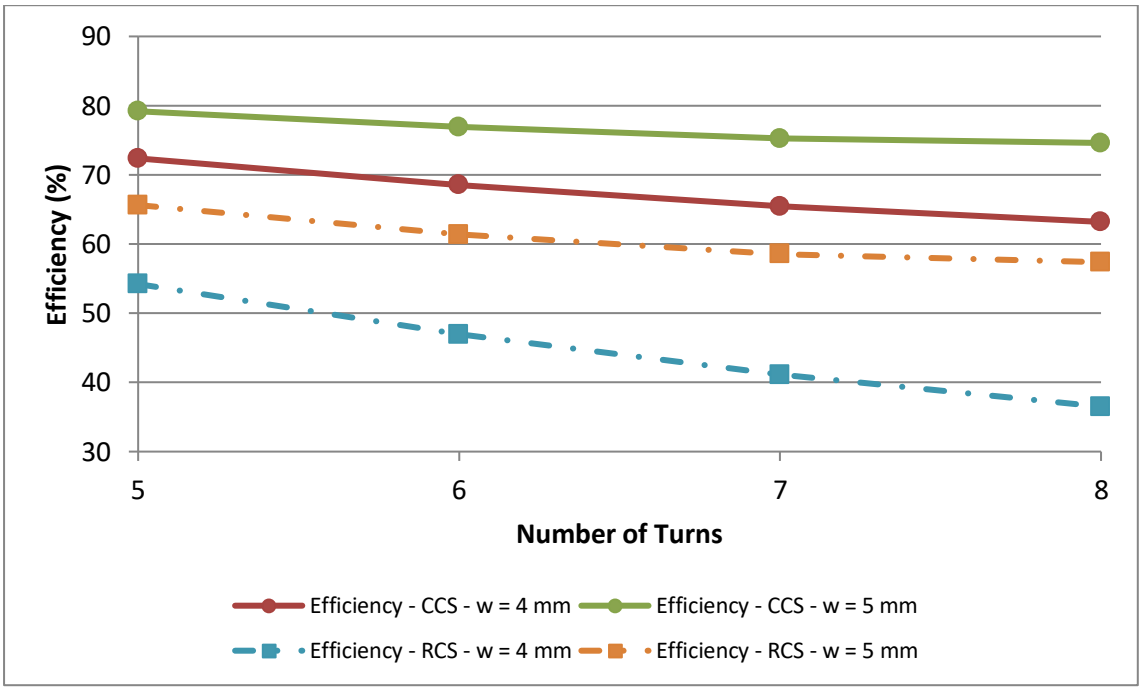

Figure 4.54: Series-Parallel – Circular vs. Rectangular Coils – Rectangular Cross-Section – Efficiency (%) vs. Number of Turns (d_{out} = 120 mm, s = 1 mm, d = 10 mm & f_o = 100 kHz)

However, it seems that according to Figures 4.55 & 4.56, in Parallel-Series and in Parallel-Parallel topologies higher efficiencies are developed in systems that use rectangular coils.

This happens, since in Series-Series and in Series-Parallel topologies higher currents can flow through the circuits with coils of rectangular shape and end up to the load, in comparison to the currents that end up to the load of circuits with circular coils. The exact opposite happens in the Parallel-Series and Parallel-Parallel topologies. Higher currents result in higher losses and thus lower efficiencies.

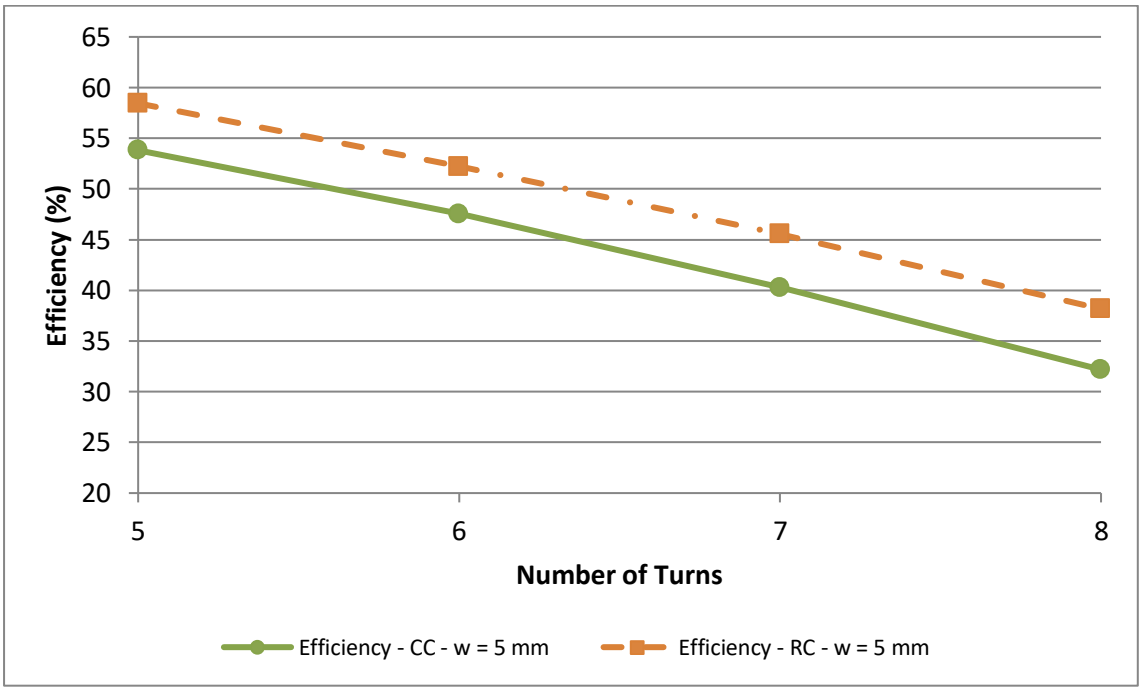

Figure 4.55: Parallel-Series – Circular vs. Rectangular Coils – Rectangular Cross-Section – Efficiency (%) vs. Number of Turns (d_{out} = 120 mm, s = 1 mm, d = 10 mm & f_o = 100 kHz)

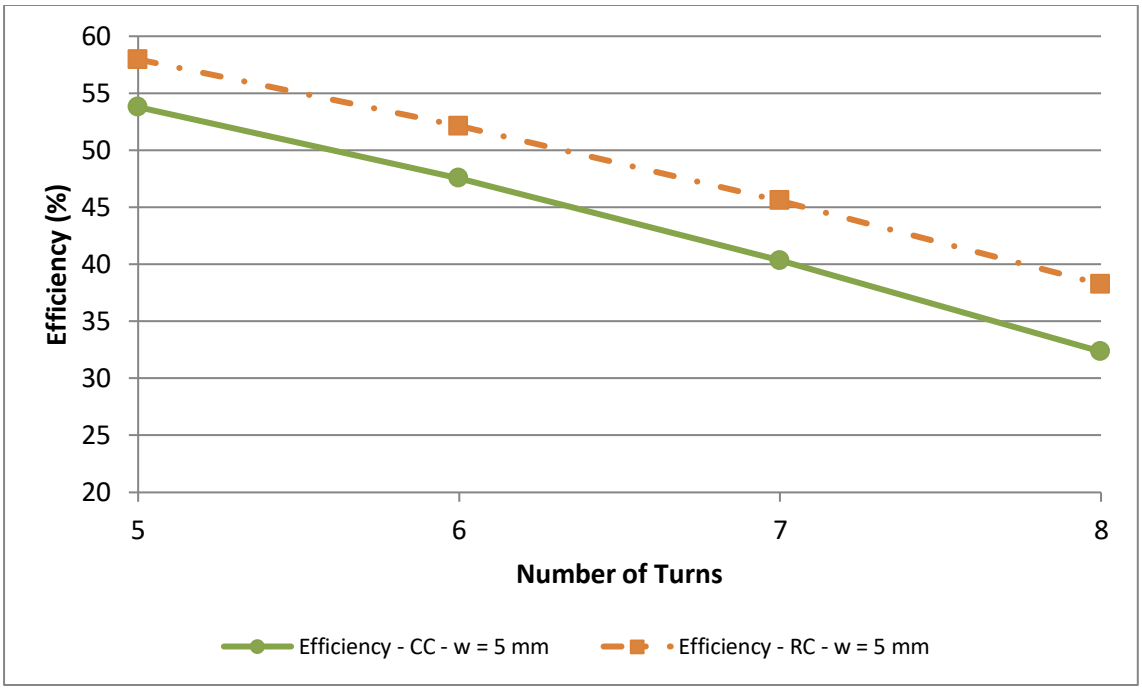

Figure 4.56: Parallel-Parallel – Circular vs. Rectangular Coils – Rectangular Cross-Section – Efficiency (%) vs. Number of Turns (d_{out} = 120 mm, s = 1 mm, d = 10 mm & f_o = 100 kHz)

In Tables 4.1 & 4.2, the exact values of the currents (I_L, I_C, I_{Load}) that flow through the capacitors, the inductors and the loads of the circuits, for both circular (CC) and rectangular (RC) coils, can be seen. The comparison has been made between the Series-Parallel and the Parallel-Series compensation topologies.

Table 4.1: Peak (MAX) & Root Mean Square (RMS) Currents for Series-Parallel Compensation Topology

CC	**I_{C1} (A)**	**I_{L1} (A)**	**I_{L2} (A)**	**I_{C2} (A)**	**I_{Load} (A)**
MAX	9,198	9,198	**6,184**	0,493	**6,171**
RMS	6,503	6,503	**4,372**	0,349	**4,363**
RC	**I_{C1} (A)**	**I_{L1} (A)**	**I_{L2} (A)**	**I_{C2} (A)**	**I_{Load} (A)**
MAX	9,258	9,258	**8,435**	0,284	**8,430**
RMS	6,545	6,545	**5,964**	0,201	**5,960**

Table 4.2: Peak (MAX) & Root Mean Square (RMS) Currents for Parallel-Series Compensation Topology

CC	I_{C1} **(A)**	I_{L1} **(A)**	I_{L2} **(A)**	I_{C2} **(A)**	I_{Load} **(A)**
MAX	0	8,025	**13,741**	13,732	**13,732**
RMS	0	5,674	**9,715**	9,709	**9,709**
RC	I_{C1} **(A)**	I_{L1} **(A)**	I_{L2} **(A)**	I_{C2} **(A)**	I_{Load} **(A)**
MAX	0	10,471	**9,733**	9,731	**9,731**
RMS	0	7,403	**6,881**	6,880	**6,880**

At this point, it should be mentioned that the systems need coils with low number of turns and high values of turn width, to achieve efficient Wireless Power Transfer. So, according to the comparisons that had been made, for a range of turn widths between 3 and 5 mm, the most ideal option seems to be coils with turn width of 5 mm and for a range of number of turns between 5 and 8, the best option seems to be coils with 5 turns.

To sum up, in Series-Series and in Series-Parallel topologies, the most ideal option is circular coils with rectangular cross-section, d_{out} = 120 mm, N = 5 turns, w = 5 mm, s = 1 mm and d = 10 mm. On the other hand, in Parallel-Series and in Parallel-Parallel topologies, the best option seems to be rectangular coils with rectangular cross-section, d_{out} = 120 mm, N = 5 turns, w = 5 mm, s = 1 mm and d = 10 mm.

4.2.3 Effect of the Compensation Topology on System's Efficiency – 1 Solar Cell

In Figure 4.57, it can be seen that in Series-Series compensation topology, the systems with circular coils and rectangular cross-section develop higher efficiencies, in comparison to the systems of the other compensation topologies.

The main reason of it is that in Series-Series topology lower currents flow through the circuits with circular coils and rectangular cross-section, in comparison to the currents that flow through the circuits of the other topologies. Therefore, the losses are less and the systems develop higher efficiencies.

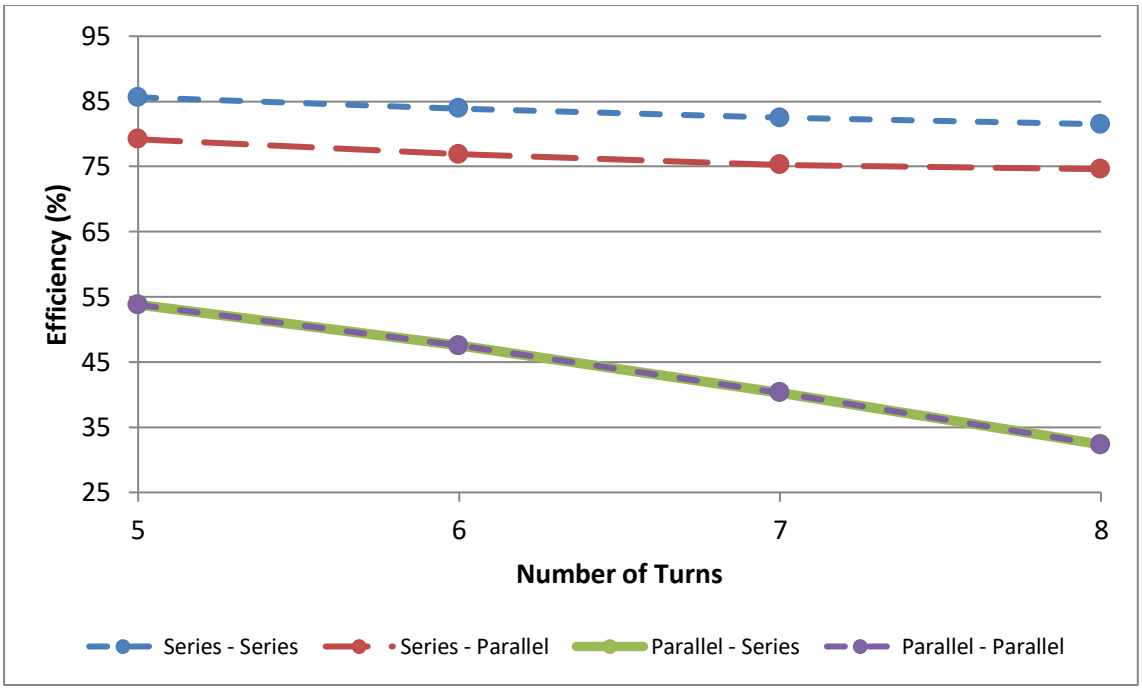

Figure 4.57: Circular Coils with Rectangular Cross-Section – Efficiency (%) vs. Number of Turns (d_{out} = 120 mm, w = 5 mm, s = 1 mm, d = 10 mm & f_o = 100 kHz)

Another thing that can be observed in Figure 4.57 is that in Parallel-Series and in Parallel-Parallel compensation topologies, the systems develop almost the same efficiencies. However, in Parallel-Series topology the efficiencies are slightly higher (0.05 – 0.09%).

The main reason of it is that in Parallel-Series topology slightly lower currents flow through the circuits, in comparison to the currents that flow through the circuits of the Parallel-Parallel topology. Therefore, the losses are slightly less and the systems in Parallel-Series topology develop slightly higher efficiencies, than the ones in Parallel-Parallel topology.

Finally, from Figure 4.58 it is clear that similar trends are obtained for systems with rectangular coils with rectangular cross-section, d_{out} = 120 mm, w = 5 mm, s = 1 mm and d = 10 mm, at 100 kHz.

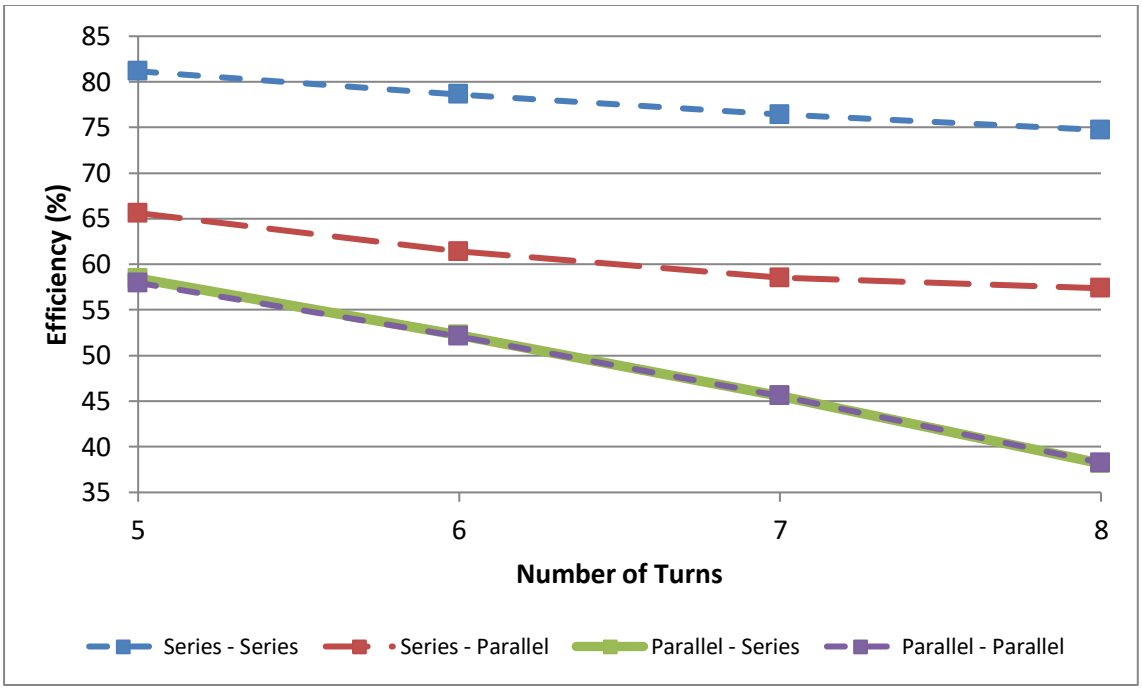

Figure 4.58: Rectangular Coils with Rectangular Cross-Section – Efficiency (%) vs. Number of Turns (d_{out} = 120 mm, w = 5 mm, s = 1 mm, d = 10 mm & f_o = 100 kHz)

4.2.4 Efficiency of Circuits Connected to 16 Solar Cells

In this section, the results for systems that are connected with a module, that consists of 16 IBC solar cells, connected in series, will be presented. The module works at MPP, with voltage (V_{mpp}) of 9.6 V and current (I_{mpp}) of 5.9 A. According to the results that were presented in the previous chapter, it is clear that the systems develop higher efficiencies in Series-Series and in Series-Parallel compensation topologies. In these topologies, the coils of circular shape with rectangular cross-section help the systems develop better efficiencies.

So, for the simulations of the circuits that are connected with the 16 solar cell module, the results of the Series-Series and Series-Parallel topologies will be presented. In these simulations that were held using Simulink, circular planar coils with rectangular cross-section, external diameter of 120 mm, number of turns equal to 5, turn width equal to 5 mm and turn spacing equal to 1 mm, were used, for a distance between the coils of 10 mm.

All these values are the values of the main parameters of the coils, for which the circuits that were connected with one solar cell worked more efficiently and at the same time balanced the coupling capabilities and the parasitic resistances of the coils. So, the exact same values were used for these simulations too.

In Figure 4.59, it can be observed that for systems with circuits connected to one module of 16 solar cells, the efficiencies are much higher, in comparison to the efficiencies of systems with circuits connected to 1 solar cell, which was expected, since higher amounts of energy can be transferred. (See also Appendix B, Tables B.81 – B.84)

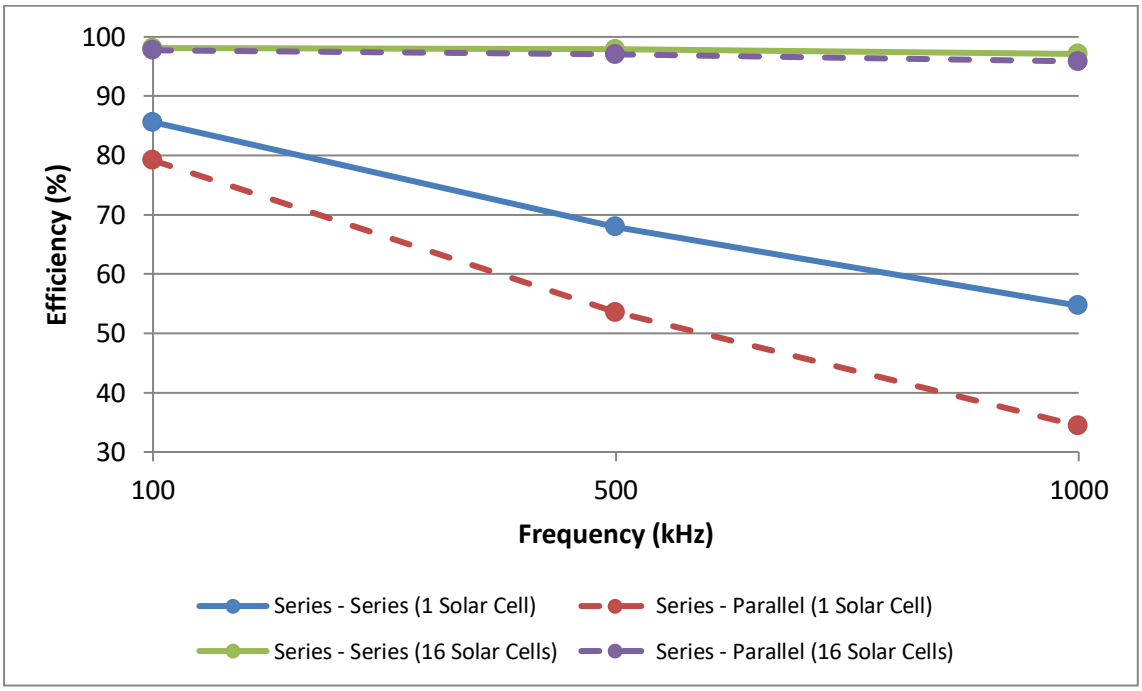

Figure 4.59: Circular Coils with Rectangular Cross-Section – Efficiency (%) vs. Frequency (d_{out} = 120 mm, N = 5 turns, w = 5 mm, s = 1 mm & d = 10 mm)

5 Conclusions & Discussion

During this project, the main goals were to understand how Wireless Power Transfer techniques and more specifically, how Magnetic Resonant Coupling can be efficiently incorporated into PV devices, such as PV cells and modules, find out whether these techniques in theory and in practice are efficient enough and suggest the best design approach as a guideline for near future prototyping.

First of all, according to the results that were presented in Chapter 4, for systems that are connected wirelessly, the most ideal coils are the planar coils of circular or rectangular shape with rectangular cross-section. This happens since the rectangular cross-section is bigger than the circular one and the skin effect less significant, resulting in lower parasitic resistances and thus lower conduction losses.

As far as the shape of coils and compensation topologies are concerned, in Series-Series and in Series-Parallel topologies, the circular planar coils help the systems develop higher efficiencies, in comparison to the rectangular ones. On the other hand, in Parallel-Series and in Parallel-Parallel compensation topologies, the rectangular planar coils help the systems develop higher efficiencies.

However, the efficiencies of the systems in Series-Series compensation topology are higher than the ones in Series-Parallel, in Parallel-Series and in Parallel-Parallel topologies. So, the most ideal option seems to be systems in which the components of the circuits are connected in series and circular planar coils, with rectangular cross-section, are used.

Furthermore, the main coil parameters are the ones that affect the self-inductances, the mutual inductance, the coupling coefficient and the parasitic resistances of the coils. The main purpose was to find combinations of coil parameters that would balance the coupling capabilities and the parasitic resistances of the coils.

After the development of the main mathematical models and the simulations that were held using both Matlab and Simulink, both types of planar coils (circular and rectangular), with external diameter equal to 120 mm, number of turns equal to 5, turn width and turn spacing equal to 5 and 1 mm, respectively and a distance between the coils of 10 mm, managed to balance the coupling capabilities and the parasitic resistances of the coils, and thus helped the systems to develop high efficiencies. Here, it should be mentioned that these values are the best options for the specific regions of values that were tested.

Also, the systems developed higher efficiencies in lower frequencies. So, for a range between 100 and 1000 kHz, the best option is a resonant frequency of 100 kHz, in which the parasitic resistances are lower and the conduction losses less.

In addition, the systems that are connected to a module of 16 series-connected IBC solar cells developed much higher efficiencies, higher than 97%, in comparison to the ones that are connected to only one IBC solar cell, which reached efficiencies of 85%. This was expected since higher amounts of power were inserted in the primary circuit, and thus higher amounts of power were transferred wirelessly from the primary circuit to the secondary one, in comparison to the amounts of power that were transferred from a solar cell.

So, in theory, for the ideal cases that were studied during this research, Magnetic Resonant Coupling method is efficient enough. However, in practice, it might be less efficient, since many other factors should be taken into account, such as the losses of DC/AC conversion and the proximity effect, and further research should be made.

Taking everything into consideration, as a follow up of this research, it is recommended to run simulations of the systems in varying ambient conditions, since they were simulated in standard test conditions (STC) only. Furthermore, it is also recommended to simulate the systems by taking into account the proximity effect and doing further research on the mathematical models of the mutual inductance in the case of the rectangular coils, since there are many

different approaches that could give more accurate results, such as the Finite Element Method (FEM), by using software packages, such as COMSOL.

Some other recommendations would be (1) further simulations on the coil parameters and finding new combinations that would lead to even or better balances between the coupling capabilities and the parasitic resistances, (2) simulations of the systems in non-ideal conditions, namely with misalignments between the coils or with losses that haven't been included in these cases, (3) developing Simulink models, that account for the frequency splitting, since is the main drawback of the Magnetic Resonant Coupling and questions on when this phenomenon happens are still open, (4) studying systems that are connected with modules that consist of higher number of solar cells, (5) studying systems for longer or shorter distances between the coils and (6) studying systems that include DC to AC conversion losses.

Also, the simulation framework developed during this project, namely the mathematical and Simulink models, represents the backbone for further research on this topic. Rather than recreating everything from scratch, the simulation framework can be updated with novel and more accurate models that for instance include a non-ideal DC/AC converter, or the resistances of the capacitors, or ways to study the frequency splitting and so on.

Bibliography

[1] V. V. Tyagi, “Progress in Solar PV Technology Research and Achievement,” *Renewable and Sustainable Energy Reviews*, p. 20, 2013.

[2] A. HM Smets, K. Jäger, O. Isabella, R. ACMM van Swaaij, and M. Zeman, *Solar Energy: The Physics and Engineering of Photovoltaic Conversion, Technologies and Systems*. 2016.

[3] “Air Pollution - Greenhouse Gases | Britannica.” https://www.britannica.com/science/air-pollution/Greenhouse-gases (accessed Nov. 03, 2021).

[4] “Climate change and coronavirus: Five charts about the biggest carbon crash,” *BBC News*, May 05, 2020. Accessed: Nov. 03, 2021. [Online]. Available: https://www.bbc.com/news/science-environment-52485712

[5] “Solar Cell,” *Brittanica*, Jun. 2020. https://www.britannica.com/technology/solar-cell (accessed Nov. 11, 2021).

[6] “History of Photovoltaics,” *Florida Solar Energy Center*. http://www.fsec.ucf.edu/en/consumer/solar_electricity/basics/history_of_pv.htm (accessed Apr. 27, 2021).

[7] Anshu Bhaeadwaj, Jain Pratah, Ghosh Saptak, and Raed Bkayrat, “Future of Solar Photovoltaic - Deployment, investment, technology, grid integration and socio-economic aspects,” International Renewable Energy Agency (IRENA), Abu Dhabi, Nov. 2019.

[8] A. Langner, “Photovoltaics Report,” p. 50.

[9] “From a Solar Cell to a PV System.” https://commons.wikimedia.org/wiki/File:From_a_solar_cell_to_a_PV_system.svg (accessed Nov. 03, 2021).

[10] A. M. Bagher, M. M. A. Vahid, and M. Mohsen, “Types of Solar Cells and Application,” p. 21.

[11] Unknown, “Earth4Energy Review: What Is Difference Between Monocrystalline Polycrystalline And Amorphous Thin Film Solar Cell?,” *Earth4Energy Review*, Dec. 08, 2013. http://earth4energyreviewinfo.blogspot.com/2013/12/what-is-difference-between.html (accessed Nov. 16, 2021).

[12] A. Blakers, “Development of the PERC Solar Cell,” *IEEE JOURNAL OF PHOTOVOLTAICS*, vol. 9, no. 3, p. 7, 2019.

[13] “High Efficiency Solar Cells | PVEducation.” https://www.pveducation.org/pvcdrom/manufacturing-si-cells/high-efficiency-solar-cells (accessed Nov. 03, 2021).

[14] “Most powerful solar panels 2021 — Clean Energy Reviews.” https://www.cleanenergyreviews.info/blog/most-powerful-solar-panels (accessed Nov. 04, 2021).

[15] H. Wirth, K.-A. Weiss, and C. Wiesmeier, *Photovoltaic Modules: Technology and Reliability*. De Gruyter, 2016.

[16] M. T. Zarmai, N. N. Ekere, C. F. Oduoza, and E. H. Amalu, "A review of interconnection technologies for improved crystalline silicon solar cell photovoltaic module assembly," School of Engineering, Faculty of Science and Engineering, University of Wolverhampton, Wolverhampton, United Kingdom, 2015.

[17] "Solder Melting Temperature - What is it and why is it important?," *AMETEK ECP.*, May 2019. www.ametek-ecp.com/resources/blog/2019/may/what-is-solder-melting-point (accessed Apr. 27, 2021).

[18] J. H. Bultman *et al.*, "PIN UP module: a design for higher efficiency, easy module manufacturing and attractive appearance," p. 5.

[19] A. Chourzamanis, "Wireless Power Transfer Extra Project," 2020.

[20] J. Serrano, M. Perez-Tarragona, C. Carretero, and J. Acero, "Modeling, Simulation and Verification of Contactless Power Transfer Systems," p. 6, 2016.

[21] Yiming Zhang and Zhengming Zhao, "Frequency Splitting Analysis of Two-Coil Resonant Wireless Power Transfer," *Antennas Wirel. Propag. Lett.*, vol. 13, pp. 400–402, 2014, doi: 10.1109/LAWP.2014.2307924.

[22] Z. Zhang, H. Pang, A. Georgiadis, and C. Cecati, "Wireless Power Transfer: An Overview," *IEEE TRANSACTIONS ON INDUSTRIAL ELECTRONICS*, p. 15.

[23] W. Zhong, D. Xu, and R. S. Y. Hui, *Wireless Power Transfer: Between Distance and Efficiency*. 2020. Accessed: Apr. 27, 2021. [Online]. Available: https://doi.org/10.1007/978-981-15-2441-7

[24] E. Electronics *et al.*, "Different Types of Wireless Power Transfer Technologies and their Working," *Circuit Digest*, Jan. 20, 2020. https://circuitdigest.com/tutorial/different-types-of-wireless-power-transmission-technologies-and-their-working (accessed Nov. 05, 2021).

[25] J. Dai and D. Ludois, "A Survey of Wireless Power Transfer and a Critical Comparison of Inductive and Capacitive Coupling for Small Gap Applications," *IEEE TRANSACTIONS ON POWER ELECTRONICS*, vol. 30, no. 11, p. 13, 2015.

[26] M. Nisshagen and E. Sjöstrand, "Wireless Power Transfer Using Resonant Inductive Coupling," Department of Energy and Envoronment, Division of Electric Power Engineering, Chalmers University of Technology, Gothenburg, Sweeden, 2017.

[27] "Mutual Inductance of Two Adjacent Inductive Coils," *Basic Electronics Tutorials*, Aug. 14, 2013. https://www.electronics-tutorials.ws/inductor/mutual-inductance.html (accessed Nov. 05, 2021).

[28] A. Kurs, A. Karalis, R. Moffatt, J. D. Joannopoulos, P. Fisher, and M. Soljačić, "Wireless Power Transfer via Strongly Coupled Magnetic Resonances," *Science*, vol. 317, no. 5834, pp. 83–86, Jul. 2007, doi: 10.1126/science.1143254.

[29] B. H. Choi, V. X. Thai, E. S. Lee, J. H. Kim, and C. T. Rim, “Dipole-Coil-Based Wide-Range Inductive Power Transfer Systems for Wireless Sensors,” *IEEE Trans. Ind. Electron.*, vol. 63, no. 5, pp. 3158–3167, May 2016, doi: 10.1109/TIE.2016.2517061.

[30] B. Minnaert and N. Stevens, “Conjugate Image Theory Applied on Capacitive Wireless Power Transfer,” *Energies*, vol. 10, no. 1, p. 46, Jan. 2017, doi: 10.3390/en10010046.

[31] R. Vinge, “Wireless Energy Transfer by Resonant Inductive Coupling,” Department of Signals and Systems, Division of Signal Proicessing and Biomedical Engineering, Chalmers University of Technology, Gothenburg, Sweeden, 2015.

[32] M. Rehman, Z. Baharudin, P. Nallagownden, and B. ul Islam, “Design and Analysis of Resonant Wireless Power Transfer System,” *MATEC Web Conf.*, vol. 225, p. 02020, 2018, doi: 10.1051/matecconf/201822502020.

[33] Fayoum University, M. M. El Rayes, G. Nagib, and W. G. Ali Abdelaal, “A Review on Wireless Power Transfer,” *IJETT*, vol. 40, no. 5, pp. 272–280, Oct. 2016, doi: 10.14445/22315381/IJETT-V40P244.

[34] “Inductive Versus Resonant Wireless Charging: A Truce May Be a Designer’s Best Choice.” https://www.digikey.com/en/articles/inductive-versus-resonant-wireless-charging (accessed Apr. 27, 2021).

[35] Y. Cheng and Y. Shu, “A New Analytical Calculation of the Mutual Inductance of the Coaxial Spiral Rectangular Coils,” *IEEE Trans. Magn.*, vol. 50, no. 4, pp. 1–6, Apr. 2014, doi: 10.1109/TMAG.2013.2290972.

[36] “NFC/RFID Planar Spiral Coil Inductance Calculator.” https://www.translatorscafe.com/unit-converter/zh/calculator/planar-coil-inductance/ (accessed May 06, 2021).

[37] S. S. Mohan, M. del Mar Hershenson, S. P. Boyd, and T. H. Lee, “Simple Accurate Expressions for Planar Spiral Inductances,” *IEEE J. Solid-State Circuits*, vol. 34, no. 10, pp. 1419–1424, Oct. 1999, doi: 10.1109/4.792620.

[38] S. R. Khan, S. K. Pavuluri, and M. P. Y. Desmulliez, “Accurate Modeling of Coil Inductance for Near-Field Wireless Power Transfer,” *IEEE Trans. Microwave Theory Techn.*, vol. 66, no. 9, pp. 4158–4169, Sep. 2018, doi: 10.1109/TMTT.2018.2854190.

[39] S. Liu, J. Su, and J. Lai, “Accurate Expressions of Mutual Inductance and Their Calculation of Archimedean Spiral Coils,” *Energies*, vol. 12, no. 10, p. 2017, May 2019, doi: 10.3390/en12102017.

[40] F. Y. Lin, C. Carretero, G. A. Covic, and J. T. Boys, “A Reduced Order Model to Determine the Coupling Factor Between Magnetic Pads Used in Wireless Power Transfer,” *IEEE Trans. Transp. Electrific.*, vol. 3, no. 2, pp. 321–331, Jun. 2017, doi: 10.1109/TTE.2016.2628793.

[41] S. Raju, R. Wu, M. Chan, and C. P. Yue, “Modeling of Mutual Coupling Between Planar Inductors in Wireless Power Applications,” *IEEE Trans. Power Electron.*, vol. 29, no. 1, pp. 481–490, Jan. 2014, doi: 10.1109/TPEL.2013.2253334.

[42] E. R. Joy, B. K. Kushwaha, G. Rituraj, and P. Kumar, “Analysis and Comparison of Four Compensation Topologies of Contactless Power Transfer System,” in *2015 4th International Conference on Electric Power and Energy Conversion Systems (EPECS)*, Sharjah, United Arab Emirates, Nov. 2015, pp. 1–6. doi: 10.1109/EPECS.2015.7368544.

[43] X. Liu, C. Xia, and X. Yuan, “Study of the Circular Flat Spiral Coil Structure Effect on Wireless Power Transfer System Performance,” *Energies*, vol. 11, no. 11, p. 2875, Oct. 2018, doi: 10.3390/en11112875.

[44] “Spiral Coil Calculator,” *Kaizer Power Electronics*, Jul. 10, 2014. https://kaizerpowerelectronics.dk/calculators/spiral-coil-calculator/ (accessed May 31, 2021).

[45] H. A. Aebischer, “Inductance Formula for Rectangular Planar Spiral Inductors with Rectangular Conductor Cross Section,” *AEM*, vol. 9, no. 1, pp. 1–18, Feb. 2020, doi: 10.7716/aem.v9i1.1346.

[46] M. H. Nguyen and H. Fortin Blanchette, “Optimizing AC Resistance of Solid PCB Winding,” *Electronics*, vol. 9, no. 5, p. 875, May 2020, doi: 10.3390/electronics9050875.

[47] “What is Proximity Effect? Definition & Factors Affecting it - Circuit Globe.” https://circuitglobe.com/proximity-effect.html (accessed Nov. 03, 2021).

[48] “Litz Wire, HF-Litz, High Frequency Litz Wire, Litz Wire for High Efficiency | ELEKTRISOLA.” https://www.elektrisola.com/en-us/Litz-Wire/Info (accessed Nov. 11, 2021).

[49] “Introduction to Capacitors, Capacitance and Charge,” *Basic Electronics Tutorials*, Jul. 26, 2013. https://www.electronics-tutorials.ws/capacitor/cap_1.html (accessed Nov. 18, 2021).

[50] A. Haque and Zaheeruddin, “A fast and reliable perturb and observe maximum power point tracker for solar PV system,” *Int J Syst Assur Eng Manag*, vol. 8, no. S2, pp. 773–787, Nov. 2017, doi: 10.1007/s13198-016-0523-2.

[51] M. A. Eltawil and Z. Zhao, “MPPT techniques for photovoltaic applications,” *Renewable and Sustainable Energy Reviews*, vol. 25, pp. 793–813, Sep. 2013, doi: 10.1016/j.rser.2013.05.022.

Appendix A: Compensation Topologies

In the following section, the derivation of the modeling equations for the Series-Parallel, Parallel-Series and Parallel-Parallel compensation topologies is shown.

A.1 Series-Parallel Compensation Topology

In Series-Parallel compensation topology the corresponding equations of the circuit model are the following:

$$z_1 \cdot I_1 + j \cdot \omega_o \cdot M_{12} \cdot I_2 = V_s \tag{A.1}$$

$$(j \cdot \omega_o \cdot M_{12}) \cdot I_1 + z_2 \cdot I_2 = 0 \tag{A.2}$$

The impedance of the primary side is the same as the impedance of the primary side in Series-Series compensation topology.

In (A.1) and (A.2), z_1 and z_2 are the impedances of the primary and the secondary sides, respectively and are equal to:

$$z_1 = R_1 + j \cdot X_1 \tag{A.3}$$

$$z_2 = R_2 + j \cdot \omega_o \cdot L_2 + \frac{R_L}{1 + j \cdot R_L \cdot \omega_o \cdot C_2} \tag{A.4}$$

Where X_1 is the reactance of resonator and is equal to:

$$X_1 = (\omega_o \cdot L_1) - \frac{1}{\omega_o \cdot C_1} \tag{A.5}$$

In Series-Parallel compensation topology, the secondary current phasor can be derived from (A.2) and it is equal to:

$$I_2 = -\frac{I_1 \cdot M_{12} \cdot \omega_o \cdot j}{R_2 + j \cdot \omega_o \cdot L_2 + \frac{R_L}{1 + j \cdot R_L \cdot C_2 \cdot \omega_o}} \tag{A.6}$$

By substituting (A.6) into (A.1), the voltage source can be calculated and it is equal to:

$$V_s = I_1 \cdot (R_1 + j \cdot \omega_o \cdot L_1 - \frac{j}{C_1 \cdot \omega_o}) + \frac{I_1 \cdot M_{12}^2 \cdot \omega_o^2}{R_2 + j \cdot \omega_o \cdot L_2 + \frac{R_L}{1 + j \cdot R_L \cdot C_2 \cdot \omega_o}} \quad \text{(A.7)}$$

The input impedance of the system can be calculated by using the following equation:

$$Z_{in} = \frac{V_s}{I_1} \quad \text{(A.8)}$$

By substituting (A.7) into (A.8), the impedance of the system can be calculated and it is equal to:

$$Z_{in} = \frac{V_s}{I_1} = R_1 + j \cdot \omega_o \cdot L_1 - \frac{j}{C_1 \cdot \omega_o} + \frac{M_{12}^2 \cdot \omega_o^2}{R_2 + j \cdot \omega_o \cdot L_2 + \frac{R_L}{1 + j \cdot R_L \cdot C_2 \cdot \omega_o}} \quad \text{(A.9)}$$

The impedance of the primary circuit is the same as the one from the Series-Series compensation topology, but the reflected impedance is different.

$$Z_{pr} = R_1 + j \cdot \omega_o \cdot L_1 - \frac{j}{C_1 \cdot \omega_o} \quad \text{(A.10)}$$

$$Z_r = \frac{M_{12}^2 \cdot \omega_o^2}{R_2 + j \cdot \omega_o \cdot L_2 + \frac{R_L}{1 + j \cdot R_L \cdot C_2 \cdot \omega_o}} \quad \text{(A.11)}$$

In Series-Parallel compensation topology, the current gain can be derived as:

$$G = \left| \frac{I_{R_L}}{I_1} \right| \quad \text{(A.12)}$$

Where I_{RL} is the current phasor of the load and can be expressed as a current partitioner for I_2.

$$I_{R_L} = I_2 \cdot \frac{\frac{1}{j \cdot \omega_o \cdot C_2}}{R_L + \frac{1}{j \cdot \omega_o \cdot C_2}} \quad \text{(A.13)}$$

By substituting (A.6) into (A.13) I_{RL} becomes:

$$I_{R_L} = -\frac{I_1 \cdot M_{12}}{C_2 \cdot (R_L - \frac{j}{C_2 \cdot \omega_o}) \cdot (R_2 + j \cdot \omega_o \cdot L_2 + \frac{R_L}{1 + j \cdot R_L \cdot C_2 \cdot \omega_o}} \quad \text{(A.14)}$$

Then, by substituting (A.14) into (A.12), the current gain can be calculated and it is equal to:

$$G = \left|\frac{I_{R_L}}{I_1}\right| = \frac{M_{12} \cdot \omega_o}{\left|R_2 + j \cdot \omega_o \cdot L_2 + \frac{R_L}{1 + j \cdot R_L \cdot C_2 \cdot \omega_o}\right| \cdot |R_L \cdot C_2 \cdot \omega_o - j|} \quad \text{(A.15)}$$

Finally, the efficiency of the system can be expressed as:

$$n_s = \frac{total\ output\ power}{total\ input\ power} = \frac{P_{sec}}{P_{pr}} \quad \text{(A.16)}$$

The total input power can be expressed as:

$$P_{pr} = V_s \cdot I_1^* = R_1 \cdot |I_1|^2 + j \cdot \omega_o \cdot L_1 \cdot |I_1|^2 - \frac{|I_1|^2 \cdot j}{C_1 \cdot \omega_o} + \frac{C_2 \cdot M_{12}^2 \cdot \omega_o^3 \cdot |I_1|^2}{C_2 \cdot R_2 \cdot \omega_o + C_2 \cdot R_L \cdot \omega_o + j \cdot \omega_o^2 \cdot C_2 \cdot L_2 - j} \quad \text{(A.17)}$$

The total output power in Series-Parallel topology can be expressed as:

$$P_{sec} = \left|I_{R_L}\right|^2 \cdot R_L \quad \text{(A.18)}$$

By substituting (A.14) into (A.18), the total output power can be calculated and it is equal to:

$$P_{sec} = \left|I_{R_L}\right|^2 \cdot R_L = \frac{R_L \cdot M_{12}^2 \cdot \omega_o^2 \cdot |I_1|^2}{\left|R_2 + j \cdot \omega_o \cdot L_2 + \frac{R_L}{1 + j \cdot R_L \cdot C_2 \cdot \omega_o}\right|^2 \cdot |R_L \cdot C_2 \cdot \omega_o - j|^2} \quad \text{(A.19)}$$

By substituting (A.17) and (A.19) into (A.16), the efficiency of the system can be calculated.

A.2 Parallel-Series Compensation Topology

In Parallel-Series compensation topology the corresponding equations of the circuit model are the following:

$$(R_1 + j \cdot \omega_o \cdot L_1) \cdot I_{L1} + j \cdot \omega_o \cdot M_{12} \cdot I_2 = V_s \quad \text{(A.20)}$$

$$(j \cdot \omega_o \cdot M_{12}) \cdot I_{L1} + z_2 \cdot I_2 = 0 \quad \text{(A.21)}$$

Where z_2 and X_2 are equal to:

$$z_2 = R_2 + R_L + j \cdot X_2 \quad \text{(A.22)}$$

$$X_2 = (\omega_o \cdot L_2) - \frac{1}{\omega_o \cdot C_2} \quad \text{(A.23)}$$

I_{L1} is the current that flows through the inductor and is equal to:

$$I_{L1} = I_1 - V_s \cdot j \cdot \omega_o \cdot C_1 \quad \text{(A.24)}$$

The secondary current phasor can be derived from (A.21) and it is equal to:

$$I_2 = -\frac{I_1 \cdot C_2 \cdot M_{12} \cdot {\omega_o}^2}{\begin{array}{c} C_1 \cdot L_1 \cdot {\omega_o}^2 - C_2 \cdot R_2 \cdot \omega_o \cdot j - C_2 \cdot R_L \cdot \omega_o \cdot j - C_1 \cdot R_1 \cdot \omega_o \cdot j + C_2 \cdot L_2 \cdot {\omega_o}^2 + C_1 \cdot C_2 \cdot {M_{12}}^2 \cdot {\omega_o}^4 - \\ - C_1 \cdot C_2 \cdot L_1 . L_2 \cdot {\omega_o}^4 + C_1 \cdot C_2 \cdot L_1 \cdot R_2 \cdot {\omega_o}^3 \cdot j + C_1 \cdot C_2 \cdot L_2 \cdot R_1 \cdot {\omega_o}^3 \cdot j + C_1 \cdot C_2 \cdot L_1 \cdot R_L \cdot {\omega_o}^3 \cdot j + \\ + C_1 \cdot C_2 \cdot R_1 \cdot R_2 \cdot {\omega_o}^2 + C_1 \cdot C_2 \cdot R_1 . R_L \cdot {\omega_o}^2 - 1 \end{array}} \quad \text{(A.25)}$$

By substituting (A.25) into (A.20), the voltage source can be calculated and it is equal to:

$$V_s = \frac{\begin{array}{c} I_1 \cdot (L_1 \cdot \omega_o - R_1 \cdot j + C_2 \cdot {M_{12}}^2 \cdot {\omega_o}^3 - C_2 \cdot L_1 . L_2 \cdot {\omega_o}^3 + C_2 \cdot L_1 . R_2 \cdot {\omega_o}^2 \cdot j + \\ + C_2 \cdot L_2 . R_1 \cdot {\omega_o}^2 \cdot j + C_2 \cdot L_1 . R_L \cdot {\omega_o}^2 \cdot j + C_2 \cdot R_1 . R_2 \cdot \omega_o + C_2 \cdot R_1 . R_L \cdot \omega_o) \end{array}}{\begin{array}{c} C_1 \cdot R_1 \cdot \omega_o + C_2 \cdot R_2 \cdot \omega_o + C_2 \cdot R_L \cdot \omega_o + C_1 \cdot L_1 \cdot {\omega_o}^2 \cdot j + C_2 \cdot L_2 \cdot {\omega_o}^2 \cdot j + \\ + C_1 \cdot C_2 \cdot {M_{12}}^2 \cdot {\omega_o}^4 \cdot j - C_1 \cdot C_2 \cdot L_1 \cdot L_2 \cdot {\omega_o}^4 \cdot j - C_1 \cdot C_2 \cdot L_1 \cdot R_2 \cdot {\omega_o}^3 - C_1 \cdot C_2 \cdot L_2 \cdot R_1 \cdot {\omega_o}^3 - C_1 \cdot C_2 \cdot L_1 \cdot R_L \cdot {\omega_o}^3 + \\ + C_1 \cdot C_2 \cdot R_1 \cdot R_2 \cdot {\omega_o}^2 \cdot j + C_1 \cdot C_2 \cdot R_1 . R_L \cdot {\omega_o}^2 \cdot j - j \end{array}} \quad \text{(A.26)}$$

By substituting (A.26) into (A.9), the impedance of the system can be calculated and it is equal to:

$$Z_{in} = \frac{V_s}{I_1} = \frac{\begin{matrix} L_1\cdot\omega_o - R_1\cdot j + C_2\cdot {M_{12}}^2\cdot {\omega_o}^3 - C_2\cdot L_1.L_2\cdot {\omega_o}^3 + C_2\cdot L_1.R_2\cdot {\omega_o}^2\cdot j + \\ + C_2\cdot L_2.R_1\cdot {\omega_o}^2\cdot j + C_2\cdot L_1.R_L\cdot {\omega_o}^2\cdot j + C_2\cdot R_1.R_2\cdot\omega_o + C_2\cdot R_1.R_L\cdot\omega_o \end{matrix}}{\begin{matrix} C_1\cdot R_1\cdot\omega_o + C_2\cdot R_2\cdot\omega_o + C_2\cdot R_L\cdot\omega_o + C_1\cdot L_1\cdot {\omega_o}^2\cdot j + C_2\cdot L_2\cdot {\omega_o}^2\cdot j + \\ + C_1\cdot C_2\cdot {M_{12}}^2\cdot {\omega_o}^4\cdot j - C_1\cdot C_2\cdot L_1\cdot L_2\cdot {\omega_o}^4\cdot j - C_1\cdot C_2\cdot L_1\cdot R_2\cdot {\omega_o}^3 - C_1\cdot C_2\cdot L_2\cdot R_1\cdot {\omega_o}^3 - C_1\cdot C_2\cdot L_1\cdot R_L\cdot {\omega_o}^3 + \\ + C_1\cdot C_2\cdot R_1\cdot R_2\cdot {\omega_o}^2\cdot j + C_1\cdot C_2\cdot R_1.R_L\cdot {\omega_o}^2\cdot j - j \end{matrix}} \quad \text{(A.27)}$$

In Parallel-Series compensation topology, the current gain can be derived as:

$$G = \left|\frac{I_2}{I_1}\right| \quad \text{(A.28)}$$

By substituting (A.25) into (A.28), the current gain can be calculated and it is equal to:

$$G = \left|\frac{I_2}{I_1}\right| = \frac{C_2\cdot M_{12}\cdot {\omega_o}^2}{\left|\begin{matrix} C_1\cdot L_1\cdot {\omega_o}^2 - C_2\cdot R_2\cdot\omega_o\cdot j - C_2\cdot R_L\cdot\omega_o\cdot j - C_1\cdot R_1\cdot\omega_o\cdot j + C_2\cdot L_2\cdot {\omega_o}^2 + C_1\cdot C_2\cdot {M_{12}}^2\cdot {\omega_o}^4 - \\ - C_1\cdot C_2\cdot L_1.L_2\cdot {\omega_o}^4 + C_1\cdot C_2\cdot L_1\cdot R_2\cdot {\omega_o}^3\cdot j + C_1\cdot C_2\cdot L_2\cdot R_1\cdot {\omega_o}^3\cdot j + C_1\cdot C_2\cdot L_1\cdot R_L\cdot {\omega_o}^3\cdot j + \\ + C_1\cdot C_2\cdot R_1\cdot R_2\cdot {\omega_o}^2 + C_1\cdot C_2\cdot R_1.R_L\cdot {\omega_o}^2 - 1 \end{matrix}\right|} \quad \text{(A.29)}$$

The total input power can be expressed as:

$$P_{pr} = V_s\cdot I_1^* \quad \text{(A.30)}$$

Where I_1^* is the conjugate of the current of the primary circuit.

The total output power can be expressed as:

$$P_{sec} = |I_2|^2\cdot R_L \quad \text{(A.31)}$$

By substituting (A.26) into (A.30) and (A.25) into (A.31), the total input and output powers can be expressed as:

$$P_{pr} = V_s\cdot I_1^* = -\frac{\begin{matrix} |I_1|^2\cdot(R_1 + L_1\cdot\omega_o\cdot j + C_2\cdot {M_{12}}^2\cdot {\omega_o}^3\cdot j - C_2\cdot L_1.L_2\cdot {\omega_o}^3\cdot j - C_2\cdot L_1.R_2\cdot {\omega_o}^2 - \\ - \frac{C}{2}\cdot L_2.R_1\cdot {\omega_o}^2 - C_2\cdot L_1.R_L\cdot {\omega_o}^2 + C_2\cdot R_1.R_2\cdot\omega_o\cdot j + C_2\cdot R_1.R_L\cdot\omega_o\cdot j)\cdot \\ \cdot(C_1\cdot L_1\cdot {\omega_o}^2 + C_2\cdot L_2\cdot {\omega_o}^2 + C_1\cdot C_2\cdot {M_{12}}^2\cdot {\omega_o}^4 - C_1\cdot C_2\cdot L_1\cdot L_2\cdot {\omega_o}^4 + C_1\cdot C_2\cdot R_1\cdot R_2\cdot {\omega_o}^2 + \\ + C_1\cdot C_2\cdot R_1.R_L\cdot {\omega_o}^2 - 1 + C_1\cdot R_1\cdot\omega_o\cdot j + C_2\cdot R_2\cdot\omega_o\cdot j + C_2\cdot R_L\cdot\omega_o\cdot j - \\ - C_1\cdot C_2\cdot L_1\cdot R_2\cdot {\omega_o}^3\cdot j - C_1\cdot C_2\cdot L_2\cdot R_1\cdot {\omega_o}^3\cdot j - C_1\cdot C_2\cdot L_1\cdot R_L\cdot {\omega_o}^3\cdot j) \end{matrix}}{\begin{matrix} (C_1\cdot L_1\cdot {\omega_o}^2 + C_2\cdot L_2\cdot {\omega_o}^2 + C_1\cdot C_2\cdot {M_{12}}^2\cdot {\omega_o}^4 - C_1\cdot C_2\cdot L_1\cdot L_2\cdot {\omega_o}^4 + C_1\cdot C_2\cdot R_1\cdot R_2\cdot {\omega_o}^2 + C_1\cdot C_2\cdot R_1\cdot R_L\cdot {\omega_o}^2 - 1)^2 + \\ + {\omega_o}^2\cdot(C_1\cdot R_1 + C_2\cdot R_2 + C_2\cdot R_L - C_1\cdot C_2\cdot L_1\cdot R_2\cdot {\omega_o}^2 - C_1\cdot C_2\cdot L_2\cdot R_1\cdot {\omega_o}^2 - C_1\cdot C_2\cdot L_1\cdot R_L\cdot {\omega_o}^2)^2 \end{matrix}} \quad \text{(A.32)}$$

$$P_{sec} = |I_2|^2 \cdot R_L = \frac{|I_1|^2 \cdot R_L \cdot {C_2}^2 \cdot {M_{12}}^2 \cdot {\omega_o}^4}{\left| \begin{matrix} C_1 \cdot L_1 \cdot {\omega_o}^2 - C_2 \cdot R_2 \cdot \omega_o \cdot j - C_2 \cdot R_L \cdot \omega_o \cdot j - C_1 \cdot R_1 \cdot \omega_o \cdot j + C_2 \cdot L_2 \cdot {\omega_o}^2 + \\ + C_1 \cdot C_2 \cdot {M_{12}}^2 \cdot {\omega_o}^4 - C_1 \cdot C_2 \cdot L_1 \cdot L_2 \cdot {\omega_o}^4 + C_1 \cdot C_2 \cdot L_1 \cdot R_2 \cdot {\omega_o}^3 \cdot j + C_1 \cdot C_2 \cdot L_2 \cdot R_1 \cdot {\omega_o}^3 \cdot j + C_1 \cdot C_2 \cdot L_1 \cdot R_L \cdot {\omega_o}^3 \cdot j + \\ + C_1 \cdot C_2 \cdot R_1 \cdot R_2 \cdot {\omega_o}^2 + C_1 \cdot C_2 \cdot R_1 \cdot R_L \cdot {\omega_o}^2 - 1 \end{matrix} \right|^2} \quad \text{(A.33)}$$

By substituting (A.32) and (A.33) into (A.16), the efficiency of the system can be calculated.

A.3 Parallel-Parallel Compensation Topology

In Parallel-Parallel compensation topology the corresponding equations of the circuit model are the same as in the Parallel-Series compensation topology:

$$(R_1 + j \cdot \omega_o \cdot L_1) \cdot I_{L1} + j \cdot \omega_o \cdot M_{12} \cdot I_2 = V_s \quad \text{(A.20)}$$

$$(j \cdot \omega_o \cdot M_{12}) \cdot I_{L1} + z_2 \cdot I_2 = 0 \quad \text{(A.21)}$$

Where z_2 is equal to:

$$z_2 = R_2 + j \cdot \omega_o \cdot L_2 + \frac{R_L}{1 + j \cdot R_L \cdot \omega_o \cdot C_2} \quad \text{(A.34)}$$

And I_{L1} is equal to:

$$I_{L1} = I_1 - V_s \cdot j \cdot \omega_o \cdot C_1 \quad \text{(A.24)}$$

The secondary current phasor can be derived from (A.21) and it is equal to:

$$I_2 = \frac{I_1 \cdot M_{12} \cdot \omega_o \cdot (j - C_2 \cdot R_L \cdot \omega_o)}{\begin{matrix} C_1 \cdot L_1 \cdot R_2 \cdot {\omega_o}^2 - R_L - L_2 \cdot \omega_o \cdot j - C_1 \cdot {M_{12}}^2 \cdot {\omega_o}^3 \cdot j + C_1 \cdot L_1 \cdot L_2 \cdot {\omega_o}^3 \cdot j - R_2 + C_1 \cdot L_2 \cdot R_1 \cdot {\omega_o}^2 + C_1 \cdot L_1 \cdot R_L \cdot {\omega_o}^2 + \\ + C_2 \cdot L_2 \cdot R_L \cdot {\omega_o}^2 - C_1 \cdot R_1 \cdot R_2 \cdot \omega_o \cdot j - C_1 \cdot R_1 \cdot R_L \cdot \omega_o \cdot j - C_2 \cdot R_2 \cdot R_L \cdot \omega_o \cdot j + \\ + C_1 \cdot C_2 \cdot {M_{12}}^2 \cdot R_L \cdot {\omega_o}^4 - C_1 \cdot C_2 \cdot L_1 \cdot L_2 \cdot R_L \cdot {\omega_o}^4 + C_1 \cdot C_2 \cdot L_1 \cdot R_2 \cdot R_L \cdot {\omega_o}^3 \cdot j + C_1 \cdot C_2 \cdot L_2 \cdot R_1 \cdot R_L \cdot {\omega_o}^3 \cdot j + C_1 \cdot C_2 \cdot R_1 \cdot R_2 \cdot R_L \cdot {\omega_o}^2 \end{matrix}} \quad \text{(A.35)}$$

By substituting (A.35) into (A.20), the voltage source can be calculated and it is equal to:

$$V_s = \frac{\begin{matrix} I_1 \cdot (L_1 \cdot R_2 \cdot \omega_o - R_1 \cdot R_L \cdot j - {M_{12}}^2 \cdot {\omega_o}^2 \cdot j - R_1 \cdot R_2 \cdot j + L_2 \cdot R_1 \cdot \omega_o + L_1 \cdot R_L \cdot \omega_o + \\ + L_1 \cdot L_2 \cdot {\omega_o}^2 \cdot j + C_2 \cdot {M_{12}}^2 \cdot R_L \cdot {\omega_o}^3 + C_2 \cdot R_1 . R_2 \cdot R_L \cdot \omega_o - C_2 \cdot L_1 \cdot L_2 \cdot R_L \cdot \omega_o^3 + C_2 \cdot L_1 \cdot R_2 \cdot R_L \cdot {\omega_o}^2 \cdot j + C_2 \cdot L_2 \cdot R_1 \cdot R_L \cdot {\omega_o}^2 \cdot j) \end{matrix}}{\begin{matrix} L_2 \cdot \omega_o - R_L \cdot j - R_2 \cdot j + C_1 \cdot {M_{12}}^2 \cdot {\omega_o}^3 - C_1 \cdot L_1 \cdot L_2 \cdot {\omega_o}^3 + C_1 \cdot L_1 \cdot R_2 \cdot {\omega_o}^2 \cdot j + C_1 \cdot L_2 \cdot R_1 \cdot {\omega_o}^2 \cdot j + C_1 \cdot L_1 \cdot R_L \cdot {\omega_o}^2 \cdot j + \\ + C_2 \cdot L_2 \cdot R_L \cdot {\omega_o}^2 \cdot j + C_1 \cdot R_1 \cdot R_2 \cdot \omega_o + C_1 \cdot R_1 \cdot R_L \cdot \omega_o + C_2 \cdot R_2 \cdot R_L \cdot \omega_o + C_1 \cdot C_2 \cdot {M_{12}}^2 \cdot R_L \cdot {\omega_o}^4 \cdot j - C_1 \cdot C_2 \cdot L_1 \cdot L_2 \cdot R_L \cdot {\omega_o}^4 \cdot j - \\ - C_1 \cdot C_2 \cdot L_1 \cdot R_2 \cdot R_L \cdot {\omega_o}^3 - C_1 \cdot C_2 \cdot L_2 \cdot R_1 \cdot R_L \cdot {\omega_o}^3 + C_1 \cdot C_2 \cdot R_1 \cdot R_2 \cdot R_L \cdot {\omega_o}^2 \cdot j \end{matrix}} \quad \text{(A.36)}$$

By substituting (A.36) into (A.9), the impedance of the system can be calculated and it is equal to:

$$Z_{in} = \frac{V_s}{I_1} = \frac{\begin{matrix} L_1 \cdot R_2 \cdot \omega_o - R_1 \cdot R_L \cdot j - {M_{12}}^2 \cdot {\omega_o}^2 \cdot j - R_1 \cdot R_2 \cdot j + L_2 \cdot R_1 \cdot \omega_o + L_1 \cdot R_L \cdot \omega_o + \\ + L_1 \cdot L_2 \cdot {\omega_o}^2 \cdot j + C_2 \cdot {M_{12}}^2 \cdot R_L \cdot {\omega_o}^3 + C_2 \cdot R_1 . R_2 \cdot R_L \cdot \omega_o - C_2 \cdot L_1 \cdot L_2 \cdot R_L \cdot \omega_o^3 + C_2 \cdot L_1 \cdot R_2 \cdot R_L \cdot {\omega_o}^2 \cdot j + C_2 \cdot L_2 \cdot R_1 \cdot R_L \cdot {\omega_o}^2 \cdot j \end{matrix}}{\begin{matrix} L_2 \cdot \omega_o - R_L \cdot j - R_2 \cdot j + C_1 \cdot {M_{12}}^2 \cdot {\omega_o}^3 - C_1 \cdot L_1 \cdot L_2 \cdot {\omega_o}^3 + C_1 \cdot L_1 \cdot R_2 \cdot {\omega_o}^2 \cdot j + C_1 \cdot L_2 \cdot R_1 \cdot {\omega_o}^2 \cdot j + C_1 \cdot L_1 \cdot R_L \cdot {\omega_o}^2 \cdot j + \\ + C_2 \cdot L_2 \cdot R_L \cdot {\omega_o}^2 \cdot j + C_1 \cdot R_1 \cdot R_2 \cdot \omega_o + C_1 \cdot R_1 \cdot R_L \cdot \omega_o + C_2 \cdot R_2 \cdot R_L \cdot \omega_o + C_1 \cdot C_2 \cdot {M_{12}}^2 \cdot R_L \cdot {\omega_o}^4 \cdot j - C_1 \cdot C_2 \cdot L_1 \cdot L_2 \cdot R_L \cdot {\omega_o}^4 \cdot j - \\ - C_1 \cdot C_2 \cdot L_1 \cdot R_2 \cdot R_L \cdot {\omega_o}^3 - C_1 \cdot C_2 \cdot L_2 \cdot R_1 \cdot R_L \cdot {\omega_o}^3 + C_1 \cdot C_2 \cdot R_1 \cdot R_2 \cdot R_L \cdot {\omega_o}^2 \cdot j \end{matrix}} \quad \text{(A.37)}$$

By substituting (A.35) into (A.28), the current gain can be calculated and it is equal to:

$$G = \left|\frac{I_2}{I_1}\right| = \frac{M_{12} \cdot \omega_o \cdot |1 + C_2 \cdot R_L \cdot \omega_o \cdot j|}{|C_2 \cdot R_L \cdot \omega_o - j| \cdot \left| \begin{matrix} C_1 \cdot L_1 \cdot R_2 \cdot {\omega_o}^2 - R_L - L_2 \cdot \omega_o \cdot j - C_1 \cdot {M_{12}}^2 \cdot {\omega_o}^3 \cdot j + C_1 \cdot L_1 \cdot L_2 \cdot {\omega_o}^3 \cdot j - R_2 + C_1 \cdot L_2 \cdot R_1 \cdot {\omega_o}^2 + C_1 \cdot L_1 \cdot R_L \cdot {\omega_o}^2 + \\ + C_2 \cdot L_2 \cdot R_L \cdot {\omega_o}^2 - C_1 \cdot R_1 \cdot R_2 \cdot \omega_o \cdot j - C_1 \cdot R_1 \cdot R_L \cdot \omega_o \cdot j - C_2 \cdot R_2 \cdot R_L \cdot \omega_o \cdot j + \\ + C_1 \cdot C_2 \cdot {M_{12}}^2 \cdot R_L \cdot {\omega_o}^4 - C_1 \cdot C_2 \cdot L_1 \cdot L_2 \cdot R_L \cdot {\omega_o}^4 + C_1 \cdot C_2 \cdot L_1 \cdot R_2 \cdot R_L \cdot {\omega_o}^3 \cdot j + \\ + C_1 \cdot C_2 \cdot L_2 \cdot R_1 \cdot R_L \cdot {\omega_o}^3 \cdot j + C_1 \cdot C_2 \cdot R_1 \cdot R_2 \cdot R_L \cdot {\omega_o}^2 \end{matrix} \right|} \quad \text{(A.38)}$$

The total input power and the total output power can be expressed as:

$$P_{pr} = V_s \cdot I_1^* \quad \text{(A.30)}$$

$$P_{sec} = \left|I_{R_L}\right|^2 \cdot R_L \quad \text{(A.18)}$$

Where

$$I_{R_L} = I_2 \cdot \frac{\frac{1}{j \cdot \omega_o \cdot C_2}}{R_L + \frac{1}{j \cdot \omega_o \cdot C_2}} \quad \text{(A.13)}$$

So, after substituting (A.13) into (A.18) and (A.36) into (A.30), the input and the output powers can be calculated. Thus, the efficiency of the system for Parallel-Parallel compensation topology can be calculated too, through equation (A.16).

Appendix B: Results

Table B.1: Increasing the Distance between Circular Coils (N = 7 Turns)

$d_{out1}=d_{out2}$ (mm)	$w_1=w_2$ (mm)	$s_1=s_2$ (mm)	$N_1=N_2$ (turns)	$d_{in1}=d_{in2}$ (mm)	$L_1=L_2$ (µH)	M_{12} (µH)	k_{12} (-)	d (mm)
120	4	1	7	52	4,9680	3,3661	0,6776	**10**
120	4	1	7	52	4,9680	2,8538	0,5744	**15**
120	4	1	7	52	4,9680	2,5071	0,5046	**20**
120	4	1	7	52	4,9680	2,2727	0,4575	**25**
120	4	1	7	52	4,9680	2,1170	0,4261	**30**
120	4	1	7	52	4,9680	2,0172	0,4060	**35**
120	4	1	7	52	4,9680	1,9576	0,3941	**40**

Table B.2: Increasing the Distance between Circular Coils (N = 8 Turns)

$d_{out1}=d_{out2}$ (mm)	$w_1=w_2$ (mm)	$s_1=s_2$ (mm)	$N_1=N_2$ (turns)	$d_{in1}=d_{in2}$ (mm)	$L_1=L_2$ (µH)	M_{12} (µH)	k_{12} (-)	d (mm)
120	4	1	8	42	5,4886	3,6580	0,6665	**10**
120	4	1	8	42	5,4886	3,1229	0,5690	**15**
120	4	1	8	42	5,4886	2,7684	0,5044	**20**
120	4	1	8	42	5,4886	2,5375	0,4623	**25**
120	4	1	8	42	5,4886	2,3924	0,4359	**30**
120	4	1	8	42	5,4886	2,3077	0,4204	**35**
120	4	1	8	42	5,4886	2,2653	0,4127	**40**

Table B.3: Increasing the Distance between Rectangular Coils (N = 7 Turns)

$d_{out1}=d_{out2}$ (mm)	$w_1=w_2$ (mm)	$s_1=s_2$ (mm)	$N_1=N_2$ (turns)	$d_{in1}=d_{in2}$ (mm)	$L_1=L_2$ (µH)	M_{12} (µH)	k_{12} (-)	d (mm)
120	4	1	7	52	5,9368	5,4570	0,9192	**10**
120	4	1	7	52	5,9368	4,6264	0,7793	**15**
120	4	1	7	52	5,9368	4,0643	0,6846	**20**
120	4	1	7	52	5,9368	3,6844	0,6206	**25**
120	4	1	7	52	5,9368	3,4319	0,5781	**30**
120	4	1	7	52	5,9368	3,2701	0,5508	**35**
120	4	1	7	52	5,9368	3,1736	0,5346	**40**

Table B.4: Increasing the Distance between Rectangular Coils (N = 8 Turns)

$d_{out1}=d_{out2}$ (mm)	$w_1=w_2$ (mm)	$s_1=s_2$ (mm)	$N_1=N_2$ (turns)	$d_{in1}=d_{in2}$ (mm)	$L_1=L_2$ (µH)	M_{12} (µH)	k_{12} (-)	d (mm)
120	4	1	8	42	6,5590	5,9302	0,9041	**10**
120	4	1	8	42	6,5590	5,0626	0,7719	**15**
120	4	1	8	42	6,5590	4,4880	0,6842	**20**
120	4	1	8	42	6,5590	4,1136	0,6272	**25**
120	4	1	8	42	6,5590	3,8785	0,5913	**30**
120	4	1	8	42	6,5590	3,7411	0,5704	**35**
120	4	1	8	42	6,5590	3,6724	0,5599	**40**

Table B.5: Increasing the Turn Spacing for Circular Coils (N = 7 Turns)

$d_{out1}=d_{out2}$ (mm)	$w_1=w_2$ (mm)	$s_1=s_2$ (mm)	$N_1=N_2$ (turns)	$d_{in1}=d_{in2}$ (mm)	$L_1=L_2$ (µH)	M_{12} (µH)	k_{12} (-)	d (mm)
120	4	**1**	7	52	4,9680	3,3661	0,6776	10
120	4	**1,1**	7	50,8	4,8704	3,3048	0,6786	10
120	4	**1,2**	7	49,6	4,7744	3,2443	0,6795	10
120	4	**1,3**	7	48,4	4,6801	3,1846	0,6805	10

Table B.6: Increasing the Turn Spacing for Circular Coils (N = 8 Turns)

$d_{out1}=d_{out2}$ (mm)	$w_1=w_2$ (mm)	$s_1=s_2$ (mm)	$N_1=N_2$ (turns)	$d_{in1}=d_{in2}$ (mm)	$L_1=L_2$ (µH)	M_{12} (µH)	k_{12} (-)	d (mm)
120	4	**1**	8	42	5,4886	3,6580	0,6665	10
120	4	**1,1**	8	40,6	5,3593	3,5750	0,6671	10
120	4	**1,2**	8	39,2	5,2325	3,4934	0,6676	10
120	4	**1,3**	8	37,8	5,1080	3,4134	0,6682	10

Table 4.7: Increasing the Turn Spacing for Rectangular Coils (N = 7 Turns)

$d_{out1}=d_{out2}$ (mm)	$w_1=w_2$ (mm)	$s_1=s_2$ (mm)	$N_1=N_2$ (turns)	$d_{in1}=d_{in2}$ (mm)	$L_1=L_2$ (µH)	M_{12} (µH)	k_{12} (-)	d (mm)
120	4	**1**	7	52	5,9368	5,4570	0,9192	10
120	4	**1,1**	7	50,8	5,8202	5,3576	0,9205	10
120	4	**1,2**	7	49,6	5,7056	5,2595	0,9218	10
120	4	**1,3**	7	48,4	5,5928	5,1626	0,9231	10

Table B.8: Increasing the Turn Spacing for Rectangular Coils (N = 8 Turns)

$d_{out1}=d_{out2}$ (mm)	$w_1=w_2$ (mm)	$s_1=s_2$ (mm)	$N_1=N_2$ (turns)	$d_{in1}=d_{in2}$ (mm)	$L_1=L_2$ (µH)	M_{12} (µH)	k_{12} (-)	d (mm)
120	4	**1**	8	42	6,5590	5,9302	0,9041	10
120	4	**1,1**	8	40,6	6,4045	5,7956	0,9049	10
120	4	**1,2**	8	39,2	6,2529	5,6633	0,9057	10
120	4	**1,3**	8	37,8	6,1042	5,5335	0,9065	10

Table B.9: Increasing the Turn Width for Circular Coils (N = 7 Turns)

$d_{out1}=d_{out2}$ (mm)	$w_1=w_2$ (mm)	$s_1=s_2$ (mm)	$N_1=N_2$ (turns)	$d_{in1}=d_{in2}$ (mm)	$L_1=L_2$ (µH)	M_{12} (µH)	k_{12} (-)	d (mm)
120	**3**	1	7	66	6,2351	4,3100	0,6912	10
120	**4**	1	7	52	4,9680	3,3661	0,6776	10
120	**5**	1	7	38	3,9243	2,5245	0,6433	10
120	**6**	1	7	24	3,0639	1,8022	0,5882	10

Table B.10: Increasing the Turn Width for Circular Coils (N = 8 Turns)

$d_{out1}=d_{out2}$ (mm)	$w_1=w_2$ (mm)	$s_1=s_2$ (mm)	$N_1=N_2$ (turns)	$d_{in1}=d_{in2}$ (mm)	$L_1=L_2$ (µH)	M_{12} (µH)	k_{12} (-)	d (mm)
120	**3**	1	8	58	7,1588	4,9682	0,6940	10
120	**4**	1	8	42	5,4886	3,6580	0,6665	10
120	**5**	1	8	26	4,1494	2,5396	0,6120	10
120	**6**	1	8	10	3,0768	1,6479	0,5356	10

Table B.11: Increasing the Turn Width for Rectangular Coils (N = 7 Turns)

$d_{out1}=d_{out2}$ (mm)	$w_1=w_2$ (mm)	$s_1=s_2$ (mm)	$N_1=N_2$ (turns)	$d_{in1}=d_{in2}$ (mm)	$L_1=L_2$ (µH)	M_{12} (µH)	k_{12} (-)	d (mm)
120	**3**	1	7	66	7,4511	6,9871	0,9377	10
120	**4**	1	7	52	5,9368	5,4570	0,9192	10
120	**5**	1	7	38	4,6897	4,0925	0,8727	10
120	**6**	1	7	24	3,6615	2,9216	0,7979	10

Table B.12: Increasing the Turn Width for Rectangular Coils (N = 8 Turns)

$d_{out1}=d_{out2}$ (mm)	$w_1=w_2$ (mm)	$s_1=s_2$ (mm)	$N_1=N_2$ (turns)	$d_{in1}=d_{in2}$ (mm)	$L_1=L_2$ (µH)	M_{12} (µH)	k_{12} (-)	d (mm)
120	**3**	1	8	58	8,5549	8,0542	0,9415	10
120	**4**	1	8	42	6,5590	5,9302	0,9041	10
120	**5**	1	8	26	4,9586	4,1170	0,8303	10
120	**6**	1	8	10	3,6769	2,6715	0,7266	10

Table B.13: Increasing the Number of Turns for Circular Coils (w = 4 mm)

$d_{out1}=d_{out2}$ (mm)	$w_1=w_2$ (mm)	$s_1=s_2$ (mm)	$N_1=N_2$ (turns)	$d_{in1}=d_{in2}$ (mm)	$L_1=L_2$ (µH)	M_{12} (µH)	k_{12} (-)	d (mm)
120	4	1	**5**	72	3,4996	2,3663	0,6761	10
120	4	1	**6**	62	4,2961	2,9243	0,6807	10
120	4	1	**7**	52	4,9680	3,3661	0,6776	10
120	4	1	**8**	42	5,4886	3,6580	0,6665	10

Table B.14: Increasing the Number of Turns for Circular Coils (w = 5 mm)

$d_{out1}=d_{out2}$ (mm)	$w_1=w_2$ (mm)	$s_1=s_2$ (mm)	$N_1=N_2$ (turns)	$d_{in1}=d_{in2}$ (mm)	$L_1=L_2$ (µH)	M_{12} (µH)	k_{12} (-)	d (mm)
120	5	1	**5**	62	2,9834	1,9998	0,6703	10
120	5	1	**6**	50	3,5311	2,3407	0,6629	10
120	5	1	**7**	38	3,9243	2,5245	0,6433	10
120	5	1	**8**	26	4,1494	2,5396	0,6120	10

Table B.15: Increasing the Number of Turns for Rectangular Coils (w = 4 mm)

$d_{out1}=d_{out2}$ (mm)	$w_1=w_2$ (mm)	$s_1=s_2$ (mm)	$N_1=N_2$ (turns)	$d_{in1}=d_{in2}$ (mm)	$L_1=L_2$ (µH)	M_{12} (µH)	k_{12} (-)	d (mm)
120	4	1	**5**	72	4,1821	3,8360	0,9172	10
120	4	1	**6**	62	5,1339	4,7407	0,9234	10
120	4	1	**7**	52	5,9368	5,4570	0,9192	10
120	4	1	**8**	42	6,5590	5,9302	0,9041	10

Table B.16: Increasing the Number of Turns for Rectangular Coils (w = 5 mm)

$d_{out1}=d_{out2}$ (mm)	$w_1=w_2$ (mm)	$s_1=s_2$ (mm)	$N_1=N_2$ (turns)	$d_{in1}=d_{in2}$ (mm)	$L_1=L_2$ (µH)	M_{12} (µH)	k_{12} (-)	d (mm)
120	5	1	**5**	62	3,5652	3,2419	0,9093	10
120	5	1	**6**	50	4,2198	3,7945	0,8992	10
120	5	1	**7**	38	4,6897	4,0925	0,8727	10
120	5	1	**8**	26	4,9586	4,1170	0,8303	10

Table B.17: Increasing Turn Width for Circular Coils with Circular Cross-Section

$d_{out1}=d_{out2}$ (mm)	$w_1=w_2$ (mm)	$s_1=s_2$ (mm)	$r_1=r_2$ (mm)	f_o (kHz)	$A_{cs1}=A_{cs2}$ (mm^2)	$R_1=R_2$ (Ohm)	$A_{cs}/2$ (mm^2)	$R'_1=R'_2$ (Ohm)
120	**3**	1	**1,5**	100	7,069	0,0192	3,534	0,0384
120	**4**	1	**2,0**	100	12,566	0,0131	6,283	0,0262
120	**5**	1	**2,5**	100	19,635	0,0095	9,817	0,0190

Table B.18: Increasing Turn Width for Rectangular Coils with Circular Cross-Section

$d_{out1}=d_{out2}$ (mm)	$w_1=w_2$ (mm)	$s_1=s_2$ (mm)	$r_1=r_2$ (mm)	f_o (kHz)	$A_{cs1}=A_{cs2}$ (mm^2)	$R_1=R_2$ (Ohm)	$A_{cs}/2$ (mm^2)	$R'_1=R'_2$ (Ohm)
120	**3**	1	**1,5**	100	7,069	0,0258	3,534	0,0516
120	**4**	1	**2**	100	12,566	0,0176	6,283	0,0352
120	**5**	1	**2,5**	100	19,635	0,0128	9,817	0,0256

Table B.19: Increasing Turn Width for Circular Coils with Rectangular Cross-Section

$d_{out1}=d_{out2}$ (mm)	$w_1=w_2$ (mm)	$s_1=s_2$ (mm)	$h_1=h_2$ (mm)	f_o (kHz)	$A_{cs1}=A_{cs2}$ (mm^2)	$R_1=R_2$ (Ohm)
120	**3**	1	**1,5**	100	4,5	0,0282
120	**4**	1	**1,5**	100	6	0,0195
120	**5**	1	**1,5**	100	7,5	0,0144
120	**3**	1	**2**	100	6	0,0282
120	**4**	1	**2**	100	8	0,0195
120	**5**	1	**2**	100	10	0,0144
120	**3**	1	**2,5**	100	7,5	0,0282
120	**4**	1	**2,5**	100	10	0,0195
120	**5**	1	**2,5**	100	12,5	0,0144

Table B.20: Increasing Turn Width for Rectangular Coils with Rectangular Cross-Section

$d_{out1}=d_{out2}$ (mm)	$w_1=w_2$ (mm)	$s_1=s_2$ (mm)	$h_1=h_2$ (mm)	f_o (kHz)	$A_{cs1}=A_{cs2}$ (mm^2)	$R_1=R_2$ (Ohm)
120	**3**	1	**1,5**	100	4,5	0,0379
120	**4**	1	**1,5**	100	6	0,0263
120	**5**	1	**1,5**	100	7,5	0,0194
120	**3**	1	**2**	100	6	0,0379
120	**4**	1	**2**	100	8	0,0263
120	**5**	1	**2**	100	10	0,0194
120	**3**	1	**2,5**	100	7,5	0,0379
120	**4**	1	**2,5**	100	10	0,0263
120	**5**	1	**2,5**	100	12,5	0,0194

Table B.21: Increasing Frequency – Circular Coils with Circular Cross-Section

f_o (kHz)	$\delta_1=\delta_2$ (mm)	$A_{cs1}=A_{cs2}$ (mm^2)	$R_1=R_2$ (Ohm)	$A_{cs}/2$ (mm^2)	$R'_1=R'_2$ (Ohm)
100	0,2090	19,635	0,0078	9,817	0,0156
500	0,0935	19,635	0,0171	9,817	0,0342
1000	0,0661	19,635	0,0241	9,817	0,0482

Table B.22: Increasing Frequency – Rectangular Coils with Circular Cross-Section

f_o (kHz)	$\delta_1=\delta_2$ (mm)	$A_{cs1}=A_{cs2}$ (mm^2)	$R_1=R_2$ (Ohm)	$A_{cs}/2$ (mm^2)	$R'_1=R'_2$ (Ohm)
100	0,2090	19,635	0,0103	9,817	0,0206
500	0,0935	19,635	0,0224	9,817	0,0488
1000	0,0661	19,635	0,0316	9,817	0,0632

Table B.23: Increasing Frequency – Circular Coils with Rectangular Cross-Section

f_o (kHz)	$\delta_1=\delta_2$ (mm)	$A_{cs1}=A_{cs2}$ (mm^2)	$R_1=R_2$ (Ohm)
100	0,2090	12,5	0,0118
500	0,0935	12,5	0,0264
1000	0,0661	12,5	0,0373

Table B.24: Increasing Frequency – Rectangular Coils with Rectangular Cross-Section

f_o (kHz)	$\delta_1=\delta_2$ (mm)	$A_{cs1}=A_{cs2}$ (mm^2)	$R_1=R_2$ (Ohm)
100	0,2090	12,5	0,0155
500	0,0935	12,5	0,0346
1000	0,0661	12,5	0,0489

Table B.25: Series-Series – Circular Coils – Capacitance vs. Number of Turns & Frequency

N (turns)	w (mm)	f_o (kHz)	$L_1=L_2$ (µH)	M_{12} (µH)	C_1 (µF)	C_2 (µF)
5	4	**100**	3,4996	2,3663	0,7238	0,7238
6	4	**100**	4,2961	2,9243	0,5896	0,5896
7	4	**100**	4,9680	3,3661	0,5099	0,5099
8	4	**100**	5,4886	3,6580	0,4615	0,4615
5	4	**500**	3,4996	2,3663	0,0290	0,0290
6	4	**500**	4,2961	2,9243	0,0236	0,0236
7	4	**500**	4,9680	3,3661	0,0204	0,0204
8	4	**500**	5,4886	3,6580	0,0185	0,0185
5	4	**1000**	3,4996	2,3663	0,0072	0,0072
6	4	**1000**	4,2961	2,9243	0,0059	0,0059
7	4	**1000**	4,9680	3,3661	0,0051	0,0051
8	4	**1000**	5,4886	3,6580	0,0046	0,0046

Table B.26: Series-Parallel – Circular Coils – Capacitance vs. Number of Turns & Frequency

N (turns)	w (mm)	f_o (kHz)	$L_1=L_2$ (µH)	M_{12} (µH)	C_1 (µF)	C_2 (µF)
5	4	**100**	3,4996	2,3663	1,3330	0,7238
6	4	**100**	4,2961	2,9243	1,0990	0,5896
7	4	**100**	4,9680	3,3661	0,9426	0,5099
8	4	**100**	5,4886	3,6580	0,8303	0,4615
5	4	**500**	3,4996	2,3663	0,0530	0,0290
6	4	**500**	4,2961	2,9243	0,0440	0,0236
7	4	**500**	4,9680	3,3661	0,0377	0,0204
8	4	**500**	5,4886	3,6580	0,0332	0,0185
5	4	**1000**	3,4996	2,3663	0,0130	0,0072
6	4	**1000**	4,2961	2,9243	0,0110	0,0059
7	4	**1000**	4,9680	3,3661	0,0094	0,0051
8	4	**1000**	5,4886	3,6580	0,0083	0,0046

Table B.27: Parallel-Series – Circular Coils – Capacitance vs. Number of Turns & Frequency

N (turns)	w (mm)	f_o (kHz)	$L_1=L_2$ (µH)	M_{12} (µH)	C_1 (µF)	C_2 (µF)
5	4	**100**	3,4996	2,3663	0,7238	1,3330
6	4	**100**	4,2961	2,9243	0,5896	1,0990
7	4	**100**	4,9680	3,3661	0,5099	0,9426
8	4	**100**	5,4886	3,6580	0,4615	0,8303
5	4	**500**	3,4996	2,3663	0,0290	0,0530
6	4	**500**	4,2961	2,9243	0,0236	0,0440
7	4	**500**	4,9680	3,3661	0,0204	0,0377
8	4	**500**	5,4886	3,6580	0,0185	0,0332
5	4	**1000**	3,4996	2,3663	0,0072	0,0130
6	4	**1000**	4,2961	2,9243	0,0059	0,0110
7	4	**1000**	4,9680	3,3661	0,0051	0,0094
8	4	**1000**	5,4886	3,6580	0,0046	0,0083

Table B.28: Parallel-Parallel – Circular Coils – Capacitance vs. Number of Turns & Frequency

N (turns)	w (mm)	f_o (kHz)	$L_1=L_2$ (µH)	M_{12} (µH)	C_1 (µF)	C_2 (µF)
5	4	**100**	3,4996	2,3663	1,3330	1,3330
6	4	**100**	4,2961	2,9243	1,0990	1,0990
7	4	**100**	4,9680	3,3661	0,9426	0,9426
8	4	**100**	5,4886	3,6580	0,8303	0,8303
5	4	**500**	3,4996	2,3663	0,0530	0,0530
6	4	**500**	4,2961	2,9243	0,0440	0,0440
7	4	**500**	4,9680	3,3661	0,0377	0,0377
8	4	**500**	5,4886	3,6580	0,0332	0,0332
5	4	**1000**	3,4996	2,3663	0,0130	0,0130
6	4	**1000**	4,2961	2,9243	0,0110	0,0110
7	4	**1000**	4,9680	3,3661	0,0094	0,0094
8	4	**1000**	5,4886	3,6580	0,0083	0,0083

Table B.29: Series-Series – Rectangular Coils – Capacitance vs. Number of Turns & Frequency

N (turns)	w (mm)	f_o (kHz)	$L_1=L_2$ (µH)	M_{12} (µH)	C_1 (µF)	C_2 (µF)
5	4	**100**	4,1821	3,8360	0,6057	0,6057
6	4	**100**	5,1339	4,7407	0,4934	0,4934
7	4	**100**	5,9368	5,4570	0,4267	0,4267

8	4	**100**	6,5590	5,9302	0,3862	0,3862
5	4	**500**	4,1821	3,8360	0,0242	0,0242
6	4	**500**	5,1339	4,7407	0,0197	0,0197
7	4	**500**	5,9368	5,4570	0,0171	0,0171
8	4	**500**	6,5590	5,9302	0,0154	0,0154
5	4	**1000**	4,1821	3,8360	0,0061	0,0061
6	4	**1000**	5,1339	4,7407	0,0049	0,0049
7	4	**1000**	5,9368	5,4570	0,0043	0,0043
8	4	**1000**	6,5590	5,9302	0,0039	0,0039

Table B.30: Series-Parallel – Rectangular Coils – Capacitance vs. Number of Turns & Frequency

N (turns)	w (mm)	f_o (kHz)	$L_1=L_2$ (µH)	M_{12} (µH)	C_1 (µF)	C_2 (µF)
5	4	**100**	4,1821	3,8360	3,8170	0,6057
6	4	**100**	5,1339	4,7407	3,3490	0,4934
7	4	**100**	5,9368	5,4570	2,7510	0,4267
8	4	**100**	6,5590	5,9302	2,1160	0,3862
5	4	**500**	4,1821	3,8360	0,1530	0,0242
6	4	**500**	5,1339	4,7407	0,1340	0,0197
7	4	**500**	5,9368	5,4570	0,1100	0,0171
8	4	**500**	6,5590	5,9302	0,0850	0,0154
5	4	**1000**	4,1821	3,8360	0,0380	0,0061
6	4	**1000**	5,1339	4,7407	0,0330	0,0049
7	4	**1000**	5,9368	5,4570	0,0280	0,0043
8	4	**1000**	6,5590	5,9302	0,0210	0,0039

Table B.31: Parallel-Series – Rectangular Coils – Capacitance vs. Number of Turns & Frequency

N (turns)	w (mm)	f_o (kHz)	$L_1=L_2$ (µH)	M_{12} (µH)	C_1 (µF)	C_2 (µF)
5	4	**100**	4,1821	3,8360	0,6057	3,8170
6	4	**100**	5,1339	4,7407	0,4934	3,3490
7	4	**100**	5,9368	5,4570	0,4267	2,7510
8	4	**100**	6,5590	5,9302	0,3862	2,1160
5	4	**500**	4,1821	3,8360	0,0242	0,1530
6	4	**500**	5,1339	4,7407	0,0197	0,1340
7	4	**500**	5,9368	5,4570	0,0171	0,1100
8	4	**500**	6,5590	5,9302	0,0154	0,0850
5	4	**1000**	4,1821	3,8360	0,0061	0,0380

6	4	**1000**	5,1339	4,7407	0,0049	0,0330
7	4	**1000**	5,9368	5,4570	0,0043	0,0280
8	4	**1000**	6,5590	5,9302	0,0039	0,0210

Table B.32: Parallel-Parallel – Rectangular Coils – Capacitance vs. Number of Turns & Frequency

N (turns)	w (mm)	f_o (kHz)	L_1=L_2 (µH)	M_{12} (µH)	C_1 (µF)	C_2 (µF)
5	4	**100**	4,1821	3,8360	3,8170	3,8170
6	4	**100**	5,1339	4,7407	3,3490	3,3490
7	4	**100**	5,9368	5,4570	2,7510	2,7510
8	4	**100**	6,5590	5,9302	2,1160	2,1160
5	4	**500**	4,1821	3,8360	0,1530	0,1530
6	4	**500**	5,1339	4,7407	0,1340	0,1340
7	4	**500**	5,9368	5,4570	0,1100	0,1100
8	4	**500**	6,5590	5,9302	0,0850	0,0850
5	4	**1000**	4,1821	3,8360	0,0380	0,0380
6	4	**1000**	5,1339	4,7407	0,0330	0,0330
7	4	**1000**	5,9368	5,4570	0,0280	0,0280
8	4	**1000**	6,5590	5,9302	0,0210	0,0210

Table B.33: Series-Series – Circular Coils (N = 5 Turns) – Capacitance vs. Turn Width & Frequency

N (turns)	w (mm)	f_o (kHz)	L_1=L_2 (µH)	M_{12} (µH)	k_{12} (-)	C_1 (µF)	C_2 (µF)
5	**3**	**100**	4,0948	2,7539	0,6725	0,6186	0,6186
5	**4**	**100**	3,4996	2,3663	0,6761	0,7238	0,7238
5	**5**	**100**	2,9834	1,9998	0,6703	0,8490	0,8490
5	**6**	**100**	2,5347	1,6577	0,6540	0,9993	0,9993
5	**3**	**500**	4,0948	2,7539	0,6725	0,0247	0,0247
5	**4**	**500**	3,4996	2,3663	0,6761	0,0290	0,0290
5	**5**	**500**	2,9834	1,9998	0,6703	0,0340	0,0340
5	**6**	**500**	2,5347	1,6577	0,6540	0,0400	0,0400
5	**3**	**1000**	4,0948	2,7539	0,6725	0,0062	0,0062
5	**4**	**1000**	3,4996	2,3663	0,6761	0,0072	0,0072
5	**5**	**1000**	2,9834	1,9998	0,6703	0,0085	0,0085
5	**6**	**1000**	2,5347	1,6577	0,6540	0,0100	0,0100

Table B.34: Series-Series – Circular Coils (N = 6 Turns) – Capacitance vs. Turn Width & Frequency

N (turns)	w (mm)	f_o (kHz)	$L_1=L_2$ (µH)	M_{12} (µH)	k_{12} (-)	C_1 (µF)	C_2 (µF)
6	3	100	5,2011	3,5578	0,6840	0,4870	0,4870
6	4	100	4,2961	2,9243	0,6807	0,5896	0,5896
6	5	100	3,5311	2,3407	0,6629	0,7173	0,7173
6	6	100	2,8832	1,8143	0,6293	0,8785	0,8785
6	3	500	5,2011	3,5578	0,6840	0,0195	0,0195
6	4	500	4,2961	2,9243	0,6807	0,0236	0,0236
6	5	500	3,5311	2,3407	0,6629	0,0287	0,0287
6	6	500	2,8832	1,8143	0,6293	0,0351	0,0351
6	3	1000	5,2011	3,5578	0,6840	0,0049	0,0049
6	4	1000	4,2961	2,9243	0,6807	0,0059	0,0059
6	5	1000	3,5311	2,3407	0,6629	0,0072	0,0072
6	6	1000	2,8832	1,8143	0,6293	0,0088	0,0088

Table B.35: Series-Series – Circular Coils (N = 7 Turns) – Capacitance vs. Turn Width & Frequency

N (turns)	w (mm)	f_o (kHz)	$L_1=L_2$ (µH)	M_{12} (µH)	k_{12} (-)	C_1 (µF)	C_2 (µF)
7	3	100	6,2351	4,3100	0,6912	0,4063	0,4063
7	4	100	4,9680	3,3661	0,6776	0,5099	0,5099
7	5	100	3,9243	2,5245	0,6433	0,6455	0,6455
7	6	100	3,0639	1,8022	0,5882	0,8267	0,8267
7	3	500	6,2351	4,3100	0,6912	0,0163	0,0163
7	4	500	4,9680	3,3661	0,6776	0,0204	0,0204
7	5	500	3,9243	2,5245	0,6433	0,0258	0,0258
7	6	500	3,0639	1,8022	0,5882	0,0331	0,0331
7	3	1000	6,2351	4,3100	0,6912	0,0041	0,0041
7	4	1000	4,9680	3,3661	0,6776	0,0051	0,0051
7	5	1000	3,9243	2,5245	0,6433	0,0065	0,0065
7	6	1000	3,0639	1,8022	0,5882	0,0083	0,0083

Table B.36: Series-Series – Circular Coils (N = 8 Turns) – Capacitance vs. Turn Width & Frequency

N (turns)	w (mm)	f_o (kHz)	$L_1=L_2$ (µH)	M_{12} (µH)	k_{12} (-)	C_1 (µF)	C_2 (µF)
8	3	100	7,1588	4,9682	0,6940	0,3538	0,3538
8	4	100	5,4886	3,6580	0,6665	0,4615	0,4615
8	5	100	4,1494	2,5396	0,6120	0,6105	0,6105

8	**6**	**100**	3,0768	1,6479	0,5356	0,8233	0,8233
8	**3**	**500**	7,1588	4,9682	0,6940	0,0142	0,0142
8	**4**	**500**	5,4886	3,6580	0,6665	0,0185	0,0185
8	**5**	**500**	4,1494	2,5396	0,6120	0,0244	0,0244
8	**6**	**500**	3,0768	1,6479	0,5356	0,0329	0,0329
8	**3**	**1000**	7,1588	4,9682	0,6940	0,0035	0,0035
8	**4**	**1000**	5,4886	3,6580	0,6665	0,0046	0,0046
8	**5**	**1000**	4,1494	2,5396	0,6120	0,0061	0,0061
8	**6**	**1000**	3,0768	1,6479	0,5356	0,0082	0,0082

Table B.37: Series-Series – Rectangular Coils (N = 5 Turns) – Capacitance vs. Turn Width & Frequency

N (turns)	**w (mm)**	**f_o (kHz)**	**L_1=L_2 (µH)**	**M_{12} (µH)**	**k_{12} (-)**	**C_1 (µF)**	**C_2 (µF)**
5	**3**	**100**	4,8934	4,4645	0,9124	0,5176	0,5176
5	**4**	**100**	4,1821	3,8360	0,9172	0,6057	0,6057
5	**5**	**100**	3,5652	3,2419	0,9093	0,7105	0,7105
5	**6**	**100**	3,0290	2,6873	0,8872	0,8363	0,8363
5	**3**	**500**	4,8934	4,4645	0,9124	0,0207	0,0207
5	**4**	**500**	4,1821	3,8360	0,9172	0,0242	0,0242
5	**5**	**500**	3,5652	3,2419	0,9093	0,0284	0,0284
5	**6**	**500**	3,0290	2,6873	0,8872	0,0335	0,0335
5	**3**	**1000**	4,8934	4,4645	0,9124	0,0052	0,0052
5	**4**	**1000**	4,1821	3,8360	0,9172	0,0061	0,0061
5	**5**	**1000**	3,5652	3,2419	0,9093	0,0071	0,0071
5	**6**	**1000**	3,0290	2,6873	0,8872	0,0084	0,0084

Table B.38: Series-Series – Rectangular Coils (N = 6 Turns) – Capacitance vs. Turn Width & Frequency

N (turns)	**w (mm)**	**f_o (kHz)**	**L_1=L_2 (µH)**	**M_{12} (µH)**	**k_{12} (-)**	**C_1 (µF)**	**C_2 (µF)**
6	**3**	**100**	6,2155	5,7676	0,9280	0,4075	0,4075
6	**4**	**100**	5,1339	4,7407	0,9234	0,4934	0,4934
6	**5**	**100**	4,2198	3,7945	0,8992	0,6003	0,6003
6	**6**	**100**	3,4455	2,9413	0,8537	0,7352	0,7352
6	**3**	**500**	6,2155	5,7676	0,9280	0,0163	0,0163
6	**4**	**500**	5,1339	4,7407	0,9234	0,0197	0,0197
6	**5**	**500**	4,2198	3,7945	0,8992	0,0240	0,0240
6	**6**	**500**	3,4455	2,9413	0,8537	0,0294	0,0294
6	**3**	**1000**	6,2155	5,7676	0,9280	0,0041	0,0041

6	**4**	**1000**	5,1339	4,7407	0,9234	0,0049	0,0049
6	**5**	**1000**	4,2198	3,7945	0,8992	0,0060	0,0060
6	**6**	**1000**	3,4455	2,9413	0,8537	0,0074	0,0074

Table B.39: Series-Series – Rectangular Coils (N = 7 Turns) – Capacitance vs. Turn Width & Frequency

N (turns)	w (mm)	f_o (kHz)	L_1=L_2 (µH)	M_{12} (µH)	k_{12} (-)	C_1 (µF)	C_2 (µF)
7	**3**	**100**	7,4511	6,9871	0,9377	0,3400	0,3400
7	**4**	**100**	5,9368	5,4570	0,9192	0,4267	0,4267
7	**5**	**100**	4,6897	4,0925	0,8727	0,5401	0,5401
7	**6**	**100**	3,6615	2,9216	0,7979	0,6918	0,6918
7	**3**	**500**	7,4511	6,9871	0,9377	0,0136	0,0136
7	**4**	**500**	5,9368	5,4570	0,9192	0,0171	0,0171
7	**5**	**500**	4,6897	4,0925	0,8727	0,0216	0,0216
7	**6**	**500**	3,6615	2,9216	0,7979	0,0277	0,0277
7	**3**	**1000**	7,4511	6,9871	0,9377	0,0034	0,0034
7	**4**	**1000**	5,9368	5,4570	0,9192	0,0043	0,0043
7	**5**	**1000**	4,6897	4,0925	0,8727	0,0054	0,0054
7	**6**	**1000**	3,6615	2,9216	0,7979	0,0069	0,0069

Table B.40: Series-Series – Rectangular Coils (N = 8 Turns) – Capacitance vs. Turn Width & Frequency

N (turns)	w (mm)	f_o (kHz)	L_1=L_2 (µH)	M_{12} (µH)	k_{12} (-)	C_1 (µF)	C_2 (µF)
8	**3**	**100**	8,5549	8,0542	0,9415	0,2961	0,2961
8	**4**	**100**	6,5590	5,9302	0,9041	0,3862	0,3862
8	**5**	**100**	4,9586	4,1170	0,8303	0,5108	0,5108
8	**6**	**100**	3,6769	2,6715	0,7266	0,6889	0,6889
8	**3**	**500**	8,5549	8,0542	0,9415	0,0118	0,0118
8	**4**	**500**	6,5590	5,9302	0,9041	0,0154	0,0154
8	**5**	**500**	4,9586	4,1170	0,8303	0,0204	0,0204
8	**6**	**500**	3,6769	2,6715	0,7266	0,0276	0,0276
8	**3**	**1000**	8,5549	8,0542	0,9415	0,0030	0,0030
8	**4**	**1000**	6,5590	5,9302	0,9041	0,0039	0,0039
8	**5**	**1000**	4,9586	4,1170	0,8303	0,0051	0,0051
8	**6**	**1000**	3,6769	2,6715	0,7266	0,0069	0,0069

Table B.41: Parallel-Parallel – Circular Coils (N = 5 Turns) – Capacitance vs. Turn Width & Frequency

N (turns)	w (mm)	f_o (kHz)	L_1=L_2 (µH)	M_{12} (µH)	k_{12} (-)	C_1 (µF)	C_2 (µF)
5	3	100	4,0948	2,7539	0,6725	1,1290	1,1290
5	4	100	3,4996	2,3663	0,6761	1,3330	1,3330
5	5	100	2,9834	1,9998	0,6703	1,5420	1,5420
5	6	100	2,5347	1,6577	0,6540	1,7460	1,7460
5	3	500	4,0948	2,7539	0,6725	0,0450	0,0450
5	4	500	3,4996	2,3663	0,6761	0,0530	0,0530
5	5	500	2,9834	1,9998	0,6703	0,0620	0,0620
5	6	500	2,5347	1,6577	0,6540	0,0700	0,0700
5	3	1000	4,0948	2,7539	0,6725	0,0110	0,0110
5	4	1000	3,4996	2,3663	0,6761	0,0130	0,0130
5	5	1000	2,9834	1,9998	0,6703	0,0150	0,0150
5	6	1000	2,5347	1,6577	0,6540	0,0170	0,0170

Table B.42: Parallel-Parallel – Circular Coils (N = 6 Turns) – Capacitance vs. Turn Width & Frequency

N (turns)	w (mm)	f_o (kHz)	L_1=L_2 (µH)	M_{12} (µH)	k_{12} (-)	C_1 (µF)	C_2 (µF)
6	3	100	5,2011	3,5578	0,6840	0,9153	0,9153
6	4	100	4,2961	2,9243	0,6807	1,0990	1,0990
6	5	100	3,5311	2,3407	0,6629	1,2800	1,2800
6	6	100	2,8832	1,8143	0,6293	1,4540	1,4540
6	3	500	5,2011	3,5578	0,6840	0,0366	0,0366
6	4	500	4,2961	2,9243	0,6807	0,0440	0,0440
6	5	500	3,5311	2,3407	0,6629	0,0510	0,0510
6	6	500	2,8832	1,8143	0,6293	0,0580	0,0580
6	3	1000	5,2011	3,5578	0,6840	0,0092	0,0092
6	4	1000	4,2961	2,9243	0,6807	0,0110	0,0110
6	5	1000	3,5311	2,3407	0,6629	0,0130	0,0130
6	6	1000	2,8832	1,8143	0,6293	0,0150	0,0150

Table B.43: Parallel-Parallel – Circular Coils (N = 7 Turns) – Capacitance vs. Turn Width & Frequency

N (turns)	w (mm)	f_o (kHz)	L_1=L_2 (µH)	M_{12} (µH)	k_{12} (-)	C_1 (µF)	C_2 (µF)
7	3	100	6,2351	4,3100	0,6912	0,7780	0,7780
7	4	100	4,9680	3,3661	0,6776	0,9426	0,9426
7	5	100	3,9243	2,5245	0,6433	1,1010	1,1010

7	**6**	**100**	3,0639	1,8022	0,5882	1,2640	1,2640
7	**3**	**500**	6,2351	4,3100	0,6912	0,0311	0,0311
7	**4**	**500**	4,9680	3,3661	0,6776	0,0377	0,0377
7	**5**	**500**	3,9243	2,5245	0,6433	0,0440	0,0440
7	**6**	**500**	3,0639	1,8022	0,5882	0,0510	0,0510
7	**3**	**1000**	6,2351	4,3100	0,6912	0,0078	0,0078
7	**4**	**1000**	4,9680	3,3661	0,6776	0,0094	0,0094
7	**5**	**1000**	3,9243	2,5245	0,6433	0,0110	0,0110
7	**6**	**1000**	3,0639	1,8022	0,5882	0,0130	0,0130

Table B.44: Parallel-Parallel – Circular Coils (N = 8 Turns) – Capacitance vs. Turn Width & Frequency

N (turns)	w (mm)	f_o (kHz)	$L_1=L_2$ (µH)	M_{12} (µH)	k_{12} (-)	C_1 (µF)	C_2 (µF)
8	**3**	**100**	7,1588	4,9682	0,6940	0,6826	0,6826
8	**4**	**100**	5,4886	3,6580	0,6665	0,8303	0,8303
8	**5**	**100**	4,1494	2,5396	0,6120	0,9761	0,9761
8	**6**	**100**	3,0768	1,6479	0,5356	1,1540	1,1540
8	**3**	**500**	7,1588	4,9682	0,6940	0,0273	0,0273
8	**4**	**500**	5,4886	3,6580	0,6665	0,0332	0,0332
8	**5**	**500**	4,1494	2,5396	0,6120	0,0390	0,0390
8	**6**	**500**	3,0768	1,6479	0,5356	0,0460	0,0460
8	**3**	**1000**	7,1588	4,9682	0,6940	0,0068	0,0068
8	**4**	**1000**	5,4886	3,6580	0,6665	0,0083	0,0083
8	**5**	**1000**	4,1494	2,5396	0,6120	0,0098	0,0098
8	**6**	**1000**	3,0768	1,6479	0,5356	0,0120	0,0120

Table B.45: Parallel-Parallel – Rectangular Coils (N = 5 Turns) – Capacitance vs. Turn Width & Frequency

N (turns)	w (mm)	f_o (kHz)	$L_1=L_2$ (µH)	M_{12} (µH)	k_{12} (-)	C_1 (µF)	C_2 (µF)
5	**3**	**100**	4,8934	4,4645	0,9124	3,0880	3,0880
5	**4**	**100**	4,1821	3,8360	0,9172	3,8170	3,8170
5	**5**	**100**	3,5652	3,2419	0,9093	4,1040	4,1040
5	**6**	**100**	3,0290	2,6873	0,8872	3,9280	3,9280
5	**3**	**500**	4,8934	4,4645	0,9124	0,1240	0,1240
5	**4**	**500**	4,1821	3,8360	0,9172	0,1530	0,1530
5	**5**	**500**	3,5652	3,2419	0,9093	0,1640	0,1640
5	**6**	**500**	3,0290	2,6873	0,8872	0,1570	0,1570
5	**3**	**1000**	4,8934	4,4645	0,9124	0,0310	0,0310

5	**4**	**1000**	4,1821	3,8360	0,9172	0,0380	0,0380
5	**5**	**1000**	3,5652	3,2419	0,9093	0,0410	0,0410
5	**6**	**1000**	3,0290	2,6873	0,8872	0,0390	0,0390

Table B.46: Parallel-Parallel – Rectangular Coils (N = 6 Turns) – Capacitance vs. Turn Width & Frequency

N (turns)	w (mm)	f_o (kHz)	$L_1=L_2$ (µH)	M_{12} (µH)	k_{12} (-)	C_1 (µF)	C_2 (µF)
6	**3**	**100**	6,2155	5,7676	0,9280	2,9330	2,9330
6	**4**	**100**	5,1339	4,7407	0,9234	3,3490	3,3490
6	**5**	**100**	4,2198	3,7945	0,8992	3,1360	3,1360
6	**6**	**100**	3,4455	2,9413	0,8537	2,7100	2,7100
6	**3**	**500**	6,2155	5,7676	0,9280	0,1170	0,1170
6	**4**	**500**	5,1339	4,7407	0,9234	0,1340	0,1340
6	**5**	**500**	4,2198	3,7945	0,8992	0,1250	0,1250
6	**6**	**500**	3,4455	2,9413	0,8537	0,1080	0,1080
6	**3**	**1000**	6,2155	5,7676	0,9280	0,0290	0,0290
6	**4**	**1000**	5,1339	4,7407	0,9234	0,0330	0,0330
6	**5**	**1000**	4,2198	3,7945	0,8992	0,0310	0,0310
6	**6**	**1000**	3,4455	2,9413	0,8537	0,0270	0,0270

Table B.47: Parallel-Parallel – Rectangular Coils (N = 7 Turns) – Capacitance vs. Turn Width & Frequency

N (turns)	w (mm)	f_o (kHz)	$L_1=L_2$ (µH)	M_{12} (µH)	k_{12} (-)	C_1 (µF)	C_2 (µF)
7	**3**	**100**	7,4511	6,9871	0,9377	2,8170	2,8170
7	**4**	**100**	5,9368	5,4570	0,9192	2,7510	2,7510
7	**5**	**100**	4,6897	4,0925	0,8727	2,2650	2,2650
7	**6**	**100**	3,6615	2,9216	0,7979	1,9040	1,9040
7	**3**	**500**	7,4511	6,9871	0,9377	0,1130	0,1130
7	**4**	**500**	5,9368	5,4570	0,9192	0,1100	0,1100
7	**5**	**500**	4,6897	4,0925	0,8727	0,0910	0,0910
7	**6**	**500**	3,6615	2,9216	0,7979	0,0760	0,0760
7	**3**	**1000**	7,4511	6,9871	0,9377	0,0280	0,0280
7	**4**	**1000**	5,9368	5,4570	0,9192	0,0280	0,0280
7	**5**	**1000**	4,6897	4,0925	0,8727	0,0230	0,0230
7	**6**	**1000**	3,6615	2,9216	0,7979	0,0190	0,0190

Table B.48: Parallel-Parallel – Rectangular Coils (N = 8 Turns) – Capacitance vs. Turn Width & Frequency

N (turns)	w (mm)	f_o (kHz)	$L_1=L_2$ (µH)	M_{12} (µH)	k_{12} (-)	C_1 (µF)	C_2 (µF)
8	3	100	8,5549	8,0542	0,9415	2,6060	2,6060
8	4	100	6,5590	5,9302	0,9041	2,1160	2,1160
8	5	100	4,9586	4,1170	0,8303	1,6440	1,6440
8	6	100	3,6769	2,6715	0,7266	1,4590	1,4590
8	3	500	8,5549	8,0542	0,9415	0,1040	0,1040
8	4	500	6,5590	5,9302	0,9041	0,0850	0,0850
8	5	500	4,9586	4,1170	0,8303	0,0660	0,0660
8	6	500	3,6769	2,6715	0,7266	0,0580	0,0580
8	3	1000	8,5549	8,0542	0,9415	0,0260	0,0260
8	4	1000	6,5590	5,9302	0,9041	0,0210	0,0210
8	5	1000	4,9586	4,1170	0,8303	0,0160	0,0160
8	6	1000	3,6769	2,6715	0,7266	0,0150	0,0150

Table B.49: Series-Parallel – Circular Coils (N = 5 Turns) – Capacitance vs. Turn Width & Frequency

N (turns)	w (mm)	f_o (kHz)	$L_1=L_2$ (µH)	M_{12} (µH)	k_{12} (-)	C_1 (µF)	C_2 (µF)
5	3	100	4,0948	2,7539	0,6725	1,1290	0,6186
5	4	100	3,4996	2,3663	0,6761	1,3330	0,7238
5	5	100	2,9834	1,9998	0,6703	1,5420	0,8490
5	6	100	2,5347	1,6577	0,6540	1,7460	0,9993
5	3	500	4,0948	2,7539	0,6725	0,0450	0,0247
5	4	500	3,4996	2,3663	0,6761	0,0530	0,0290
5	5	500	2,9834	1,9998	0,6703	0,0620	0,0340
5	6	500	2,5347	1,6577	0,6540	0,0700	0,0400
5	3	1000	4,0948	2,7539	0,6725	0,0110	0,0062
5	4	1000	3,4996	2,3663	0,6761	0,0130	0,0072
5	5	1000	2,9834	1,9998	0,6703	0,0150	0,0085
5	6	1000	2,5347	1,6577	0,6540	0,0170	0,0100

Table B.50: Series-Parallel – Circular Coils (N = 6 Turns) – Capacitance vs. Turn Width & Frequency

N (turns)	w (mm)	f_o (kHz)	$L_1=L_2$ (µH)	M_{12} (µH)	k_{12} (-)	C_1 (µF)	C_2 (µF)
6	3	100	5,2011	3,5578	0,6840	0,9153	0,4870
6	4	100	4,2961	2,9243	0,6807	1,0990	0,5896
6	5	100	3,5311	2,3407	0,6629	1,2800	0,7173

6	6	100	2,8832	1,8143	0,6293	1,4540	0,8785
6	3	500	5,2011	3,5578	0,6840	0,0366	0,0195
6	4	500	4,2961	2,9243	0,6807	0,0440	0,0236
6	5	500	3,5311	2,3407	0,6629	0,0510	0,0287
6	6	500	2,8832	1,8143	0,6293	0,0580	0,0351
6	3	1000	5,2011	3,5578	0,6840	0,0092	0,0049
6	4	1000	4,2961	2,9243	0,6807	0,0110	0,0059
6	5	1000	3,5311	2,3407	0,6629	0,0130	0,0072
6	6	1000	2,8832	1,8143	0,6293	0,0150	0,0088

Table B.51: Series-Parallel – Circular Coils (N = 7 Turns) – Capacitance vs. Turn Width & Frequency

N (turns)	w (mm)	f_o (kHz)	$L_1=L_2$ (µH)	M_{12} (µH)	k_{12} (-)	C_1 (µF)	C_2 (µF)
7	3	100	6,2351	4,3100	0,6912	0,7780	0,4063
7	4	100	4,9680	3,3661	0,6776	0,9426	0,5099
7	5	100	3,9243	2,5245	0,6433	1,1010	0,6455
7	6	100	3,0639	1,8022	0,5882	1,2640	0,8267
7	3	500	6,2351	4,3100	0,6912	0,0311	0,0163
7	4	500	4,9680	3,3661	0,6776	0,0377	0,0204
7	5	500	3,9243	2,5245	0,6433	0,0440	0,0258
7	6	500	3,0639	1,8022	0,5882	0,0510	0,0331
7	3	1000	6,2351	4,3100	0,6912	0,0078	0,0041
7	4	1000	4,9680	3,3661	0,6776	0,0094	0,0051
7	5	1000	3,9243	2,5245	0,6433	0,0110	0,0065
7	6	1000	3,0639	1,8022	0,5882	0,0130	0,0083

Table B.52: Series-Parallel – Circular Coils (N = 8 Turns) – Capacitance vs. Turn Width & Frequency

N (turns)	w (mm)	f_o (kHz)	$L_1=L_2$ (µH)	M_{12} (µH)	k_{12} (-)	C_1 (µF)	C_2 (µF)
8	3	100	7,1588	4,9682	0,6940	0,6826	0,3538
8	4	100	5,4886	3,6580	0,6665	0,8303	0,4615
8	5	100	4,1494	2,5396	0,6120	0,9761	0,6105
8	6	100	3,0768	1,6479	0,5356	1,1540	0,8233
8	3	500	7,1588	4,9682	0,6940	0,0273	0,0142
8	4	500	5,4886	3,6580	0,6665	0,0332	0,0185
8	5	500	4,1494	2,5396	0,6120	0,0390	0,0244
8	6	500	3,0768	1,6479	0,5356	0,0460	0,0329
8	3	1000	7,1588	4,9682	0,6940	0,0068	0,0035

8	**4**	**1000**	5,4886	3,6580	0,6665	0,0083	0,0046
8	**5**	**1000**	4,1494	2,5396	0,6120	0,0098	0,0061
8	**6**	**1000**	3,0768	1,6479	0,5356	0,0120	0,0082

Table B.53: Series-Parallel – Rectangular Coils (N = 5 Turns) – Capacitance vs. Turn Width & Frequency

N (turns)	w (mm)	f_o (kHz)	$L_1=L_2$ (µH)	M_{12} (µH)	k_{12} (-)	C_1 (µF)	C_2 (µF)
5	**3**	**100**	4,8934	4,4645	0,9124	3,0880	0,5176
5	**4**	**100**	4,1821	3,8360	0,9172	3,8170	0,6057
5	**5**	**100**	3,5652	3,2419	0,9093	4,1040	0,7105
5	**6**	**100**	3,0290	2,6873	0,8872	3,9280	0,8363
5	**3**	**500**	4,8934	4,4645	0,9124	0,1240	0,0207
5	**4**	**500**	4,1821	3,8360	0,9172	0,1530	0,0242
5	**5**	**500**	3,5652	3,2419	0,9093	0,1640	0,0284
5	**6**	**500**	3,0290	2,6873	0,8872	0,1570	0,0335
5	**3**	**1000**	4,8934	4,4645	0,9124	0,0310	0,0052
5	**4**	**1000**	4,1821	3,8360	0,9172	0,0380	0,0061
5	**5**	**1000**	3,5652	3,2419	0,9093	0,0410	0,0071
5	**6**	**1000**	3,0290	2,6873	0,8872	0,0390	0,0084

Table B.54: Series-Parallel – Rectangular Coils (N = 6 Turns) – Capacitance vs. Turn Width & Frequency

N (turns)	w (mm)	f_o (kHz)	$L_1=L_2$ (µH)	M_{12} (µH)	k_{12} (-)	C_1 (µF)	C_2 (µF)
6	**3**	**100**	6,2155	5,7676	0,9280	2,9330	0,4075
6	**4**	**100**	5,1339	4,7407	0,9234	3,3490	0,4934
6	**5**	**100**	4,2198	3,7945	0,8992	3,1360	0,6003
6	**6**	**100**	3,4455	2,9413	0,8537	2,7100	0,7352
6	**3**	**500**	6,2155	5,7676	0,9280	0,1170	0,0163
6	**4**	**500**	5,1339	4,7407	0,9234	0,1340	0,0197
6	**5**	**500**	4,2198	3,7945	0,8992	0,1250	0,0240
6	**6**	**500**	3,4455	2,9413	0,8537	0,1080	0,0294
6	**3**	**1000**	6,2155	5,7676	0,9280	0,0290	0,0041
6	**4**	**1000**	5,1339	4,7407	0,9234	0,0330	0,0049
6	**5**	**1000**	4,2198	3,7945	0,8992	0,0310	0,0060
6	**6**	**1000**	3,4455	2,9413	0,8537	0,0270	0,0074

Table B.55: Series-Parallel – Rectangular Coils (N = 7 Turns) – Capacitance vs. Turn Width & Frequency

N (turns)	w (mm)	f_o (kHz)	L_1=L_2 (µH)	M_{12} (µH)	k_{12} (-)	C_1 (µF)	C_2 (µF)
7	3	100	7,4511	6,9871	0,9377	2,8170	0,3400
7	4	100	5,9368	5,4570	0,9192	2,7510	0,4267
7	5	100	4,6897	4,0925	0,8727	2,2650	0,5401
7	6	100	3,6615	2,9216	0,7979	1,9040	0,6918
7	3	500	7,4511	6,9871	0,9377	0,1130	0,0136
7	4	500	5,9368	5,4570	0,9192	0,1100	0,0171
7	5	500	4,6897	4,0925	0,8727	0,0910	0,0216
7	6	500	3,6615	2,9216	0,7979	0,0760	0,0277
7	3	1000	7,4511	6,9871	0,9377	0,0280	0,0034
7	4	1000	5,9368	5,4570	0,9192	0,0280	0,0043
7	5	1000	4,6897	4,0925	0,8727	0,0230	0,0054
7	6	1000	3,6615	2,9216	0,7979	0,0190	0,0069

Table B.56: Series-Parallel – Rectangular Coils (N = 8 Turns) – Capacitance vs. Turn Width & Frequency

N (turns)	w (mm)	f_o (kHz)	L_1=L_2 (µH)	M_{12} (µH)	k_{12} (-)	C_1 (µF)	C_2 (µF)
8	3	100	8,5549	8,0542	0,9415	2,6060	0,2961
8	4	100	6,5590	5,9302	0,9041	2,1160	0,3862
8	5	100	4,9586	4,1170	0,8303	1,6440	0,5108
8	6	100	3,6769	2,6715	0,7266	1,4590	0,6889
8	3	500	8,5549	8,0542	0,9415	0,1040	0,0118
8	4	500	6,5590	5,9302	0,9041	0,0850	0,0154
8	5	500	4,9586	4,1170	0,8303	0,0660	0,0204
8	6	500	3,6769	2,6715	0,7266	0,0580	0,0276
8	3	1000	8,5549	8,0542	0,9415	0,0260	0,0030
8	4	1000	6,5590	5,9302	0,9041	0,0210	0,0039
8	5	1000	4,9586	4,1170	0,8303	0,0160	0,0051
8	6	1000	3,6769	2,6715	0,7266	0,0150	0,0069

Table B.57: Parallel-Series – Circular Coils (N = 5 Turns) – Capacitance vs. Turn Width & Frequency

N (turns)	w (mm)	f_o (kHz)	L_1=L_2 (µH)	M_{12} (µH)	k_{12} (-)	C_1 (µF)	C_2 (µF)
5	3	100	4,0948	2,7539	0,6725	0,6186	1,1290
5	4	100	3,4996	2,3663	0,6761	0,7238	1,3330
5	5	100	2,9834	1,9998	0,6703	0,8490	1,5420

5	6	100	2,5347	1,6577	0,6540	0,9993	1,7460
5	3	500	4,0948	2,7539	0,6725	0,0247	0,0450
5	4	500	3,4996	2,3663	0,6761	0,0290	0,0530
5	5	500	2,9834	1,9998	0,6703	0,0340	0,0620
5	6	500	2,5347	1,6577	0,6540	0,0400	0,0700
5	3	1000	4,0948	2,7539	0,6725	0,0062	0,0110
5	4	1000	3,4996	2,3663	0,6761	0,0072	0,0130
5	5	1000	2,9834	1,9998	0,6703	0,0085	0,0150
5	6	1000	2,5347	1,6577	0,6540	0,0100	0,0170

Table B.58: Parallel-Series – Circular Coils (N = 6 Turns) – Capacitance vs. Turn Width & Frequency

N (turns)	w (mm)	f_o (kHz)	$L_1=L_2$ (µH)	M_{12} (µH)	k_{12} (-)	C_1 (µF)	C_2 (µF)
6	3	100	5,2011	3,5578	0,6840	0,4870	0,9153
6	4	100	4,2961	2,9243	0,6807	0,5896	1,0990
6	5	100	3,5311	2,3407	0,6629	0,7173	1,2800
6	6	100	2,8832	1,8143	0,6293	0,8785	1,4540
6	3	500	5,2011	3,5578	0,6840	0,0195	0,0366
6	4	500	4,2961	2,9243	0,6807	0,0236	0,0440
6	5	500	3,5311	2,3407	0,6629	0,0287	0,0510
6	6	500	2,8832	1,8143	0,6293	0,0351	0,0580
6	3	1000	5,2011	3,5578	0,6840	0,0049	0,0092
6	4	1000	4,2961	2,9243	0,6807	0,0059	0,0110
6	5	1000	3,5311	2,3407	0,6629	0,0072	0,0130
6	6	1000	2,8832	1,8143	0,6293	0,0088	0,0150

Table B.59: Parallel-Series – Circular Coils (N = 7 Turns) – Capacitance vs. Turn Width & Frequency

N (turns)	w (mm)	f_o (kHz)	$L_1=L_2$ (µH)	M_{12} (µH)	k_{12} (-)	C_1 (µF)	C_2 (µF)
7	3	100	6,2351	4,3100	0,6912	0,4063	0,7780
7	4	100	4,9680	3,3661	0,6776	0,5099	0,9426
7	5	100	3,9243	2,5245	0,6433	0,6455	1,1010
7	6	100	3,0639	1,8022	0,5882	0,8267	1,2640
7	3	500	6,2351	4,3100	0,6912	0,0163	0,0311
7	4	500	4,9680	3,3661	0,6776	0,0204	0,0377
7	5	500	3,9243	2,5245	0,6433	0,0258	0,0440
7	6	500	3,0639	1,8022	0,5882	0,0331	0,0510
7	3	1000	6,2351	4,3100	0,6912	0,0041	0,0078

7	**4**	**1000**	4,9680	3,3661	0,6776	0,0051	0,0094
7	**5**	**1000**	3,9243	2,5245	0,6433	0,0065	0,0110
7	**6**	**1000**	3,0639	1,8022	0,5882	0,0083	0,0130

Table B.60: Parallel-Series – Circular Coils (N = 8 Turns) – Capacitance vs. Turn Width & Frequency

N (turns)	w (mm)	f_o (kHz)	$L_1=L_2$ (µH)	M_{12} (µH)	k_{12} (-)	C_1 (µF)	C_2 (µF)
8	**3**	**100**	7,1588	4,9682	0,6940	0,3538	0,6826
8	**4**	**100**	5,4886	3,6580	0,6665	0,4615	0,8303
8	**5**	**100**	4,1494	2,5396	0,6120	0,6105	0,9761
8	**6**	**100**	3,0768	1,6479	0,5356	0,8233	1,1540
8	**3**	**500**	7,1588	4,9682	0,6940	0,0142	0,0273
8	**4**	**500**	5,4886	3,6580	0,6665	0,0185	0,0332
8	**5**	**500**	4,1494	2,5396	0,6120	0,0244	0,0390
8	**6**	**500**	3,0768	1,6479	0,5356	0,0329	0,0460
8	**3**	**1000**	7,1588	4,9682	0,6940	0,0035	0,0068
8	**4**	**1000**	5,4886	3,6580	0,6665	0,0046	0,0083
8	**5**	**1000**	4,1494	2,5396	0,6120	0,0061	0,0098
8	**6**	**1000**	3,0768	1,6479	0,5356	0,0082	0,0120

Table B.61: Parallel-Series – Rectangular Coils (N = 5 Turns) – Capacitance vs. Turn Width & Frequency

N (turns)	w (mm)	f_o (kHz)	$L_1=L_2$ (µH)	M_{12} (µH)	k_{12} (-)	C_1 (µF)	C_2 (µF)
5	**3**	**100**	4,8934	4,4645	0,9124	0,5176	3,0880
5	**4**	**100**	4,1821	3,8360	0,9172	0,6057	3,8170
5	**5**	**100**	3,5652	3,2419	0,9093	0,7105	4,1040
5	**6**	**100**	3,0290	2,6873	0,8872	0,8363	3,9280
5	**3**	**500**	4,8934	4,4645	0,9124	0,0207	0,1240
5	**4**	**500**	4,1821	3,8360	0,9172	0,0242	0,1530
5	**5**	**500**	3,5652	3,2419	0,9093	0,0284	0,1640
5	**6**	**500**	3,0290	2,6873	0,8872	0,0335	0,1570
5	**3**	**1000**	4,8934	4,4645	0,9124	0,0052	0,0310
5	**4**	**1000**	4,1821	3,8360	0,9172	0,0061	0,0380
5	**5**	**1000**	3,5652	3,2419	0,9093	0,0071	0,0410
5	**6**	**1000**	3,0290	2,6873	0,8872	0,0084	0,0390

Table B.62: Parallel-Series – Rectangular Coils (N = 6 Turns) – Capacitance vs. Turn Width & Frequency

N (turns)	w (mm)	f_o (kHz)	$L_1=L_2$ (µH)	M_{12} (µH)	k_{12} (-)	C_1 (µF)	C_2 (µF)
6	3	100	6,2155	5,7676	0,9280	0,4075	2,9330
6	4	100	5,1339	4,7407	0,9234	0,4934	3,3490
6	5	100	4,2198	3,7945	0,8992	0,6003	3,1360
6	6	100	3,4455	2,9413	0,8537	0,7352	2,7100
6	3	500	6,2155	5,7676	0,9280	0,0163	0,1170
6	4	500	5,1339	4,7407	0,9234	0,0197	0,1340
6	5	500	4,2198	3,7945	0,8992	0,0240	0,1250
6	6	500	3,4455	2,9413	0,8537	0,0294	0,1080
6	3	1000	6,2155	5,7676	0,9280	0,0041	0,0290
6	4	1000	5,1339	4,7407	0,9234	0,0049	0,0330
6	5	1000	4,2198	3,7945	0,8992	0,0060	0,0310
6	6	1000	3,4455	2,9413	0,8537	0,0074	0,0270

Table B.63: Parallel-Series – Rectangular Coils (N = 7 Turns) – Capacitance vs. Turn Width & Frequency

N (turns)	w (mm)	f_o (kHz)	$L_1=L_2$ (µH)	M_{12} (µH)	k_{12} (-)	C_1 (µF)	C_2 (µF)
7	3	100	7,4511	6,9871	0,9377	0,3400	2,8170
7	4	100	5,9368	5,4570	0,9192	0,4267	2,7510
7	5	100	4,6897	4,0925	0,8727	0,5401	2,2650
7	6	100	3,6615	2,9216	0,7979	0,6918	1,9040
7	3	500	7,4511	6,9871	0,9377	0,0136	0,1130
7	4	500	5,9368	5,4570	0,9192	0,0171	0,1100
7	5	500	4,6897	4,0925	0,8727	0,0216	0,0910
7	6	500	3,6615	2,9216	0,7979	0,0277	0,0760
7	3	1000	7,4511	6,9871	0,9377	0,0034	0,0280
7	4	1000	5,9368	5,4570	0,9192	0,0043	0,0280
7	5	1000	4,6897	4,0925	0,8727	0,0054	0,0230
7	6	1000	3,6615	2,9216	0,7979	0,0069	0,0190

Table B.64: Parallel-Series – Rectangular Coils (N = 8 Turns) – Capacitance vs. Turn Width & Frequency

N (turns)	w (mm)	f_o (kHz)	$L_1=L_2$ (µH)	M_{12} (µH)	k_{12} (-)	C_1 (µF)	C_2 (µF)
8	3	100	8,5549	8,0542	0,9415	0,2961	2,6060
8	4	100	6,5590	5,9302	0,9041	0,3862	2,1160
8	5	100	4,9586	4,1170	0,8303	0,5108	1,6440

8	6	100	3,6769	2,6715	0,7266	0,6889	1,4590
8	3	500	8,5549	8,0542	0,9415	0,0118	0,1040
8	4	500	6,5590	5,9302	0,9041	0,0154	0,0850
8	5	500	4,9586	4,1170	0,8303	0,0204	0,0660
8	6	500	3,6769	2,6715	0,7266	0,0276	0,0580
8	3	1000	8,5549	8,0542	0,9415	0,0030	0,0260
8	4	1000	6,5590	5,9302	0,9041	0,0039	0,0210
8	5	1000	4,9586	4,1170	0,8303	0,0051	0,0160
8	6	1000	3,6769	2,6715	0,7266	0,0069	0,0150

Table B.65: Series-Series – Circular Coils with Circular Cross-Section – Efficiency (f_o = 100 kHz)

w (mm)	N (turns)	L (µH)	M_{12} (µH)	k_{12} (-)	$A_{cs}/2$ (mm^2)	R' (Ω)	δ (mm)	C_1 (µF)	C_2 (µF)	P_{in} (W)	P_{out} (W)	n (%)
3	5	4,0948	2,7539	0,6725	3,5343	0,0298	0,2090	0,6186	0,6186	3,540	2,259	63,814
3	6	5,2011	3,5578	0,6840	3,5343	0,0344	0,2090	0,4870	0,4870	3,540	2,060	58,192
3	7	6,2351	4,3100	0,6912	3,5343	0,0384	0,2090	0,4063	0,4063	3,540	1,885	53,249
3	8	7,1588	4,9682	0,6940	3,5343	0,0420	0,2090	0,3538	0,3538	3,540	1,725	48,729
4	5	3,4996	2,3663	0,6761	6,2832	0,0208	0,2090	0,7238	0,7238	3,540	2,645	74,718
4	6	4,2961	2,9243	0,6807	6,2832	0,0238	0,2090	0,5896	0,5896	3,540	2,516	71,073
4	7	4,9680	3,3661	0,6776	6,2832	0,0262	0,2090	0,5099	0,5099	3,540	2,413	68,164
4	8	5,4886	3,6580	0,6665	6,2832	0,0282	0,2090	0,4615	0,4615	3,540	2,325	65,678
5	5	2,9834	1,9998	0,6703	9,8175	0,0156	0,2090	0,8490	0,8490	3,540	2,868	81,017
5	6	3,5311	2,3407	0,6629	9,8175	0,0176	0,2090	0,7173	0,7173	3,540	2,782	78,588
5	7	3,9243	2,5245	0,6433	9,8175	0,0190	0,2090	0,6455	0,6455	3,540	2,722	76,893
5	8	4,1494	2,5396	0,6120	9,8175	0,0202	0,2090	0,6105	0,6105	3,540	2,671	75,452

Table B.66: Series-Series – Circular Coils with Rectangular Cross-Section – Efficiency (f_o = 100 kHz)

w (mm)	N (turns)	L (µH)	M_{12} (µH)	k_{12} (-)	A_{cs} (mm^2)	R (Ω)	δ (mm)	C_1 (µF)	C_2 (µF)	P_{in} (W)	P_{out} (W)	n (%)
3	5	4,0948	2,7539	0,6725	4,5	0,0219	0,2090	0,6186	0,6186	3,540	2,598	73,390
3	6	5,2011	3,5578	0,6840	4,5	0,0252	0,2090	0,4870	0,4870	3,540	2,455	69,350
3	7	6,2351	4,3100	0,6912	4,5	0,0282	0,2090	0,4063	0,4063	3,540	2,322	65,593
3	8	7,1588	4,9682	0,6940	4,5	0,0308	0,2090	0,3538	0,3538	3,540	2,203	62,232
4	5	3,4996	2,3663	0,6761	8,0	0,0156	0,2090	0,7238	0,7238	3,540	2,868	81,017
4	6	4,2961	2,9243	0,6807	8,0	0,0177	0,2090	0,5896	0,5896	3,540	2,778	78,475
4	7	4,9680	3,3661	0,6776	8,0	0,0195	0,2090	0,5099	0,5099	3,540	2,700	76,271
4	8	5,4886	3,6580	0,6665	8,0	0,0210	0,2090	0,4615	0,4615	3,540	2,634	74,407
5	5	2,9834	1,9998	0,6703	12,5	0,0118	0,2090	0,8490	0,8490	3,540	3,031	85,621

5	**6**	3,5311	2,3407	0,6629	12,5	0,0132	0,2090	0,7173	0,7173	3,540	2,971	83,927
5	**7**	3,9243	2,5245	0,6433	12,5	0,0144	0,2090	0,6455	0,6455	3,540	2,920	82,486
5	**8**	4,1494	2,5396	0,6120	12,5	0,0152	0,2090	0,6105	0,6105	3,540	2,885	81,497

Table B.67: Series-Series – Rectangular Coils with Circular Cross-Section – Efficiency (f_o = 100 kHz)

w (mm)	N (turns)	L (µH)	M_{12} (µH)	k_{12} (-)	$A_{cs}/2$ (mm^2)	R' (Ω)	δ (mm)	C_1 (µF)	C_2 (µF)	P_{in} (W)	P_{out} (W)	n (%)
3	**5**	4,8934	4,4645	0,9124	3,5343	0,0392	0,2090	0,5176	0,5176	3,540	1,855	52,401
3	**6**	6,2155	5,7676	0,9280	3,5343	0,0456	0,2090	0,4075	0,4075	3,540	1,577	44,548
3	**7**	7,4511	6,9871	0,9377	3,5343	0,0516	0,2090	0,3400	0,3400	3,540	1,313	37,090
3	**8**	8,5549	8,0542	0,9415	3,5343	0,0572	0,2090	0,2961	0,2961	3,540	1,066	30,113
4	**5**	4,1821	3,8360	0,9172	6,2832	0,0274	0,2090	0,6057	0,6057	3,540	2,362	66,723
4	**6**	5,1339	4,7407	0,9234	6,2832	0,0316	0,2090	0,4934	0,4934	3,540	2,181	61,610
4	**7**	5,9368	5,4570	0,9192	6,2832	0,0352	0,2090	0,4267	0,4267	3,540	2,024	57,175
4	**8**	6,5590	5,9302	0,9041	6,2832	0,0386	0,2090	0,3862	0,3862	3,540	1,875	52,966
5	**5**	3,5652	3,2419	0,9093	9,8175	0,0206	0,2090	0,7105	0,7105	3,540	2,654	74,972
5	**6**	4,2198	3,7945	0,8992	9,8175	0,0234	0,2090	0,6003	0,6003	3,540	2,534	71,582
5	**7**	4,6897	4,0925	0,8727	9,8175	0,0256	0,2090	0,5401	0,5401	3,540	2,439	68,898
5	**8**	4,9586	4,1170	0,8303	9,8175	0,0276	0,2090	0,5108	0,5108	3,540	2,353	66,469

Table B.68: Series-Series – Rectangular Coils with Rectangular Cross-Section – Efficiency (f_o = 100 kHz)

w (mm)	N (turns)	L (µH)	M_{12} (µH)	k_{12} (-)	A_{cs} (mm^2)	R (Ω)	δ (mm)	C_1 (µF)	C_2 (µF)	P_{in} (W)	P_{out} (W)	n (%)
3	**5**	4,8934	4,4645	0,9124	4,5	0,0287	0,2090	0,5176	0,5176	3,540	2,306	65,141
3	**6**	6,2155	5,7676	0,9280	4,5	0,0335	0,2090	0,4075	0,4075	3,540	2,095	59,181
3	**7**	7,4511	6,9871	0,9377	4,5	0,0379	0,2090	0,3400	0,3400	3,540	1,897	53,588
3	**8**	8,5549	8,0542	0,9415	4,5	0,0420	0,2090	0,2961	0,2961	3,540	1,708	48,249
4	**5**	4,1821	3,8360	0,9172	8,0	0,0205	0,2090	0,6057	0,6057	3,540	2,658	75,085
4	**6**	5,1339	4,7407	0,9234	8,0	0,0236	0,2090	0,4934	0,4934	3,540	2,524	71,299
4	**7**	5,9368	5,4570	0,9192	8,0	0,0263	0,2090	0,4267	0,4267	3,540	2,405	67,938
4	**8**	6,5590	5,9302	0,9041	8,0	0,0288	0,2090	0,3862	0,3862	3,540	2,294	64,802
5	**5**	3,5652	3,2419	0,9093	12,5	0,0155	0,2090	0,7105	0,7105	3,540	2,873	81,158
5	**6**	4,2198	3,7945	0,8992	12,5	0,0176	0,2090	0,6003	0,6003	3,540	2,783	78,616
5	**7**	4,6897	4,0925	0,8727	12,5	0,0194	0,2090	0,5401	0,5401	3,540	2,705	76,412
5	**8**	4,9586	4,1170	0,8303	12,5	0,0208	0,2090	0,5108	0,5108	3,540	2,645	74,718

Table B.69: Series-Parallel – Circular Coils with Circular Cross-Section – Efficiency (f_o = 100 kHz)

w (mm)	N (turns)	L (µH)	M_{12} (µH)	k_{12} (-)	$A_{cs}/2$ (mm^2)	R' (Ω)	δ (mm)	C_1 (µF)	C_2 (µF)	P_{in} (W)	P_{out} (W)	n (%)
3	**5**	4,0948	2,7539	0,6725	3,5343	0,0298	0,2090	1,1290	0,6186	3,540	1,681	47,486
3	**6**	5,2011	3,5578	0,6840	3,5343	0,0344	0,2090	0,9153	0,4870	3,540	1,570	44,350
3	**7**	6,2351	4,3100	0,6912	3,5343	0,0384	0,2090	0,7780	0,4063	3,540	1,103	31,158
3	**8**	7,1588	4,9682	0,6940	3,5343	0,0420	0,2090	0,6826	0,3538	3,540	0,868	24,508
4	**5**	3,4996	2,3663	0,6761	6,2832	0,0208	0,2090	1,3330	0,7238	3,540	2,237	63,192
4	**6**	4,2961	2,9243	0,6807	6,2832	0,0238	0,2090	1,0990	0,5896	3,540	2,043	57,712
4	**7**	4,9680	3,3661	0,6776	6,2832	0,0262	0,2090	0,9426	0,5099	3,540	1,898	53,616
4	**8**	5,4886	3,6580	0,6665	6,2832	0,0282	0,2090	0,8303	0,4615	3,540	1,790	50,565
5	**5**	2,9834	1,9998	0,6703	9,8175	0,0156	0,2090	1,5420	0,8490	3,540	2,567	72,514
5	**6**	3,5311	2,3407	0,6629	9,8175	0,0176	0,2090	1,2800	0,7173	3,540	2,450	69,209
5	**7**	3,9243	2,5245	0,6433	9,8175	0,0190	0,2090	1,1010	0,6455	3,540	2,385	67,373
5	**8**	4,1494	2,5396	0,6120	9,8175	0,0202	0,2090	0,9761	0,6105	3,540	2,346	66,271

Table B.70: Series-Parallel – Circular Coils with Rectangular Cross-Section – Efficiency (f_o = 100 kHz)

w (mm)	N (turns)	L (µH)	M_{12} (µH)	k_{12} (-)	A_{cs} (mm^2)	R (Ω)	δ (mm)	C_1 (µF)	C_2 (µF)	P_{in} (W)	P_{out} (W)	n (%)
3	**5**	4,0948	2,7539	0,6725	4,5	0,0219	0,2090	1,1290	0,6186	3,540	2,173	61,384
3	**6**	5,2011	3,5578	0,6840	4,5	0,0252	0,2090	0,9153	0,4870	3,540	1,951	55,113
3	**7**	6,2351	4,3100	0,6912	4,5	0,0282	0,2090	0,7780	0,4063	3,540	1,750	49,435
3	**8**	7,1588	4,9682	0,6940	4,5	0,0308	0,2090	0,6826	0,3538	3,540	1,580	44,633
4	**5**	3,4996	2,3663	0,6761	8,0	0,0156	0,2090	1,3330	0,7238	3,540	2,562	72,373
4	**6**	4,2961	2,9243	0,6807	8,0	0,0177	0,2090	1,0990	0,5896	3,540	2,426	68,531
4	**7**	4,9680	3,3661	0,6776	8,0	0,0195	0,2090	0,9426	0,5099	3,540	2,317	65,452
4	**8**	5,4886	3,6580	0,6665	8,0	0,0210	0,2090	0,8303	0,4615	3,540	2,237	63,192
5	**5**	2,9834	1,9998	0,6703	12,5	0,0118	0,2090	1,5420	0,8490	3,540	2,803	79,181
5	**6**	3,5311	2,3407	0,6629	12,5	0,0132	0,2090	1,2800	0,7173	3,540	2,722	76,893
5	**7**	3,9243	2,5245	0,6433	12,5	0,0144	0,2090	1,1010	0,6455	3,540	2,664	75,254
5	**8**	4,1494	2,5396	0,6120	12,5	0,0152	0,2090	0,9761	0,6105	3,540	2,641	74,605

Table B.71: Series-Parallel – Rectangular Coils with Circular Cross-Section – Efficiency (f_o = 100 kHz)

w (mm)	N (turns)	L (µH)	M_{12} (µH)	k_{12} (-)	$A_{cs}/2$ (mm^2)	R' (Ω)	δ (mm)	C_1 (µF)	C_2 (µF)	P_{in} (W)	P_{out} (W)	n (%)
3	**5**	4,8934	4,4645	0,9124	3,5343	0,0392	0,2090	3,0880	0,5176	3,540	0,456	12,870
3	**6**	6,2155	5,7676	0,9280	3,5343	0,0456	0,2090	2,9330	0,4075	-	-	-
3	**7**	7,4511	6,9871	0,9377	3,5343	0,0516	0,2090	2,8170	0,3400	-	-	-

3	**8**	8,5549	8,0542	0,9415	3,5343	0,0572	0,2090	2,6060	0,2961	-	-	-
4	**5**	4,1821	3,8360	0,9172	6,2832	0,0274	0,2090	3,8170	0,6057	3,540	1,373	38,785
4	**6**	5,1339	4,7407	0,9234	6,2832	0,0316	0,2090	3,3490	0,4934	3,540	1,026	28,983
4	**7**	5,9368	5,4570	0,9192	6,2832	0,0352	0,2090	2,7510	0,4267	3,540	0,751	21,223
4	**8**	6,5590	5,9302	0,9041	6,2832	0,0386	0,2090	2,1160	0,3862	3,540	0,527	14,898
5	**5**	3,5652	3,2419	0,9093	9,8175	0,0206	0,2090	4,1040	0,7105	3,540	1,924	54,350
5	**6**	4,2198	3,7945	0,8992	9,8175	0,0234	0,2090	3,1360	0,6003	3,540	1,722	48,644
5	**7**	4,6897	4,0925	0,8727	9,8175	0,0256	0,2090	2,2650	0,5401	3,540	1,603	45,282
5	**8**	4,9586	4,1170	0,8303	9,8175	0,0276	0,2090	1,6440	0,5108	3,540	1,537	43,418

Table B.72: Series-Parallel – Rectangular Coils with Rectangular Cross-Section – Efficiency (f_o = 100 kHz)

w (mm)	N (turns)	L (µH)	M_{12} (µH)	k_{12} (-)	A_{cs} (mm^2)	R (Ω)	δ (mm)	C_1 (µF)	C_2 (µF)	P_{in} (W)	P_{out} (W)	n (%)
3	**5**	4,8934	4,4645	0,9124	4,5	0,0287	0,2090	3,0880	0,5176	3,540	1,282	36,215
3	**6**	6,2155	5,7676	0,9280	4,5	0,0335	0,2090	2,9330	0,4075	3,540	0,863	24,370
3	**7**	7,4511	6,9871	0,9377	4,5	0,0379	0,2090	2,8170	0,3400	3,540	0,481	13,596
3	**8**	8,5549	8,0542	0,9415	4,5	0,0420	0,2090	2,6060	0,2961	3,540	0,138	3,890
4	**5**	4,1821	3,8360	0,9172	8,0	0,0205	0,2090	3,8170	0,6057	3,540	1,919	54,209
4	**6**	5,1339	4,7407	0,9234	8,0	0,0236	0,2090	3,3490	0,4934	3,540	1,662	46,949
4	**7**	5,9368	5,4570	0,9192	8,0	0,0263	0,2090	2,7510	0,4267	3,540	1,456	41,130
4	**8**	6,5590	5,9302	0,9041	8,0	0,0288	0,2090	2,1160	0,3862	3,540	1,292	36,497
5	**5**	3,5652	3,2419	0,9093	12,5	0,0155	0,2090	4,1040	0,7105	3,540	2,323	65,621
5	**6**	4,2198	3,7945	0,8992	12,5	0,0176	0,2090	3,1360	0,6003	3,540	2,173	61,384
5	**7**	4,6897	4,0925	0,8727	12,5	0,0194	0,2090	2,2650	0,5401	3,540	2,072	58,531
5	**8**	4,9586	4,1170	0,8303	12,5	0,0208	0,2090	1,6440	0,5108	3,540	2,031	57,373

Table B.73: Parallel-Series – Circular Coils with Circular Cross-Section – Efficiency (f_o = 100 kHz)

w (mm)	N (turns)	L (µH)	M_{12} (µH)	k_{12} (-)	$A_{cs}/2$ (mm^2)	R' (Ω)	δ (mm)	C_1 (µF)	C_2 (µF)	P_{in} (W)	P_{out} (W)	n (%)
3	**5**	4,0948	2,7539	0,6725	3,5343	0,0298	0,2090	0,6186	1,1290	-	-	-
3	**6**	5,2011	3,5578	0,6840	3,5343	0,0344	0,2090	0,4870	0,9153	-	-	-
3	**7**	6,2351	4,3100	0,6912	3,5343	0,0384	0,2090	0,4063	0,7780	-	-	-
3	**8**	7,1588	4,9682	0,6940	3,5343	0,0420	0,2090	0,3538	0,6826	-	-	-
4	**5**	3,4996	2,3663	0,6761	6,2832	0,0208	0,2090	0,7238	1,3330	3,540	0,694	19,596
4	**6**	4,2961	2,9243	0,6807	6,2832	0,0238	0,2090	0,5896	1,0990	3,540	0,313	8,833
4	**7**	4,9680	3,3661	0,6776	6,2832	0,0262	0,2090	0,5099	0,9426	-	-	-
4	**8**	5,4886	3,6580	0,6665	6,2832	0,0282	0,2090	0,4615	0,8303	-	-	-
5	**5**	2,9834	1,9998	0,6703	9,8175	0,0156	0,2090	0,8490	1,5420	3,540	1,379	38,955

5	**6**	3,5311	2,3407	0,6629	9,8175	0,0176	0,2090	0,7173	1,2800	3,540	1,064	30,056
5	**7**	3,9243	2,5245	0,6433	9,8175	0,0190	0,2090	0,6455	1,1010	3,540	0,752	21,243
5	**8**	4,1494	2,5396	0,6120	9,8175	0,0202	0,2090	0,6105	0,9761	3,540	0,356	10,045

Table B.74: Parallel-Series – Circular Coils with Rectangular Cross-Section – Efficiency (f_o = 100 kHz)

w (mm)	N (turns)	L (µH)	M_{12} (µH)	k_{12} (-)	A_{cs} (mm^2)	R (Ω)	δ (mm)	C_1 (µF)	C_2 (µF)	P_{in} (W)	P_{out} (W)	n (%)
3	**5**	4,0948	2,7539	0,6725	4,5	0,0219	0,2090	0,6186	1,1290	3,540	0,521	14,709
3	**6**	5,2011	3,5578	0,6840	4,5	0,0252	0,2090	0,4870	0,9153	3,540	0,145	4,107
3	**7**	6,2351	4,3100	0,6912	4,5	0,0282	0,2090	0,4063	0,7780	-	-	-
3	**8**	7,1588	4,9682	0,6940	4,5	0,0308	0,2090	0,3538	0,6826	-	-	-
4	**5**	3,4996	2,3663	0,6761	8,0	0,0156	0,2090	0,7238	1,3330	3,540	1,405	39,689
4	**6**	4,2961	2,9243	0,6807	8,0	0,0177	0,2090	0,5896	1,0990	3,540	1,139	32,175
4	**7**	4,9680	3,3661	0,6776	8,0	0,0195	0,2090	0,5099	0,9426	3,540	0,877	24,777
4	**8**	5,4886	3,6580	0,6665	8,0	0,0210	0,2090	0,4615	0,8303	3,540	0,605	17,093
5	**5**	2,9834	1,9998	0,6703	12,5	0,0118	0,2090	0,8490	1,5420	3,540	1,905	53,814
5	**6**	3,5311	2,3407	0,6629	12,5	0,0132	0,2090	0,7173	1,2800	3,540	1,683	47,542
5	**7**	3,9243	2,5245	0,6433	12,5	0,0144	0,2090	0,6455	1,1010	3,540	1,426	40,282
5	**8**	4,1494	2,5396	0,6120	12,5	0,0152	0,2090	0,6105	0,9761	3,540	1,139	32,175

Table B.75: Parallel-Series – Rectangular Coils with Circular Cross-Section – Efficiency (f_o = 100 kHz)

w (mm)	N (turns)	L (µH)	M_{12} (µH)	k_{12} (-)	$A_{cs}/2$ (mm^2)	R' (Ω)	δ (mm)	C_1 (µF)	C_2 (µF)	P_{in} (W)	P_{out} (W)	n (%)
3	**5**	4,8934	4,4645	0,9124	3,5343	0,0392	0,2090	0,5176	3,0880	-	-	-
3	**6**	6,2155	5,7676	0,9280	3,5343	0,0456	0,2090	0,4075	2,9330	-	-	-
3	**7**	7,4511	6,9871	0,9377	3,5343	0,0516	0,2090	0,3400	2,8170	-	-	-
3	**8**	8,5549	8,0542	0,9415	3,5343	0,0572	0,2090	0,2961	2,6060	-	-	-
4	**5**	4,1821	3,8360	0,9172	6,2832	0,0274	0,2090	0,6057	3,8170	3,540	0,965	27,268
4	**6**	5,1339	4,7407	0,9234	6,2832	0,0316	0,2090	0,4934	3,3490	3,540	0,592	16,726
4	**7**	5,9368	5,4570	0,9192	6,2832	0,0352	0,2090	0,4267	2,7510	3,540	0,240	6,777
4	**8**	6,5590	5,9302	0,9041	6,2832	0,0386	0,2090	0,3862	2,1160	-	-	-
5	**5**	3,5652	3,2419	0,9093	9,8175	0,0206	0,2090	0,7105	4,1040	3,540	1,585	44,774
5	**6**	4,2198	3,7945	0,8992	9,8175	0,0234	0,2090	0,6003	3,1360	3,540	1,293	36,525
5	**7**	4,6897	4,0925	0,8727	9,8175	0,0256	0,2090	0,5401	2,2650	3,540	0,997	28,172
5	**8**	4,9586	4,1170	0,8303	9,8175	0,0276	0,2090	0,5108	1,6440	3,540	0,636	17,963

Table B.76: Parallel-Series – Rectangular Coils with Rectangular Cross-Section – Efficiency (f_o = 100 kHz)

w (mm)	N (turns)	L (µH)	M_{12} (µH)	k_{12} (-)	A_{cs} (mm^2)	R (Ω)	δ (mm)	C_1 (µF)	C_2 (µF)	P_{in} (W)	P_{out} (W)	n (%)
3	**5**	4,8934	4,4645	0,9124	4,5	0,0287	0,2090	0,5176	3,0880	3,540	0,827	23,370
3	**6**	6,2155	5,7676	0,9280	4,5	0,0335	0,2090	0,4075	2,9330	3,540	0,431	12,178
3	**7**	7,4511	6,9871	0,9377	4,5	0,0379	0,2090	0,3400	2,8170	3,540	0,062	1,751
3	**8**	8,5549	8,0542	0,9415	4,5	0,0420	0,2090	0,2961	2,6060	-	-	-
4	**5**	4,1821	3,8360	0,9172	8,0	0,0205	0,2090	0,6057	3,8170	3,540	1,613	45,565
4	**6**	5,1339	4,7407	0,9234	8,0	0,0236	0,2090	0,4934	3,3490	3,540	1,338	37,797
4	**7**	5,9368	5,4570	0,9192	8,0	0,0263	0,2090	0,4267	2,7510	3,540	1,074	30,339
4	**8**	6,5590	5,9302	0,9041	8,0	0,0288	0,2090	0,3862	2,1160	3,540	0,791	22,331
5	**5**	3,5652	3,2419	0,9093	12,5	0,0155	0,2090	0,7105	4,1040	3,540	2,069	58,446
5	**6**	4,2198	3,7945	0,8992	12,5	0,0176	0,2090	0,6003	3,1360	3,540	1,849	52,232
5	**7**	4,6897	4,0925	0,8727	12,5	0,0194	0,2090	0,5401	2,2650	3,540	1,613	45,565
5	**8**	4,9586	4,1170	0,8303	12,5	0,0208	0,2090	0,5108	1,6440	3,540	1,351	38,164

Table B.77: Parallel-Parallel – Circular Coils with Circular Cross-Section – Efficiency (f_o = 100 kHz)

w (mm)	N (turns)	L (µH)	M_{12} (µH)	k_{12} (-)	$A_{cs}/2$ (mm^2)	R' (Ω)	δ (mm)	C_1 (µF)	C_2 (µF)	P_{in} (W)	P_{out} (W)	n (%)
3	**5**	4,0948	2,7539	0,6725	3,5343	0,0298	0,2090	1,1290	1,1290	-	-	-
3	**6**	5,2011	3,5578	0,6840	3,5343	0,0344	0,2090	0,9153	0,9153	-	-	-
3	**7**	6,2351	4,3100	0,6912	3,5343	0,0384	0,2090	0,7780	0,7780	-	-	-
3	**8**	7,1588	4,9682	0,6940	3,5343	0,0420	0,2090	0,6826	0,6826	-	-	-
4	**5**	3,4996	2,3663	0,6761	6,2832	0,0208	0,2090	1,3330	1,3330	3,540	0,698	19,715
4	**6**	4,2961	2,9243	0,6807	6,2832	0,0238	0,2090	1,0990	1,0990	3,540	0,317	8,958
4	**7**	4,9680	3,3661	0,6776	6,2832	0,0262	0,2090	0,9426	0,9426	-	-	-
4	**8**	5,4886	3,6580	0,6665	6,2832	0,0282	0,2090	0,8303	0,8303	-	-	-
5	**5**	2,9834	1,9998	0,6703	9,8175	0,0156	0,2090	1,5420	1,5420	3,540	1,381	39,011
5	**6**	3,5311	2,3407	0,6629	9,8175	0,0176	0,2090	1,2800	1,2800	3,540	1,066	30,113
5	**7**	3,9243	2,5245	0,6433	9,8175	0,0190	0,2090	1,1010	1,1010	3,540	0,755	21,331
5	**8**	4,1494	2,5396	0,6120	9,8175	0,0202	0,2090	0,9761	0,9761	3,540	0,360	10,164

Table B.78: Parallel-Parallel – Circular Coils with Rectangular Cross-Section – Efficiency (f_o = 100 kHz)

w (mm)	N (turns)	L (µH)	M_{12} (µH)	k_{12} (-)	A_{cs} (mm^2)	R (Ω)	δ (mm)	C_1 (µF)	C_2 (µF)	P_{in} (W)	P_{out} (W)	n (%)
3	**5**	4,0948	2,7539	0,6725	4,5	0,0219	0,2090	1,1290	1,1290	3,540	0,524	14,814
3	**6**	5,2011	3,5578	0,6840	4,5	0,0252	0,2090	0,9153	0,9153	3,540	0,149	4,215
3	**7**	6,2351	4,3100	0,6912	4,5	0,0282	0,2090	0,7780	0,7780	-	-	-

3	**8**	7,1588	4,9682	0,6940	4,5	0,0308	0,2090	0,6826	0,6826	-	-	-
4	**5**	3,4996	2,3663	0,6761	8,0	0,0156	0,2090	1,3330	1,3330	3,540	1,406	39,718
4	**6**	4,2961	2,9243	0,6807	8,0	0,0177	0,2090	1,0990	1,0990	3,540	1,141	32,232
4	**7**	4,9680	3,3661	0,6776	8,0	0,0195	0,2090	0,9426	0,9426	3,540	0,880	24,864
4	**8**	5,4886	3,6580	0,6665	8,0	0,0210	0,2090	0,8303	0,8303	3,540	0,610	17,226
5	**5**	2,9834	1,9998	0,6703	12,5	0,0118	0,2090	1,5420	1,5420	3,540	1,904	53,785
5	**6**	3,5311	2,3407	0,6629	12,5	0,0132	0,2090	1,2800	1,2800	3,540	1,682	47,514
5	**7**	3,9243	2,5245	0,6433	12,5	0,0144	0,2090	1,1010	1,1010	3,540	1,425	40,254
5	**8**	4,1494	2,5396	0,6120	12,5	0,0152	0,2090	0,9761	0,9761	3,540	1,138	32,147

Table B.79: Parallel-Parallel – Rectangular Coils with Circular Cross-Section – Efficiency (f_o = 100 kHz)

w (mm)	N (turns)	L (µH)	M_{12} (µH)	k_{12} (-)	$A_{cs}/2$ (mm^2)	R' (Ω)	δ (mm)	C_1 (µF)	C_2 (µF)	P_{in} (W)	P_{out} (W)	n (%)
3	**5**	4,8934	4,4645	0,9124	3,5343	0,0392	0,2090	3,0880	3,0880	-	-	-
3	**6**	6,2155	5,7676	0,9280	3,5343	0,0456	0,2090	2,9330	2,9330	-	-	-
3	**7**	7,4511	6,9871	0,9377	3,5343	0,0516	0,2090	2,8170	2,8170	-	-	-
3	**8**	8,5549	8,0542	0,9415	3,5343	0,0572	0,2090	2,6060	2,6060	-	-	-
4	**5**	4,1821	3,8360	0,9172	6,2832	0,0274	0,2090	3,8170	3,8170	3,540	1,009	28,503
4	**6**	5,1339	4,7407	0,9234	6,2832	0,0316	0,2090	3,3490	3,3490	3,540	0,650	18,364
4	**7**	5,9368	5,4570	0,9192	6,2832	0,0352	0,2090	2,7510	2,7510	3,540	0,294	8,314
4	**8**	6,5590	5,9302	0,9041	6,2832	0,0386	0,2090	2,1160	2,1160	-	-	-
5	**5**	3,5652	3,2419	0,9093	9,8175	0,0206	0,2090	4,1040	4,1040	3,540	1,590	44,915
5	**6**	4,2198	3,7945	0,8992	9,8175	0,0234	0,2090	3,1360	3,1360	3,540	1,307	36,921
5	**7**	4,6897	4,0925	0,8727	9,8175	0,0256	0,2090	2,2650	2,2650	3,540	1,011	28,559
5	**8**	4,9586	4,1170	0,8303	9,8175	0,0276	0,2090	1,6440	1,6440	3,540	0,647	18,274

Table B.80: Parallel-Parallel – Rectangular Coils with Rectangular Cross-Section – Efficiency (f_o = 100 kHz)

w (mm)	N (turns)	L (µH)	M_{12} (µH)	k_{12} (-)	A_{cs} (mm^2)	R (Ω)	δ (mm)	C_1 (µF)	C_2 (µF)	P_{in} (W)	P_{out} (W)	n (%)
3	**5**	4,8934	4,4645	0,9124	4,5	0,0287	0,2090	3,0880	3,0880	3,540	0,863	24,390
3	**6**	6,2155	5,7676	0,9280	4,5	0,0335	0,2090	2,9330	2,9330	3,540	0,484	13,678
3	**7**	7,4511	6,9871	0,9377	4,5	0,0379	0,2090	2,8170	2,8170	3,540	0,129	3,638
3	**8**	8,5549	8,0542	0,9415	4,5	0,0420	0,2090	2,6060	2,6060	-	-	-
4	**5**	4,1821	3,8360	0,9172	8,0	0,0205	0,2090	3,8170	3,8170	3,540	1,616	45,650
4	**6**	5,1339	4,7407	0,9234	8,0	0,0236	0,2090	3,3490	3,3490	3,540	1,353	38,220
4	**7**	5,9368	5,4570	0,9192	8,0	0,0263	0,2090	2,7510	2,7510	3,540	1,093	30,876
4	**8**	6,5590	5,9302	0,9041	8,0	0,0288	0,2090	2,1160	2,1160	3,540	0,808	22,831
5	**5**	3,5652	3,2419	0,9093	12,5	0,0155	0,2090	4,1040	4,1040	3,540	2,052	57,966

5	**6**	4,2198	3,7945	0,8992	12,5	0,0176	0,2090	3,1360	3,1360	3,540	1,845	52,119
5	**7**	4,6897	4,0925	0,8727	12,5	0,0194	0,2090	2,2650	2,2650	3,540	1,612	45,537
5	**8**	4,9586	4,1170	0,8303	12,5	0,0208	0,2090	1,6440	1,6440	3,540	1,350	38,136

Table B.81: Series-Series – Circular Coils with Rectangular Cross-Section – Efficiency (1 Solar Cell)

f_o (kHz)	w (mm)	h (mm)	N (turns)	L (µH)	M_{12} (µH)	k_{12} (-)	A_{cs} (mm^2)	R (Ω)	δ (mm)	P_{in} (W)	P_{out} (W)	n (%)
100	5	2,5	5	2,9834	1,9998	0,6703	12,5	0,0118	0,2090	3,540	3,031	85,621
500	5	2,5	5	2,9834	1,9998	0,6703	12,5	0,0264	0,0935	3,540	2,405	67,938
1000	5	2,5	5	2,9834	1,9998	0,6703	12,5	0,0373	0,0661	3,540	1,935	54,661

Table B.82: Series-Parallel – Circular Coils with Rectangular Cross-Section – Efficiency (1 Solar Cell)

f_o (kHz)	w (mm)	h (mm)	N (turns)	L (µH)	M_{12} (µH)	k_{12} (-)	A_{cs} (mm^2)	R (Ω)	δ (mm)	P_{in} (W)	P_{out} (W)	n (%)
100	5	2,5	5	2,9834	1,9998	0,6703	12,5	0,0118	0,2090	3,540	2,803	79,181
500	5	2,5	5	2,9834	1,9998	0,6703	12,5	0,0264	0,0935	3,540	1,896	53,559
1000	5	2,5	5	2,9834	1,9998	0,6703	12,5	0,0373	0,0661	3,540	1,218	34,407

Table B.83: Series-Series – Circular Coils with Rectangular Cross-Section – Efficiency (16 Solar Cells)

f_o (kHz)	w (mm)	h (mm)	N (turns)	L (µH)	M_{12} (µH)	k_{12} (-)	A_{cs} (mm^2)	R (Ω)	δ (mm)	P_{in} (W)	P_{out} (W)	n (%)
100	5	2,5	5	2,9834	1,9998	0,6703	12,5	0,0118	0,2090	56,640	55,580	98,129
500	5	2,5	5	2,9834	1,9998	0,6703	12,5	0,0264	0,0935	56,640	55,450	97,899
1000	5	2,5	5	2,9834	1,9998	0,6703	12,5	0,0373	0,0661	56,640	55,010	97,122

Table B.84: Series-Parallel – Circular Coils with Rectangular Cross-Section – Efficiency (16 Solar Cells)

f_o (kHz)	w (mm)	h (mm)	N (turns)	L (µH)	M_{12} (µH)	k_{12} (-)	A_{cs} (mm^2)	R (Ω)	δ (mm)	P_{in} (W)	P_{out} (W)	n (%)
100	5	2,5	5	2,9834	1,9998	0,6703	12,5	0,0118	0,2090	56,640	55,360	97,740
500	5	2,5	5	2,9834	1,9998	0,6703	12,5	0,0264	0,0935	56,640	54,950	97,016
1000	5	2,5	5	2,9834	1,9998	0,6703	12,5	0,0373	0,0661	56,640	54,300	95,869